# THEORETICAL STUDY OF RAIN INDUCED PROPAGATION EFFECTS ON SATELLITE TELECOMMUNICATION IN SOME TROPICAL LOCATIONS

OMOTOSHO TEMIDAYO VICTOR

(PHY/91/3363)

A THESIS SUBMITTED IN PARTIAL FULFILMENT OF THE REQUIREMENTS FOR THE AWARD OF THE DEGREE OF

MASTERS OF TECHNOLOGY (M.TECH.)

IN

COMMUNICATION PHYSICS

DEPARTMENT OF PHYSICS

FEDERAL UNIVERSITY OF TECHNOLOGY,

AKURE, NIGERIA

DECEMBER 2003

## CERTIFICATION

I certify that Mr. T.V Omotosho has carried out this work under my supervision in the Department of Physics, Federal University of Technology, Akure, Ondo State Nigeria.

31/1/04

**M.O. Ajewole. B.Sc., M.Sc (Ilorin) Ph.D (Akure)**

Department of Physics,

Federal University of Technology,

Akure, Nigeria.

**December 2003**

# DEDICATION

This work is dedicated to my beloved wife, **Elizabeth Olufisayo Omolola**

And my son, **David Praise Iremitide**

## ACKNOWLEDGEMENTS.

I wish to express my profound gratitude to Dr. M.O Ajewole who encouraged my coming into academics and who thoroughly supervised this work. I appreciate very much his words of encouragement; guidance, his assistance in making his library available to me and his support in providing the most recent journal and conference papers relevant to this dissertation. This support enabled me to carry out this work with the most recent techniques. I appreciate him also for his readiness to attend to my questions on this work.

I acknowledge with thanks the encouragement received from members of staff of Department of Physics, Federal University of Technology, Akure, most especially Dr. (Mrs.) I.A Fuwape, Dr. M.T Babalola, Dr A.B Rabiu and Mr. A.S Adekola.

I wish to show my sincere appreciation to the Federal University of Technology, Akure for the staff development scholarship award offered me for this programme.

I am expressing my deep gratitude to my wife, Olufisayo Omolola and my Son David Praise Iremitide for their love, prayers, understanding, support and encouragement during the period of this work. They stood as catalyst to the success of the project.

Finally, I am grateful to the Lord Jesus My Lord and Saviour, the power and the Wisdom of God. His grace and promises kept me going throughout the course of this dissertation.

## TABLE OF CONTENTS

## LIST OF FIGURES.

## LIST OF TABLES

## ABSTRACT

The study investigates the scattering effect of oblate spheroidal raindrops on Earth-space wave communication in the frequency band 1–52 GHz in three tropical locations Ile-Ife, Nigeria (4.34°E, 7.33°N), Douala, Cameroon (9.70°E, 4.05°N), and Nairobi, Kenya (36.75°E, 1.30°S). Elevation angles of 23° and 55° are assumed for wave propagation in the regions. The incident waves are assumed to be linearly polarized that is, the incident waves are horizontally and vertically polarized. The tropical lognormal raindrop size distribution model has been used to estimate the raindrops number density. The specific attenuation and specific phase shift are calculated in terms of the power law relationship between attenuation and rainfall rate since measured cumulative distribution of rain rates are available from the locations. The total slant path attenuation is then computed using the International Telecommunication Union (ITU) recommended model. Rain rates measured at the locations are used. The calculation of the propagation parameters is based on the measured Mean Annual (MA) and Mean Worst Month (MWM) rainfall rates in each location. Differential propagation parameters are also computed at the frequencies and elevation angles investigated. The results are then used to compute the Cross Polarization Discrimination (XPD) and the Co-Polarized Attenuation (CPA) at the two rain rates and elevation angles for rain rates exceeded for 0.01 % of time (99.99% time availability). The total slant path attenuation for other time percentages such as 0.001% and 0.1 % of time are calculated using the scaling formula also recommended by the ITU. The total slant path attenuation, co-polarized attenuation, and cross polarization discrimination in Cameroon and Kenya are compared with that of Nigeria. The predicted slant path attenuation, CPA, and XPD for Cameroon is closer to those obtained for

Nigeria than that for Kenya. Further, at the elevation angle of $55^0$, and for links over the Atlantic Ocean Region (AOR), the CPA and XPD are higher in Cameroon than Nigeria by about 24% at the most. At the elevation angle of $23^0$, and for links over the Indian Ocean Region (IOR), the percentage difference between CPA and XPD in Cameroon is higher than in Nigeria by about 1136%. Therefore, it can be safely said that rain induced degradation of Earth-space communication will be most severe in Cameroon and least severe in Kenya.

# CHAPTER ONE

## 1.0 INTRODUCTION

Attenuation due to rainfall plays a significant role in the design of earth –satellite radio links at frequencies above 10GHz. The increasing use of satellites for telecommunication and broadcasting services has necessitated more than before the need for earth – space attenuation studies in the tropics. Most of the attenuation studies on earth – satellite paths have been carried out in the temperate regions of the world (Ajayi et al., 1996). Apart from the use of the 6 / 4 GHz band for satellite communication, satellite systems are already operating in the 14 / 12 GHz band and above. The use of the 30/20 GHz is in fact at advance stage (Ajayi et al., 1996). The precipitation characteristics in the tropics differ appreciably from those of the temperate regions in that empirical relationships obtained in the latter have not be very suitable for system design in the former (Ajayi et al., 1996). Rain attenuation can be obtained directly through measurement or predicted from the knowledge of rain rate and drop – size distribution. It is thus possible to estimate the attenuation by means of indirect measurements. The procedure for predicting the attenuation is based on the relationship between specific attenuation and rain rate established through the modeling of the rain microstructure e.g. shape, size, temperature and terminal speed of the raindrops. The rain-induced attenuation is computed by integrating the specific attenuation along the propagating path. The non- uniform character of the rain along the path is taken into account by means of a statistical model for the rain intensity. The statistical distribution of rain

attenuation is thus, obtained from the rain rate distribution for the region considered. Raindrops both absorb and scatter microwave energy on earth – satellite links. Both may contribute, to the attenuation of a radio path, while scatter may also cause interference between radio paths. Other important effects of rain on micro- wave propagation (Ajayi et al., 1996) are: -

1. Depolarization due to non- spherical nature of raindrops.
2. Rapid amplitude and phase scintillation caused by equivalent multipath propagation.
3. Antenna degradation due to phase dispersion of ray paths reaching the antenna.

## 1.1 CROSS – POLARIZATION

To increase channel capacity without increasing bandwidth, orthogonal polarization (linear or circular) may be independently used for transmission at the same frequency over the same path. However, "frequency re – use" may be impaired by the possibility that in propagating through the atmosphere, some of the energy transmitted in one polarization state can be transferred to the orthogonal polarization state thus causing interference between the two channels (CCIR, 1986). Rain and other hydrometors may cause this phenomenon. This is usually referred to as cross polarization. Cross - polarization may occur during periods of multipath propagation. Additionally, cross - polarization may arise due to the characteristics of the antenna systems at each terminal, and this cross – polarised component will then exist at a base level. When two orthogonal polarization 'a' and 'b' (fig 1.1) are transmitted at the same level, the ratio of the co – polarised signal ('ac' or 'bc') in a given receiving channel to the cross – polarised signal

('bx' or 'ax') in that channel, is known as the cross – polarization isolation (XPI = ac/bx) and this is of prime importance in system design. The two-ratio ac/bx and bc/ax are not necessarily the same. Propagation experiment on the other hand usually measure cross polarization discrimination (XPD = ac/ax) which is the ratio of the co – polarized received signal 'ac' to the cross – polarized received signal 'ax' when one polarization only, 'a' is transmitted (ITU-R, 1994). That is, the co – polar signal ac and the cross – polar signal ax is each measured independently and in the absence of any orthogonal polarized transmitted signal 'b'. In the context of rain – induced cross - polarization, the above expressions ac/bx, bc/ax and ac/ax may be considered to be the same [Oguchi, 1975, Watson et al., 1974]. Both the cross polarization isolation (XPI) and cross - polarization discrimination (XPD) are normally expressed in decibels. A dual – polarized receiver that is designed to receive orthogonal channels simultaneously will detect both wanted, or co – polarized, signals ac and bc and the unwanted, or cross – polarized signals bx and ax. The isolation in channel a will be the ratio ac/bx. In general, experiment use only mono – polarized transmissions and so what is measured is the discrimination ratio ac/ax or bc/bx.

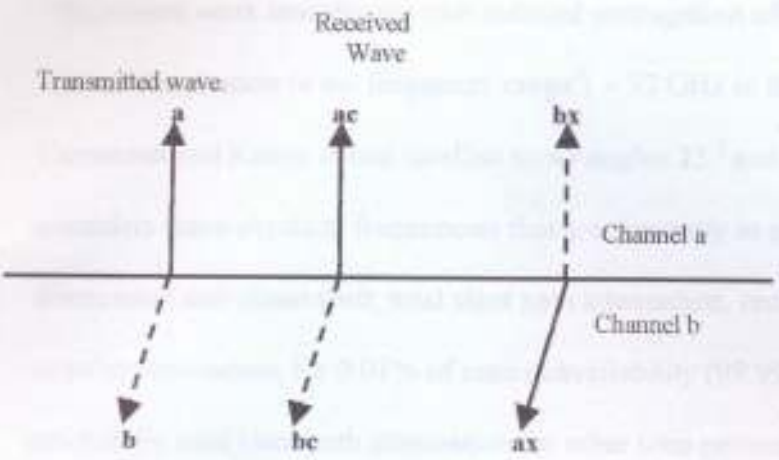


Fig. 1.1 Term used to define the difference between XPD and XPI ac and bc are the co – polarized components of signal transmitted in channels a and b, respectively. ax and bx are the cross – polarized components of signals transmitted in channels a and b respectively.

## 1.2 The scope of the present work

The present work investigates rain induced propagation effects on satellite telecommunication in the frequency range 1 – 52 GHz in three tropical locations Nigeria, Cameroon and Kenya at two satellite looks angles 23 $^0$ and 55$^0$. The study particularly considers some practical frequencies that are presently in use. It evaluates the specific attenuation and phase shift, total slant path attenuation, cross polarization, and the copolar attenuation, for 0.01% of time unavailability (99.99% availability) and then predict the total slant path attenuation for other time percentages unavailability such as 0.1%and 0.001% (99.9% and 99.999% availability) of time. The computed results of each location are compared. In Cameroon in particular, there are no reports in literature on rain-induced impairments. In Kenya on the other hand, few studies utilizing the measured rain rate exists in literature ( Allnut and Haidara, 1998). However, most of the studies on microwave depolarisation in sub-saharan Africa have been done in Nigeria. The study is thus significant in providing regional information and data for satellite telecommunication system designers to determine the extent of the distortion of propagating signals through tropical rain. These parameters are evaluated to assist system designers to determine the most suitable transmitting power, best choice of elevation angle for receiving radio signals, and antenna gain that will cope with rain induced effects on propagating signals across the region.

# CHAPTER TWO

## 2. THEORETICAL BACKGROUND

The present work presents the study of some rain-induced propagation effects on satellite telecommunication in some tropical locations. Rain attenuation is the major factor limiting the reliability of both terrestrial and Earth – to – satellite links operating at frequencies above 10GHz. Short integration – time rainfall rate is the most essential input parameter needed in the prediction models for rain attenuation.

### 2.1 Characteristics of rainfall in tropical regions

Broadly speaking, rainfall can be classified into:

(i) Stratiform

(ii) Convective

Stratiform precipitation results from the formation of small ice particles joined together to form bigger nuclei. The growing nuclei become unstable and as they pass through the so – called melting layer, extending from about 500m to 1km below the $0^{o}C$ isothermal, turn into raindrops that fall down to the earth surface.

### 2.2 Classification of rain

Stratiform consist of drizzle and widespread while the convective consist of shower and thunderstorm (Joss et al., 1968)

Drizzle distribution is associated with drops of diameter of the order of 1.0mm and the maximum rainfall intensity is about 5mm/h.

Widespread rain is made up of raindrops with diameter range between 1.0mm and 3.5mm. The rainfall time duration is usually long (greater than 1.0 hour) and has a maximum rainfall intensity of 50mm/h.

Shower rainfall consists of extremely few raindrops above 2.0mm diameter. It is of small time duration and its maximum rainfall intensity is about 150mm/h.

Thunderstorm rain distribution, on the other hand has a distribution of relatively high concentration of large drops typically greater than 3.0mm. The maximum rainfall intensity is 210mm/h.

These classifications are often used in the calculation of propagation parameters when their variations are examined with respect to the change of size distribution ( Joss et al., 1968)

Convective precipitation is associated with clouds that are formed in general below the $0^0$C isothermal and are stirred up by the strong movement of air masses caused by differences in tropospheric pressure. In this process water drops are created and grow in size, until gravity precipitate them.

Tropical rainfall is predominantly convective and characterized by high precipitation rates, it occurs in general, over limited extensions and for short duration of time. However during precipitation, stratiform structures develop which extends over wider areas (about 100km) with smaller intensities (0 - 25mm/h). Studies undertaken in the last decades concerning rain attenuation in different regions of the world combine convective and stratiform rainfalls. Regardless of the precipitation type, rainfall is characterized by space and time variable structure constituted by cells of various dimensions that move horizontally with speed depending on the tropospheric winds and the height of the clouds

(Ajayi et al., 1996). Radar measurements have shown that typical dimension of strong rain rate cells range from 2 to 5km (Ajayi et al., 1996). The height of the rain cell (rain height) is an important parameter in the calculation of slant path attenuation. It is generally considered that the rain structure reaches a maximum height equal to the $0^0$C isothermal. Above this, precipitation is assumed to have the form of ice, snow or melting snow (ITU-R, 2001). However it should be noted that tropical rainstorms, of convective nature, reach altitudes of 6 to 10km (Ajayi et al., 1996).

## 2.3 Propagation Losses

The propagation losses on Earth – space path relative to the free – space loss, is the sum of different contribution such as (ITU-R, 2003):

(i) Attenuation by atmospheric gases

(ii) Attenuation by rain, and other precipitation clouds

(iii) Focusing and defocusing

(iv) Decrease in antenna gain due to wave – front incoherence.

(v) Scintillation and multipath effects

(vi) Attenuation by sand and dust storms.

### 2.3.1 Attenuation due to atmospheric gases

Attenuation by atmospheric gases, which is entirely caused by absorption, depends mainly on frequency, elevation angle, the altitude above sea level and water vapour density (absolute humidity). At frequencies below 10 GHz, it may normally be neglected. Above 10 GHz its importance increases with frequencies, especially at low elevation

angles. At a given frequency the oxygen contribution to atmospheric absorption is relatively constant. However, both water vapour density and its vertical profile are quite variable (ITU-R, 2003). Typically, the maximum gaseous attenuation occurs during the season of maximum rainfall.

### 2.3.2 Scintillation and multipath fading

The magnitude of tropospheric scintillation depends on the magnitude and structure of the refractive index variation. It increases with frequency and path length through the medium and decreasing as the antenna beam width decreases because of aperture averaging.

### 2.3.3 Attenuation by sand and dust storms

Very little is known about the effect of sand dust on radio signals on slant – paths. Available data (ITU-R, 2003) has indicated that at frequencies below 30GHz, high particle concentration and / or high moisture content are required to produce significant propagation effects.

## 2.4 Raindrop size distribution models

Various raindrops size distribution models are in use in various regions of the world for estimating radiowave impairment on both terrestrial and earth – space paths. Among the most widely used are the Laws and Parsons (1943), Marshall and Palmer (1948) and the Joss et al., (1968). The over – estimation of the small diameter raindrops by the Laws and Parsons and the under-estimation by the Joss model when applied to the tropical path necessitated the study of Adimula and Ajayi (1996) to obtain distinct drop size distribution models for drizzle, widespread, shower, and thunderstorm rain for the

tropical region. The present study employs the lognormal distribution of Ajayi and Olsen (1985) in the calculations. Raindrop size distribution is required for the evaluation of wave propagation effects due to rainfall. Theoretical calculations are usually based on the best available empirical data of the drop size distribution (Ajayi and Olsen, 1985). Most of the existing models are based on drops size data from the temperate regions of the world. The most widely used raindrop size distributions are therefore described as follows:

### 2.4.1 Laws and Parson's distribution model.

This is probably the best – known drop size distribution and is currently recommended by the ITU – R for the calculation of specific attenuation in the temperate region (ITU –R – 1982). This distribution was obtained experimentally using quite rudimentary technique. It was concluded that the actual drop size distribution on the ground could be obtained from the volume distribution with a fall velocity, v (a) as

$$n(a) = \frac{10^3 R\beta(m)da}{4.8\pi a^3 v(a)}(m^{-3}) \qquad (2.1)$$

Where $\beta$(m) da is the volume percentages, a is the radius in m, da represent the size interval from a – da/2 to a + da/2 and R is the rain rate in mm/h

### 2.4.2 Marshall and palmer distribution model

Distributions, which describe N (D) directly, via an analytical expression, were initially proposed by Marshall and Palmer (1948) and later by Joss et al., 1968) for different types of rainfall. Both suggested a negative exponential model for the raindrops size distribution of the form.

$$N(D) = N_0 \exp(-\Lambda D) \quad (2.2)$$

Where $N_0$ is a constant often obtained from

$$N_0 = \frac{4}{3\pi} \int N(D) D^3 V(D) dD \quad (2.3)$$

And $\Lambda$ is a constant that tends to increase with rain rate. It is expressed as

$$\Lambda = 4.1R^{0.21} mm^{-1} \quad (2.4)$$

V(D) is raindrop terminal velocity expressed by Battan (1973) for diameter range $1-4$mm as $V(D) = \sqrt{200.8a}$. It describes the variation of the raindrop sizes in terms of an analytical expression. The Marshall and Palmer distribution is particularly very close to the Laws and Parsons for $N_0 = 8000 mm^{-1} m^{-1}$.

$\Lambda$ satisfies the equation above so much that meteorologist regard it to be most applicable to widespread rain especially in the continental temperate regions (Hall and Barclay, 1989). A disadvantage of the distribution is its tendency to overestimate the number of small drops below the diameter of about 1 – 5mm because of its exponential increase when D tends to zero. Therefore the use of the distribution will yield attenuation much higher than the actual attenuation at frequencies higher than about 30 GHz especially outside the continental temperate regions (Ajewole et al., 1999).

### 2.4.3 Modified Gamma distribution model

The distribution also present N (D) directly, but in contrast to the negative exponential, it corrects the exponential increase of the raindrop number per unit volume when D tends to zero. It is expressed as

$$N(D) = N_0 D^m \exp(-\Lambda D^\beta) \quad (2.5)$$

Where $N_0$, m $\Lambda$, and $\beta$ are constant which are positive and real. The greatest difficulty in the use of this distribution is in obtaining experimentally the above four parameters. Another difficulty of using the distribution could be its tendency of cutting off both the large and small ends of the raindrop size spectrum for values of m in the range 3 – 5 (ITU- R, 1995).

### 2.4.4 Joss et al., distribution model

The use of electronic devices has been employed in the measurement of rain drop size distribution. Example is the electromechanical sensor called the distrometer that transforms the momentum of falling raindrops on a diaphragm into electrical pulses. Other types include electrostatic sensor that can measure the size dependent electric charges on the drops, and optical detector that is made up of two parallel light beams capable of measuring both size and fall velocity of raindrops as they pass through the beam. Joss et al., (1968) measure raindrop size distribution with a distrometer at Lurcarno, Switzerland and found the distribution to vary considerably for different types of rain. Their work represents the first attempt to model raindrop size distribution with respect to the variation of drop size within each storm (Ajewole, 1997).

### 2.4.5 Lognormal distribution model

Due to the inadequacies of the negative exponential model as well as the modified gamma distribution in describing the small diameter drop range, a number of investigators have studied the lognormal distribution, which is expressed in the form

$$N(D) = \frac{N_T}{\sigma D\sqrt{2\pi}} \exp[-\tfrac{1}{2}\{\frac{\ln(D)-\mu}{\sigma}\}^2] \qquad (2.6)$$

where N (D) is the numbers of drops per unit volume per diameter interval, $\mu$ is the Mean of ln (D), $\sigma^2$ is the standard deviation and $N_T$ depends on climate, geographical location of measurement and rainfall type. Ajayi and Olsen (1985) employed the lognormal distribution with a method of moment regression to produce a good theoretical fit to the measure data at Ile – Ife Nigeria. This was developed mainly for the tropical rainfall. The model is also expressed as equation (2.6) with the three parameters related to the rain rates as $N_T = a_0 R^{b_0}$

$$\mu = A_\mu + B_\mu \ln R \qquad (2.7)$$

$$\sigma^2 = A_\sigma + B_\sigma \ln R$$

Adimula and Ajayi (1996) extended the results further by making measurement for a period of three years at two more locations in Nigeria. The distributions obtained confirmed the four classifications of raindrop size. The authors combined their results to obtain the propagation parameters; $\sigma^2$, $\mu$, and $N_T$ for the four rain types, which are useful for investigating rain induced microwave signal losses in tropical environments.

### 2.4.6 General formulation of the problem

A linearly polarized wave is assumed, that is the incident waves are horizontally or vertically polarized or both for dual polarised systems. The tropical lognormal raindrop size distribution model is used to estimate the specific attenuation and specific phase shift in terms of the power law relationships between attenuation and rainfall rate. The total slant path attenuation is computed using the International Telecommunication Union

models of (ITU – R, 2001 and the ITU – R, 2003). Rain rates measured during the Joint Africa Radiometric measurement program (1987 – 1988) at three locations in Africa; namely (Ile-Ife) Nigeria, (Douala) Cameroon, and (Nairobi) Kenya are used. The calculations of the propagation parameters are based on the Mean Annual (MA) and Mean Worst Months (MWM) rainfall rates data.

An oblate spheroidal raindrop shape is assumed, while the frequency band 1 - 52GHz and elevation angles of $23^0$ and $55^0$ which are the two principal look angles in Nigeria are used. Differential propagation parameters are computed and the results are used to compute the cross – polarization discrimination (XPD) and the copolar attenuation (CPA) at two rain rates and for the two elevation angles, for 0.01% of time unavailability. Scaling formula is then used to predict the total slant path attenuation for other time unavailability percentages such as 0.001% and 0.1%.

### 2.4 .7 Rain Induced Attenuation and Phase Shift

The rain induced specific attenuation (dB/km) of a wave propagating through an ensemble of raindrops is defined as the rate of attenuation per unit distance (Oguchi, 1973). It is expressed in terms of the total scattering cross section $Q_t$ of raindrops as

$$A = 4.343\times10^{3}\int_{0}^{\infty} Q_t(D)N(D)dD(dB/km)$$

or in terms of the scattering amplitude function as

$$A = 4.343\times10^{3}\frac{\lambda^2}{\pi}\sum_{n=1}^{n}\mathrm{Re}[S_{n,n}(0^0)]N(D)\Delta D \qquad (2.8)$$

$Q_t$ is the total cross section and N (D) dD is the raindrop size density. N (D) can be obtained from equation (2.6) and Re [$S_{H,V}$ ($0^0$)] is the real part of the forward scattering amplitude function. H, V stands for horizontal and vertical polarization, respectively and $\lambda$ is the wavelength in meters.

The specific phase shift can be evaluated using the expression (Chu, 1974)

$$\phi = 9.0 \times 10^4 \frac{\lambda^2}{\pi^2} \int_0^\infty \mathrm{Im}\, S_{H,V}(0^0) N(D) dD (\mathrm{deg}/km) \qquad (2.9)$$

Im S ($0^0$) is the imaginary part of the forward scattering amplitude function.

$$S(0^0) = \frac{1}{2} \sum_{n=1}^{\infty} (2n+1)(a_n + b_n) \qquad (2.10)$$

where $a_n$ and $b_n$ are the Mie coefficient of the scattered fields which depends on frequency, complex refractive index of water e.t.c.

### 2.4.8 Empirical scaling formulation

The use of an empirical scaling relationship can be employed to estimate specific attenuation and phase shift for practical applications. The relationship between specific attenuation, A (dB/km) and rain rate R (mm/h) can be approximated by a power law (Olsen et al., 1978)

$$A = aR^b \qquad (2.11)$$

A similar law has been found to be applicable to specific phase shift, $\phi$ (deg/km)(Maggoori, 1981)

$$\phi = hR^s \qquad (2.12)$$

The constant a, b, h, k are polarization, frequency and temperature dependent and R is rain rate. These parameters were taken from tropical drop size distribution given by (Ajayi and Olsen, 1985).

**Table 2.0 Tropical drop size distribution values for the expression $A = aR^b$ and $\phi = hR^k$ at a Temperature of 20$^0$C**

| FREQ | HOR.POL a | HOR.POL b | VER.POL a | VER.POL b | FREQ | HOR. POL h | HOR. POL k | VER. POL h | VER. POL k |
|---|---|---|---|---|---|---|---|---|---|
| 1 | 3.52E-05 | 0.9273 | 3.11E-05 | 0.894 | 1 | 0.1027 | 0.9107 | 0.967 | 0.891 |
| 2 | 0.000142 | 0.9627 | 0.000124 | 0.9323 | 2 | 0.205 | 0.9131 | 0.1936 | 0.893 |
| 4 | 0.000651 | 1.072 | 0.000573 | 1.043 | 4 | 0.4052 | 0.9243 | 0.3981 | 0.9 |
| 6 | 0.001848 | 1.214 | 0.001634 | 1.177 | 6 | 0.6018 | 0.94 | 0.5882 | 0.911 |
| 8 | 0.004724 | 1.273 | 0.004102 | 1.253 | 8 | 0.8555 | 0.932 | 0.801 | 0.914 |
| 10 | 0.01063 | 1.252 | 0.009238 | 1.242 | 10 | 1.199 | 0.8995 | 1.035 | 0.902 |
| 12 | 0.02015 | 1.204 | 0.01774 | 1.195 | 12 | 1.557 | 0.8687 | 1.28 | 0.883 |
| 15 | 0.04007 | 1.139 | 0.03599 | 1.126 | 15 | 2.002 | 0.8429 | 1.633 | 0.857 |
| 20 | 0.08195 | 1.083 | 0.07477 | 1.057 | 20 | 2.66 | 0.8159 | 2.152 | 0.832 |
| 25 | 0.1333 | 1.055 | 0.1206 | 1.026 | 25 | 3.618 | 0.7613 | 2.649 | 0.807 |
| 30 | 0.1977 | 1.024 | 0.1761 | 1.001 | 30 | 4.966 | 0.6815 | 3.154 | 0.772 |
| 35 | 0.2764 | 0.986 | 0.2438 | 0.9697 | 35 | 6.552 | 0.5924 | 3.648 | 0.727 |
| 40 | 0.3672 | 0.9437 | 0.3096 | 0.9335 | 40 | 8.053 | 0.5078 | 4.084 | 0.678 |
| 45 | 0.4648 | 0.9022 | 0.4097 | 0.8963 | 45 | 9.11 | 0.4362 | 4.408 | 0.631 |
| 50 | 0.5618 | 0.8649 | 0.4964 | 0.8617 | 50 | 9.463 | 0.3822 | 4.584 | 0.59 |
| 55 | 0.6507 | 0.8338 | 0.5823 | 0.8321 | 55 | 9.112 | 0.3452 | 4.609 | 0.556 |

### 2.4.9 The Propagation Constant of Transmission

The propagation constant associated with wave transmission through rain is defined as the rate of wave attenuation per unit distant and the rate of phase dispersion per unit distance. It means that the propagation constant will provide information for the specific attenuation and phase shift of a radio signal. It is generally expressed as

$$\gamma = aR^b + hR^k \tag{2.13}$$

### 2.5.0 The Total Slant Path Attenuation

The following ITU –R procedure provide estimates of the Long – term statistics of the slant – path rain attenuation at a given location for frequencies up to 55GHz. The following parameters are required.

$R_{0.01}$: Point rainfall for the location for 0.01% of an average year (mm/h)

hs: Height above sea level of the earth station (km)

$\theta$: Elevation angle (degree)

$\varphi$: Latitude of the earth station (degree)

f: frequency (GHz)

$R_e$: Effective radius of the earth (8,500km)

The Geometry is illustrated in fig 2.1

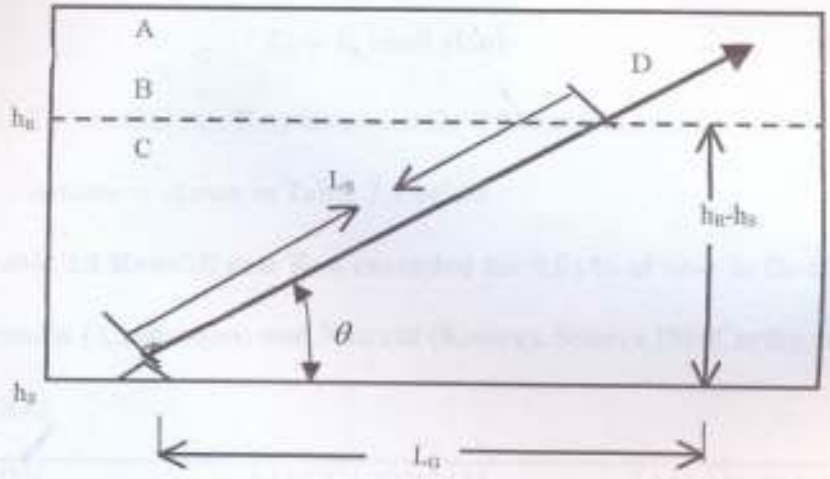


A: Frozen Precipitation

B: Rain Height

C: Liquid Precipitation

D: Earth - Space

Fig 2.1: Schematic representation of an Earth-space path.

### 2.5.1 Calculation of Long – term Attenuation Statistics from point rainfall rate

1. $h_R = 4.5$km for the tropical regions (ITU –R, 2001)
2. Since two elevation angles are consider $23^0$ and $55^0$ ,hence elevation angle $\theta \geq 5^0$ hence the slant – path length $L_s$ below the rain height is given by

$$L_s = \frac{h_R - h_s}{\sin\theta}(km) \qquad (2.14)$$

3. The Horizontal projection, $L_G$ of the slant – path length is given by

$$L_G = L_s \cos\theta \text{ (km)} \qquad (2.15)$$

4. The rainfall rate $R_{0.01}$ exceeded for 0.01% of an average year for the three stations is shown in Table 2.1 below.

**Table 2.1 Rainfall rate $R_{0.01}$ exceeded for 0.01% of time in Ile-Ife(Nigeria), Douala ( Cameroon) and Nairobi (Kenya). Source (McCarthy et al., 1994 a,b,c)**

| LOCATION | MEAN ANNUAL RAINFALL RATE FOR 0.01% TIME | MEAN WORST MONTH RAINFALL RATE FOR 0.01% TIME |
|---|---|---|
| ILE – IFE (NIGERIA) | 108mm/h | 130mm/h |
| DOUALA (CAMEROON) | 126mm/h | 160mm/h |
| NAIROBI (KENYA) | 65mm/h | 100mm/h |

Tables 2.2 shows the geometrical and electrical parameters used in the study.

**Table 2.2: Some geometrical and electrical parameters relevant to the study**

| ELEVATION ANGLE OF $55^0$ | | | | | | | | | |
|---|---|---|---|---|---|---|---|---|---|
| LOCATION | HEIGHT ABOVE SEA LEVEL | POLARISATION TILT | LONGITUDE | LATITUDE | $h_s$/km | $h_R$/km | $h_S$-$h_R$/ km | $L_S$ /km | $L_G$ km |
| ILE-IFE (NIGERIA) | 274m | Horizontal Polarization | $4.34^0$E | $7.33^0$N | 0.274km | 4.5km | 4.226km | 5.159km | 2.959km |
| DOUALA (CAMEROON) | 15m | Horizontal Polarization | $9.7^0$E | $4.05^0$N | 0.015km | 4.5km | 4.485km | 5.475km | 3.140km |
| NAIROBI (KENYA) | 1800m | Horizontal Polarization | $36.75^0$E | $1.30^0$N | 1.8km | 4.5km | 2.700km | 3.296km | 1.189km |
| **ELEVATION ANGLE OF $23^0$** | | | | | | | | | |
| LOCATION | HEIGHT ABOVE SEA LEVEL | POLARISATION TILT | LONGITUDE | LATITUDE | $h_s$ /km | $h_R$/km | $h_S$-$h_R$ /km | $L_S$ /km | $L_G$ /km |
| ILE-IFE (NIGERIA) | 274m | Horizontal Polarization | $4.34^0$E | $7.33^0$N | 0.274km | 4.5km | 4.226km | 10.82km | 9.956km |
| DOUALA (CAMEROON) | 15m | Horizontal Polarization | $9.7^0$E | $4.05^0$N | 0.015km | 4.5km | 4.485km | 11.47km | 10.566km |
| NAIROBI (KENYA) | 1800m | Horizontal Polarization | $36.75^0$E | $1.30^0$N | 1.8km | 4.5km | 2.700km | 6.910km | 6.361km |

$h_S$ = height of station above sea level

$h_R$ = Rain height

$L_S$ = Slant – path length;

$L_G$ = Horizontal projection of slant path length.

5. The next step is to obtain the specific attenuation $\gamma_{R_{0.01}}$ for 0.01% of time using the expression

$$\gamma_{R_{0.01}} = k(R_{0.01})^{\alpha} \qquad (2.16)$$

Where k and α are constants in Table 2 and R is the rain rates given in Table 2.1

6. The next step is to calculate the horizontal reduction factor $r_{0.01}$ using

$$r_{0.01} = \frac{1}{1 + 0.78\sqrt{\frac{L_G \gamma}{f}} - 0.38(1 - e^{-2L_G})} \qquad (2.17)$$

The vertical adjustment factor, $v_{0.01}$ is then calculated using the relation

$$\xi = \tan^{-1}\left(\frac{h_R - h_s}{L_G r_{0.01}}\right)$$

where $\xi$ is the true angle between slant-path length and the horizontal projection.

For $\xi > \theta$,

$$L_R = \frac{L_G r_{0.01}}{\cos\theta} km$$

Else,

$$L_R = \left(\frac{h_R - h_s}{\sin\theta}\right) km$$

If $|\varphi| < 36, \chi = 36 - |\varphi| \deg ree$

Where $\chi$ is latitude adjustment factor

Else, $\chi = 0 \deg ree$

$$v_{0.01} = \frac{1}{1+\sqrt{\sin\theta}\left(31\left(1-e^{-\left(\frac{\theta}{1+\chi}\right)}\right)\frac{\sqrt{L_R\gamma_R}}{f^2}-0.45\right)} \quad (2.18)$$

8.The effective path length to the rain region is then calculated using

$$L_E = L_R v_{0.01} km \quad (2.19)$$

9. The predicted attenuation exceeded for 0.01% of an average year is then obtained from

$$A_{0.01} = \gamma_R L_E dB \quad (2.20)$$

10. The attenuation to be exceeded for other percentages of an average year p, in the range 0.001% - 5% is determined from the attenuation to be exceeded for 0.01% of an average year.

If $P \geq 1\%$ or $|\varphi| \geq 36, \beta = 0$

If $P < 1\%$ and $|\varphi| < 36^{\circ}$ and $\theta \geq 25^{\circ}$

$$\beta = -0.005(|\varphi| - 36)$$

Otherwise,

$$\beta = -0.005(|\varphi| - 36) + 1.8 - 4.25\sin\theta$$

$$A_P = A_{0.01}\left(\frac{P}{0.01}\right)^{-(0.655+0.033\ln(P)-0.045\ln(A_{0.01})-\beta(1-P)\sin\theta)} \text{ dB} \quad (2.21)$$

## 2.5.2 Depolarization Effect

### Basic hydrometeor depolarization consideration

Depolarization occurs due to the anisotropy of the propagation medium. The shapes of the raindrops distort owing to hydrodynamic forces. The drops as well as becoming non – symmetrical in shape, also tends to be tilted away from the local horizontal and vertical axes of symmetry owing to wind gusting. This tilt of the incident electric field vector away from the axes of symmetry of the raindrop will cause signal depolarization. The depolarization will be caused by "differential attenuation" and "differential phase effect" between the two axes of symmetry of the raindrop. The amount of differential attenuation and differential phase experienced by a signal passing through an ensemble of raindrops will depend upon a number of factors, including frequency and rainfall rate. The maximum effect will be observed when the raindrops present the largest cross – sectional area towards the signal that is the major axis of the ellipsoidal raindrop.

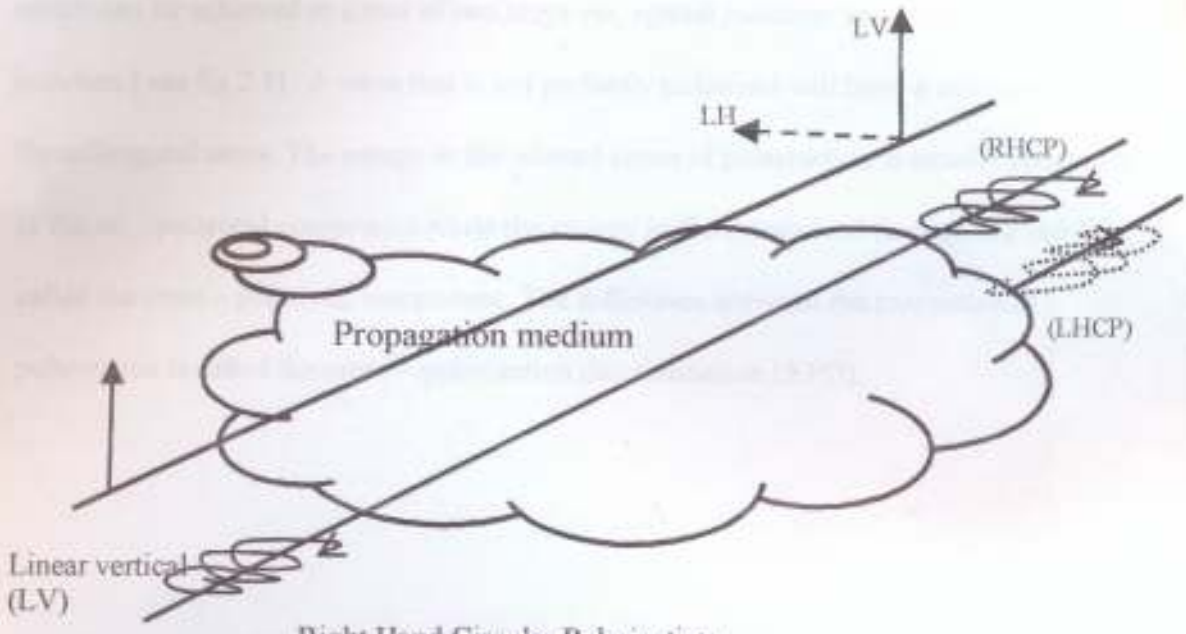


Fig 2.2 Schematic representation of the Depolarization of radio wave signal by a propagation medium.

The pressure to conserve the bandwidth has led to the "concept of frequency re – use", which can be achieved in either of two ways viz; spatial isolation and Polarization isolation ( see fig 2.3) . A wave that is not perfectly polarized will have a component in the orthogonal sense. The energy in the wanted sense of polarization is usually referred to as the co – polarized component while the energy in the orthogonal (unwanted) sense is called the cross – polarized component. The difference between the two sense of polarization is called the cross – polarization discrimination (XPD).

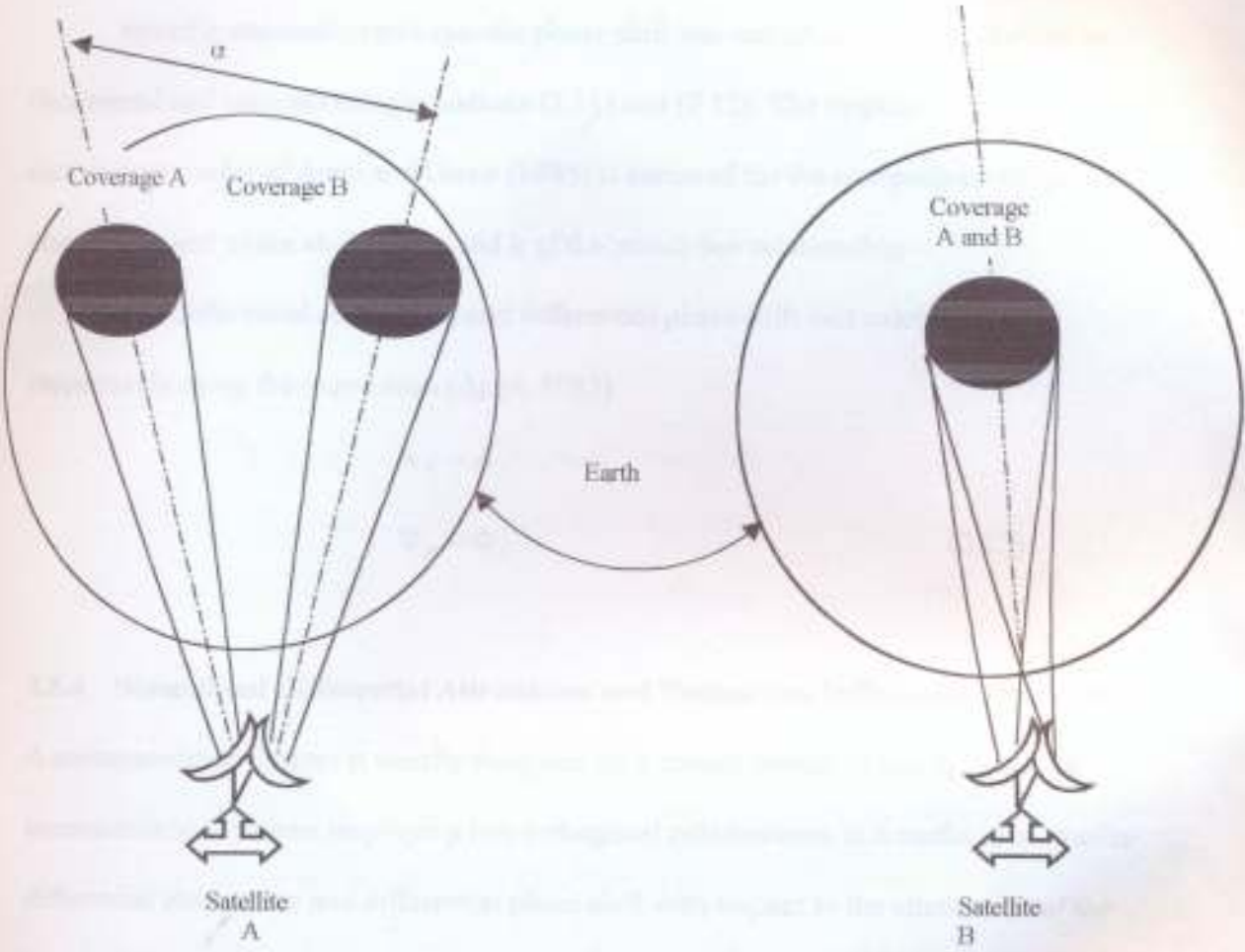


Fig 2.3 Illustration of two techniques of frequency re-use.

A Spatial isolation
B Polarization isolation

In both cases, identical frequency bands are used. In (A), the angle α between the two beams provide the spatial isolation, while in (b), the use of orthogonal polarization provides the isolation.

### 2.5.3 Differential Attenuation and Differential Phase shift

Specific attenuation and specific phase shift was calculated for two polarization (horizontal and vertical) using equations (2.11) and (2.12). The tropical drop size distribution model of Ajayi and Olsen (1985) is assumed for the computation of specific attenuation and phase shift a, b, h, and k of the power law relationship.

The differential attenuation and differential phase shift was calculated respectively using the expression (Ajayi, 1985)

$$A_H - A_V$$

$$\Phi_H - \Phi_V \qquad (2.22)$$

### 2.5.4 Normalized Differential Attenuation and Normalized Differential Phase Shift

A communication system is usually designed for a certain margin of fading, hence in communication systems employing two orthogonal polarizations, it is useful to normalize differential attenuation and differential phase shift with respect to the attenuation of the vertical polarization.

The normalized differential attenuation is defined as

$$\Delta A = \frac{A_H - A_V}{A_V} \qquad (2.23)$$

The normalized differential phase shift is defined as

$$\Delta\Phi = \frac{\Phi_H - \Phi_V}{A_V} \qquad (2.24)$$

### 2.5.5 Canting Angle Distribution models

#### Canting angles of raindrops

The axes of non- spherical raindrops in the atmosphere will not necessarily be aligned in the vertical direction, but will cant from the vertical direction due to various aerodynamic forces acting on the raindrops. The angle of raindrops axes measured from the vertical will differ from drop to drop thus forming an angular distribution with a mean angle near the vertical.

#### Existing measurement on drop canting

Measurement of raindrops canting angle has been carried out by a number of researchers such as Saunders (1971); Maher et al., (1977); Ugai and Akimoto (1983) ; and Brussard (1976)

Saunders in 1964 analyzed the photographs of 463 raindrops taken with a raindrop camera during two rainstorms. He measured the angle between the major axis of a raindrop image and the horizontal axis. The measured angle is based on two – dimensional image of the raindrops in a plane perpendicular to the optical axis of the camera. Only the component of the angles in a plane perpendicular to the propagation direction is however important in the propagation phenomena.

Ugai and Akimoto proposed a canting angle model as shown in fig 2.4. The canting angle $\theta$ of the model is made up of two angle components $\Psi$ and $\Theta$, where $\Psi$ is the angle between the vertical axis and the trace of fall, and $\Theta$ is the angle between the trace of fall and drop axis. The angle $\Theta$ may be regarded as the angle of drop oscillation. All these angles are based on two – dimensional drop images perpendicular to the optical axis. The result of measurement in two-rain events show that the cumulative

distributions of these angles are roughly regarded as normal distribution. The mean angle of the distribution for $\theta$ and $\Psi$ depend on wind direction, while the mean angle of oscillation $\Theta$ was close to zero during one rain event.

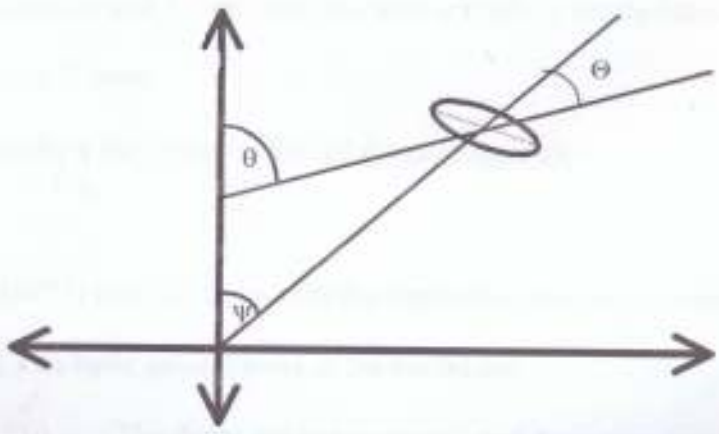


2.4 A model of drops canting angles.

A physical model of raindrop canting angle by Brussard (1976) shows that the symmetry axis of the drops is always parallel to the direction of the air flow around the drop. The direction of air flow is determined by:

(i) The vertical component due to the fall of raindrops

(ii) The horizontal component due to vertical gradient of the horizontal wind speed. He calculated the canting angle of various sizes of raindrops. It was shown that the larger the distance from the ground the smaller is the canting angle. The canting angle increases with increasing raindrop size. However the rate of increase reduced when the drop radius exceeded 1.0mm and the canting angle is nearly constant for drops with radii greater than 2.0mm.

This model predicts the "mean value" of the canting angle for each drop size.

Maher et al., (1977) tries to account for the angle distribution by considering the effect of wind gusting. The basic assumptions in the model are:

(i) The drops are axisymmetric and their axes are always in the direction of airflow.

(ii) That the horizontal wind velocity around the raindrop is made up of a steady component which play a sinusoidal oscillating component with small amplitude. Due to its mass, the raindrop cannot follow the oscillation and hence is subjected to a differential horizontal airflow of either positive or negative direction with time. They considered that the difference force corresponding to such horizontal airflow is responsible for the angle distribution around the mean canting angle, while the mean canting angle itself is the one defined by Brussard.

### 2.5.6 Canting angle distribution used in this work

Some studies of cross polarization discrimination (XPD) such as Ajayi et al., (1987); Ajayi (1990) and Ajose et al., (1995) assume equi – orientation of the raindrops along the paths. In this work a more realistic distribution of canting angle along the path is assumed. In order to estimate the XPD on a tropical slant propagation path this work assumed an effective canting angle of $10^0$ with a standard deviation of $\sigma = 10^0$ for 0.01% of time as recommended by the ITU – R, 2003

### 2.5.7 Cross polarization

Cross polarization is defined as the appearance in the course of propagation of a polarization component, which is orthogonal to the expected polarization.
Cross-polarization discrimination (XPD) is defined for a wave transmitted with a given polarization as the ratio at the reception point of the power received with the expected polarization to the power received with the orthogonal polarization.

$$XPD = \frac{E_{cross}}{E_{co}} = 20\log_{10}\left|\frac{E_{cross}}{E_{co}}\right| dB \qquad (2.25)$$

In order to distinguish increasing value of XPD from decreasing value equation (2.25) is usually written as

$$XPD = 20\log_{10}\left|\frac{E_{co}}{E_{cross}}\right| dB \qquad (2.26)$$

Cross polarization isolation (XPI) is defined for two radio waves transmitted with same power and orthogonal polarization as the ratio of the co-polarized power in a given receiver to the cross polarized power in that receiver

Fig 1.1 illustrate the difference between XPD and XPI

$$XPD = 20\log_{10}\frac{ac}{ax}dB$$

$$XPI = 20\log_{10}\frac{ac}{bx}dB \qquad (2.26)$$

For a rain medium, XPD and XPI are equivalent. Measurements have confirmed this (Cox and Arnold, 1984). A dual – polarized receiver that is designed to receive orthogonal channels simultaneously will detect both the wanted (or co – polarized) signals ac and bc and the unwanted (or cross – polarized) signals bx and ax. In general, experiment use only mono – polarized transmission and so what is measured is the discrimination ratio ac/ax or bc/bx. In propagation experiments, attenuation and cross - polarization are often measured simultaneously for correlation with each other. If the differential attenuation and differential phase induced by the propagation medium can be measured, the XPD can be obtained immediately from

$$XPD = 20\log_{10}\left|\frac{e^{-(\alpha+j\beta)}+1}{e^{-(\alpha+j\beta)}-1}\right|dB \qquad (2.27)$$

where $\alpha$ = differential attenuation, in nepers.

where $\beta$ = differential phase, in radians.

## 2.5.8 CROSS POLARIZATION DISCRIMINATION USED IN THIS WORK

Based on small argument approximations, Olsen (1981) proposed a semi-empirical

amodel

for calculating XPD and CPA. The expressions were derived from the earlier work of Oguchi (1977). Thus XPD is expressed approximately as

$$XPD \equiv -20\log(l\cos^2 \in |\Delta k| e^{-2\sigma^2} \sin\frac{|\phi - \tau|}{2} \qquad (2.28)$$

and $$CPA \equiv \left[A_H + A_V + (A_H - A_V)\cos^2 \in e^{-2\sigma^2} \cos 2(\phi - \tau)\right]\frac{l}{2} \qquad (2.29)$$

where $A_H$ and $A_V$ are the specific attenuation associated with the principal planes of the raindrops axis i.e major and minor axes of the raindrop.

$$|\Delta k| = |k_H - k_V| = (\Delta\alpha^2 + \Delta\beta^2)^{\frac{1}{2}} \qquad (2.30)$$

where $\Delta\alpha$ and $\Delta\beta$ are the differential attenuation, and differential phase shift, respectively. $\phi$ defines the effective canting angle and $\tau$ is the polarization tilt angle ( $\tau = 0$ for horizontal polarization and $\frac{\pi}{2}$ for vertical polarization) $\sigma$ is the effective standard deviation of the canting angle distribution, $\in$ represents the path elevation angle (for this work $23^0$ and $55^0$ ) and $l$ is the path length through uniform rain. The specific attenuation has been calculated using the power law relationship between attenuation and rain rate proposed by Olsen et al.,(1985). This is expressed as $A = aR^b$, R is rainfall rate and the parameters a and b are taken from the work of Ajayi (1985). A similar power law relationship has been used to calculate the specific phase shift. The phase shift is expressed as

$\phi = hR^k$.

# CHAPTER THREE

# RESULTS AND DISCUSSION

## 3.1 SPECIFIC ATTENUATION

The specific attenuation due to rain has been calculated at some frequencies for rain rates exceeded for 0.01% of time at three stations, Nigeria, Cameroon and Kenya .The mean annual (MA) and mean worst month (MWM) rainfall rates used are shown in Table 2.1. Oblate spheroidal raindrops are assumed. The frequency characteristics of the specific attenuation at the two-rain rate for the three locations are presented in fig 3.1 – 3.2. Generally the specific attenuation increases with increasing frequency with highest attenuation in Douala for both MA and MWM.The reason is due to the higher rainfall rate in Douala as shown in Table 2.1 compared to the other two stations.

### 3.2.0 Specific Phase shift

The specific phase shift has been calculated for the three stations in the frequency range 1-52GHz band for the two rain rates shown in Table 2.1, and the slant path lengths shown in Table 2.2 The frequency characteristic of the specific phase shift at the two rain rate for the three locations are presented in fig 3.3 –3.5. The specific phase shift increases with frequency up to a maximum and then decreases after the peak frequency. The peak frequency for the three stations is 25GHz. The reason is due to the high rainfall rate in the three stations as shown in Table 2.1,the rainfall rates are greater than 50 mm/h, hence the more intense the rainfall the smaller the peak frequency.

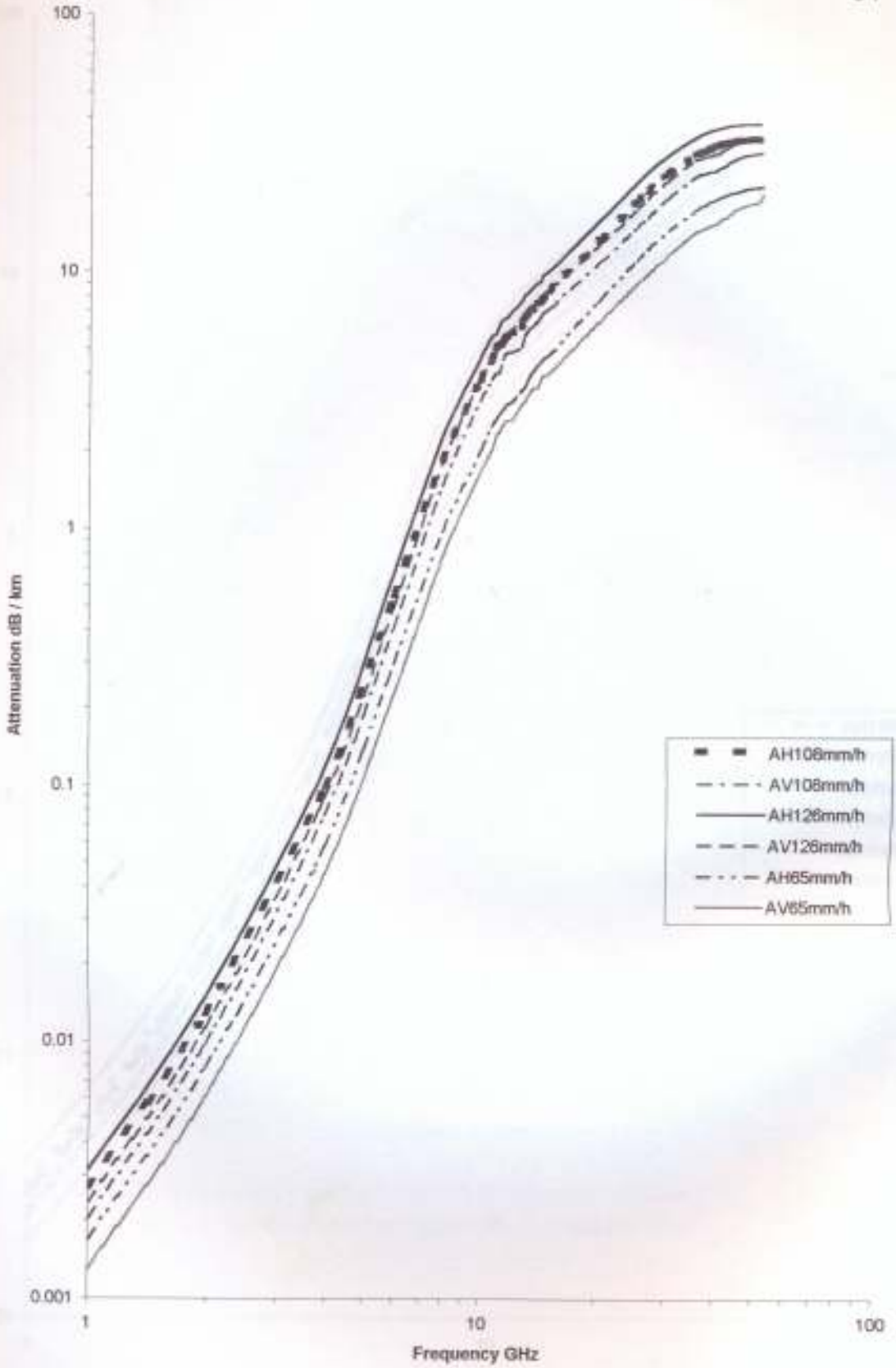


**Fig 3.1 Frequency charateristics of specific attenuation for Ile-Ife, Douala,and Nairobi for mean annual rainfall rates 108,126,65mm/h respectively**

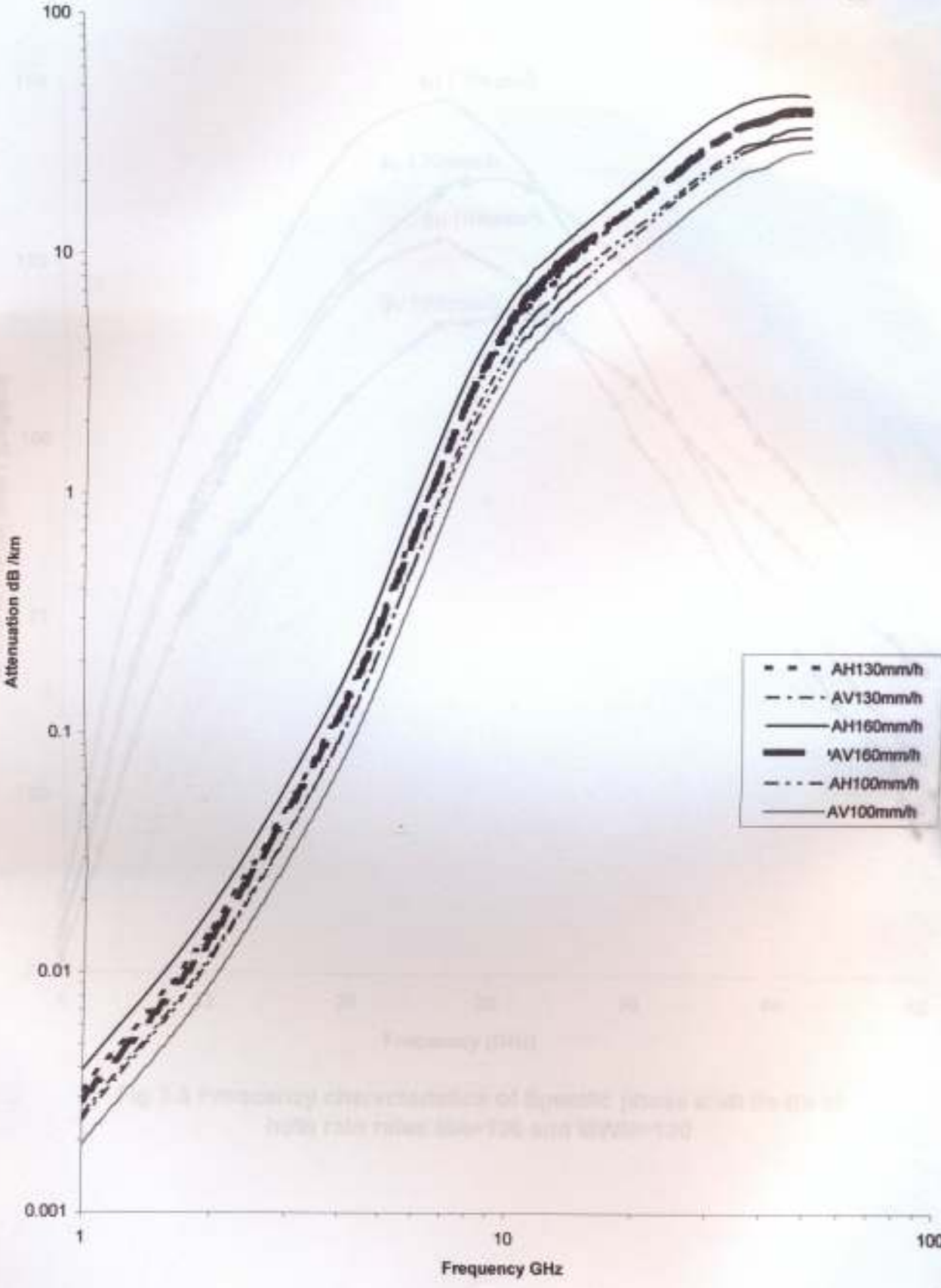


**Fig 3.2 Frequency charateristics of specific attenuation for Ile-Ife, Douala,and Nairobi for mean worst month rainfall rates 130,160,100mm/h respectively**

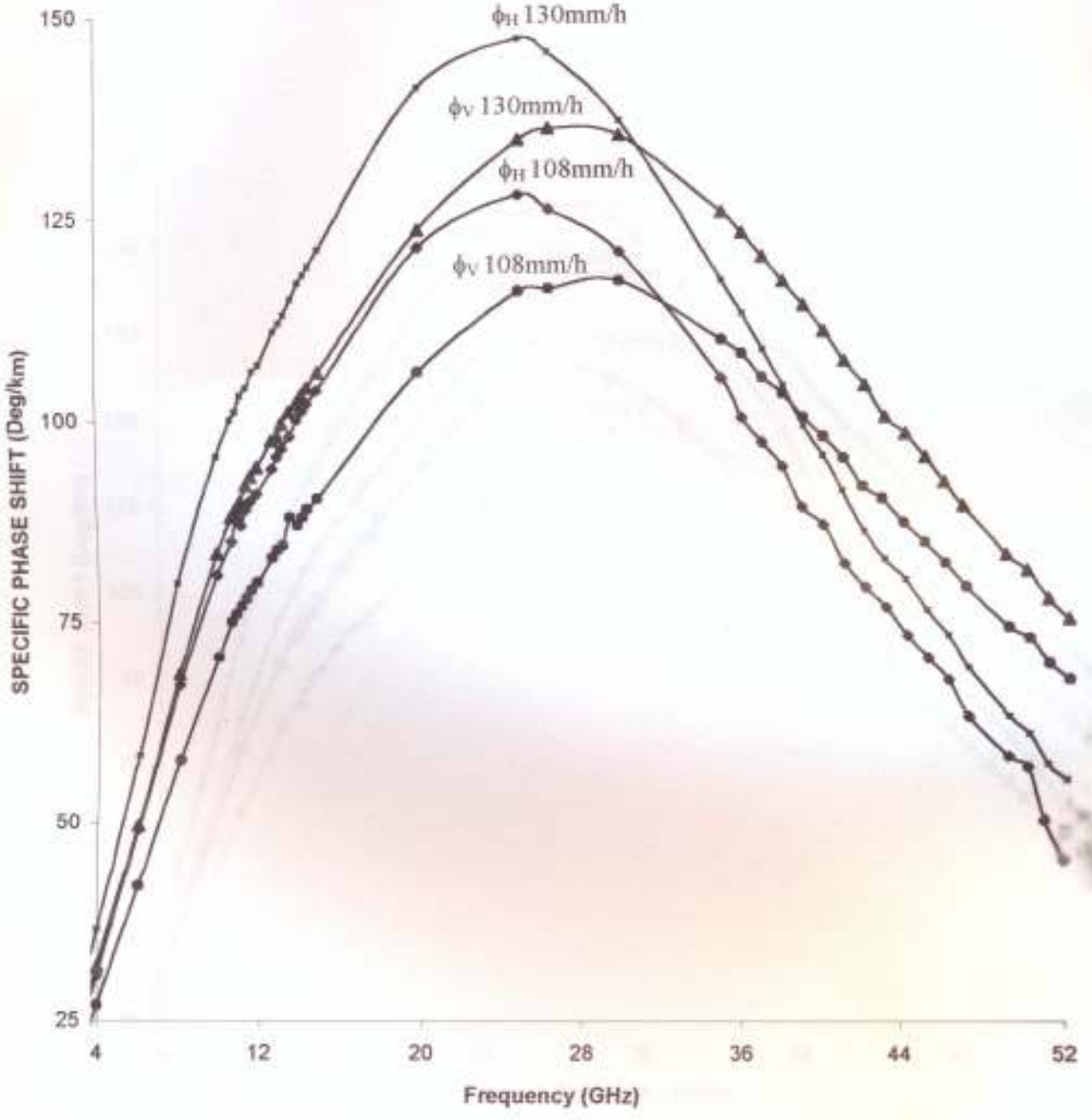


**Fig 3.3 Frequency characteristics of Specific phase shift Ile-Ife at both rain rates MA=108 and MWM=130**

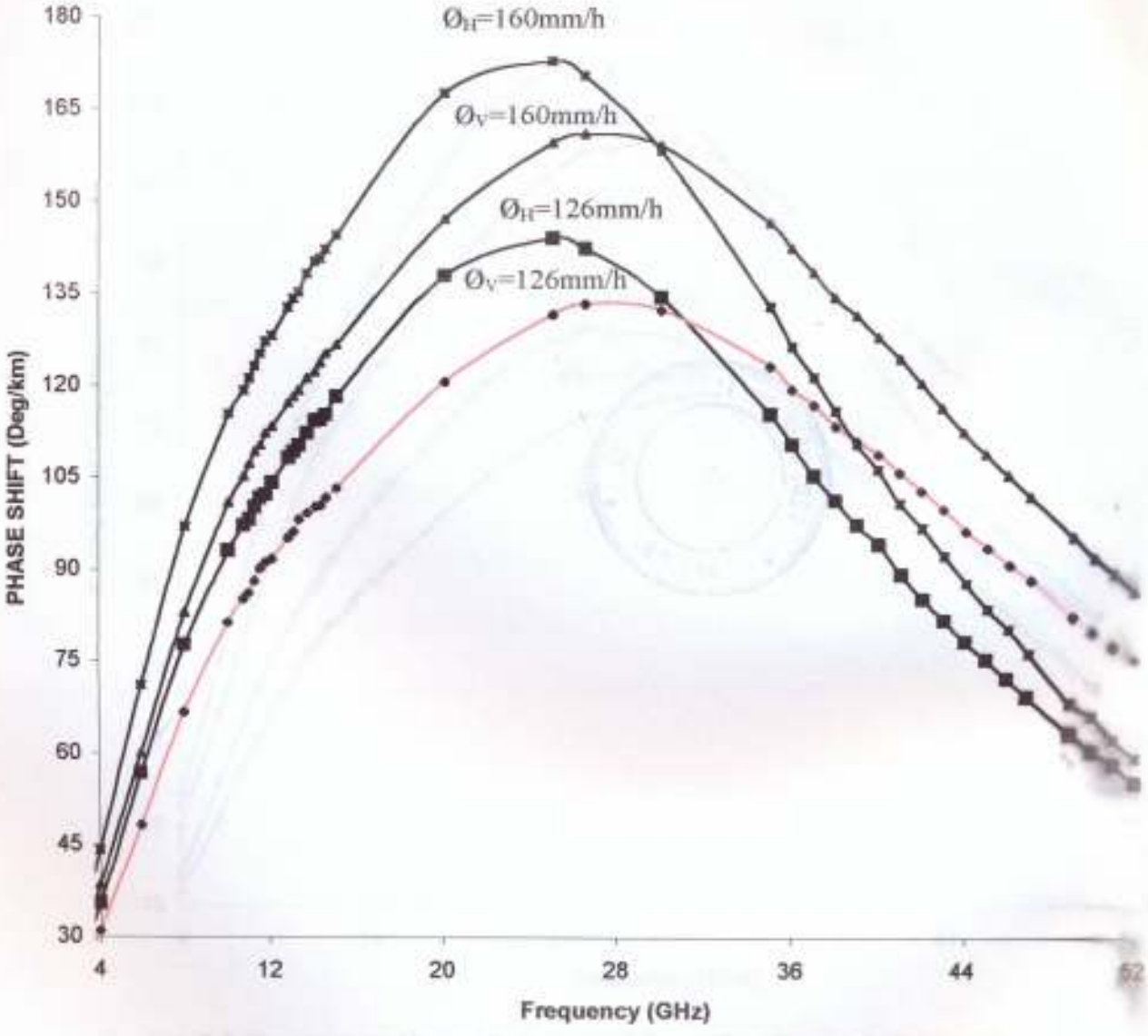


**Fig 3.4 Frequency characteristics of Specific phase shift Douala at both rain rates MA=160 and MWM=126**

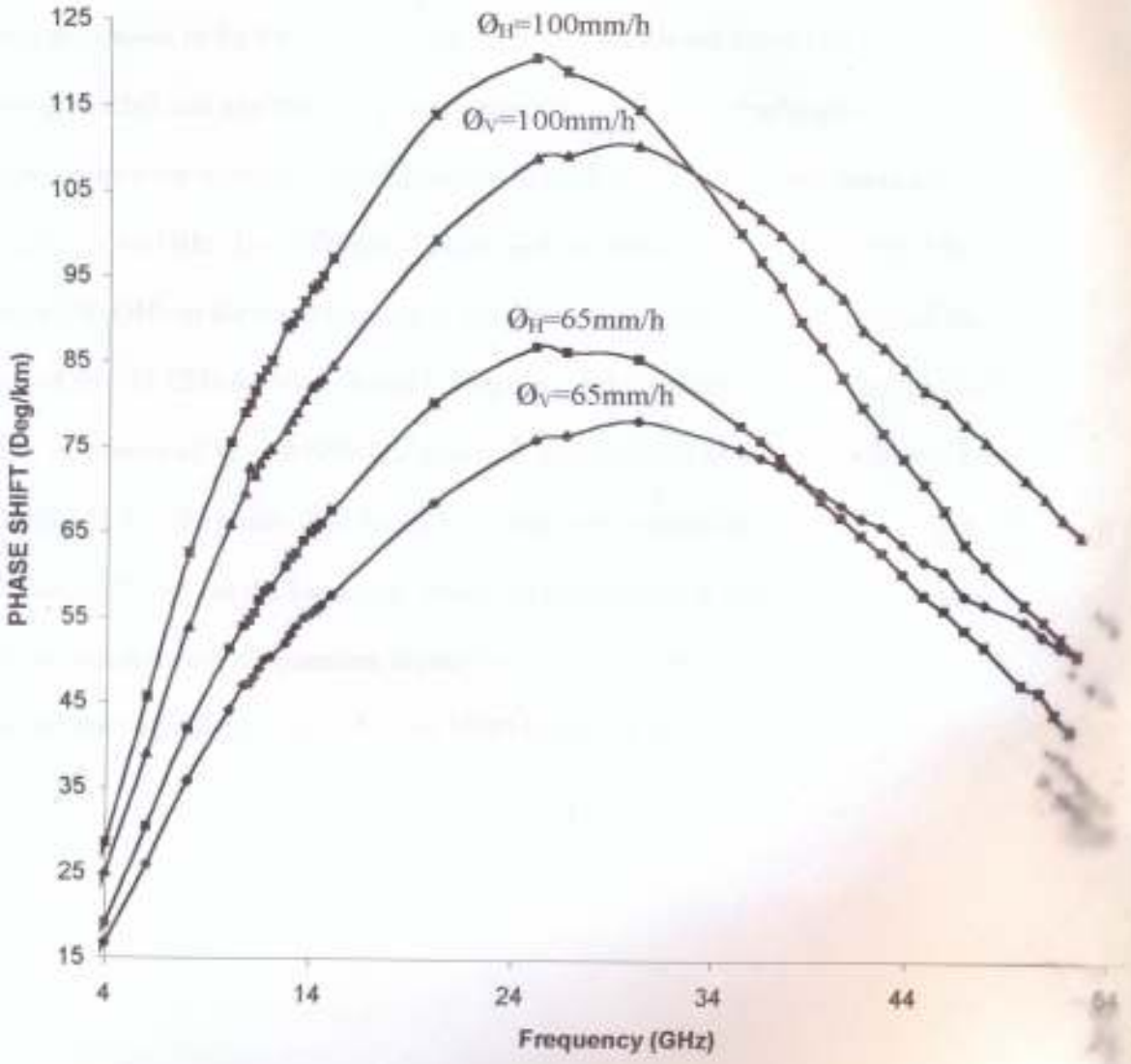


**Fig 3.5 Frequency characteristics of Specific phase shift Nairobi at both rain rates MA=65 and MWM=100**

### 3.2.1 Differential attenuation and differential phase shift

The results of the frequency characteristics of the differential attenuation and differential phase shift are shown in fig 3.6 – 3.11. In the diagrams, results are presented using the mean annual rainfall rate and the mean worst month rain rate. The results show that the differential attenuation increases with frequency in the three locations and peaks around the frequency of 40 GHz. The differential phase shift on the other hand peak (Fig 3.9-3.11) around 20 GHz in the three stations. It crosses over to negative values around the frequency of 30 - 31 GHz for Nigeria and Cameroon while in Kenya it becomes negative around the frequency of 32 - 38 GHz for both rain rates MA and MWM respectively. The reason for this is that the phase shift decreases rapidly after attaining a peak around the frequency of 24-25 GHz at the locations. Therefore the difference between the two low values become negative at frequencies higher than about 24GHz. Results are also presented for the two rainfall rates, MA and MWM respectively.

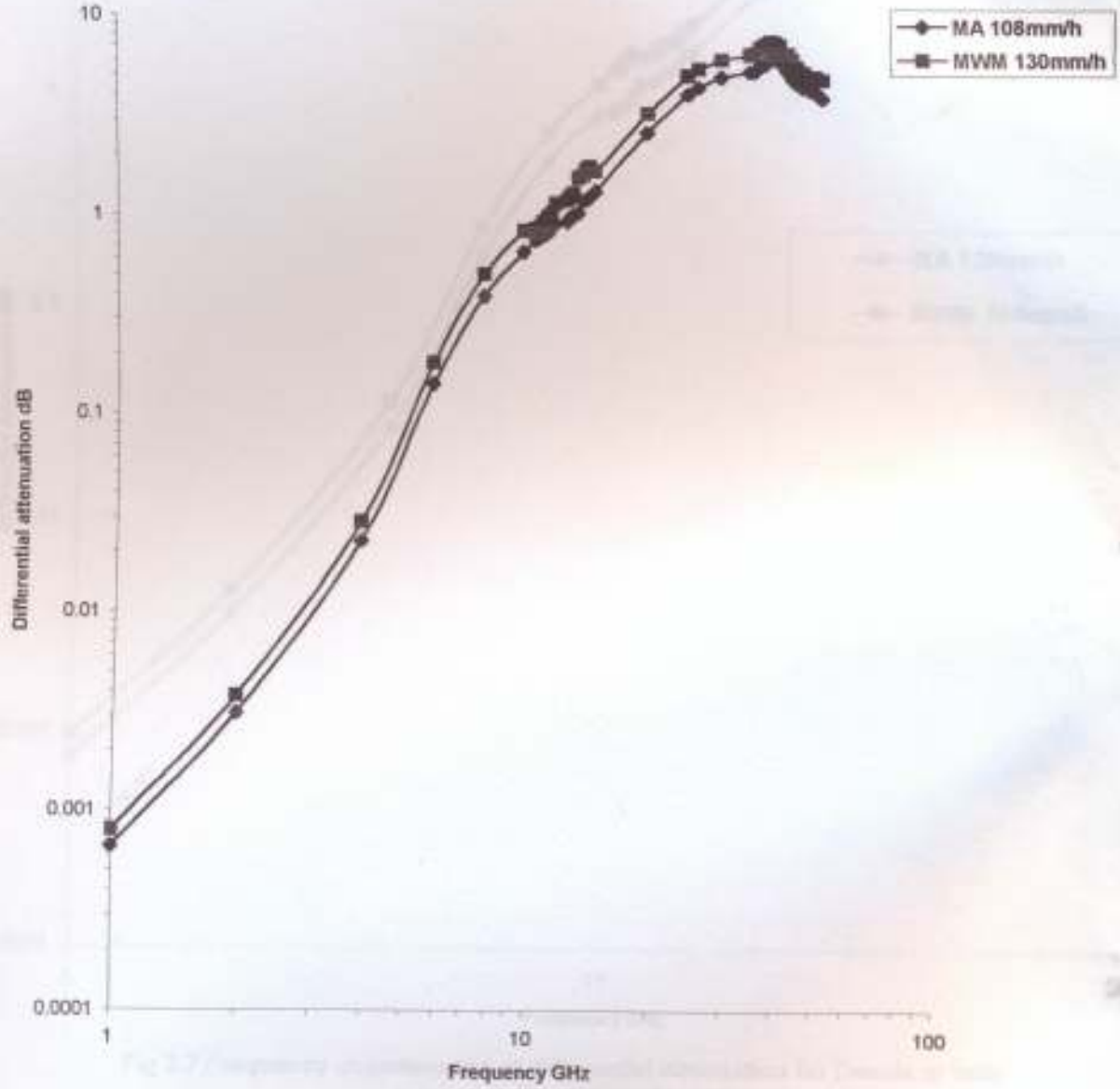


Fig 3.6 Frequency charateristics of differential attenuation for Ile-Ife at both rain rates MA=108 MWM=130

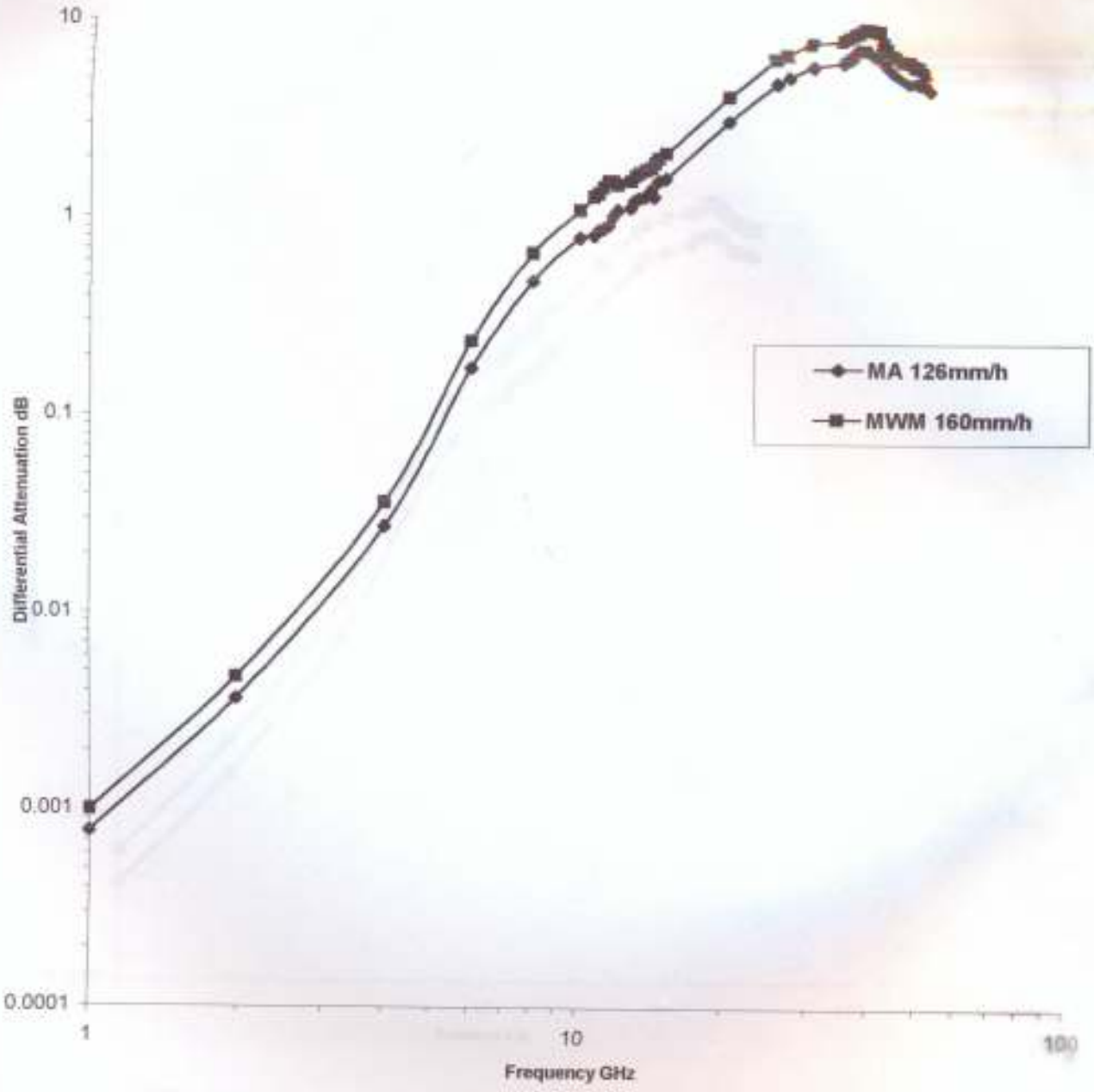


Fig 3.7 Frequency charateristics of differential attenuation for Douala at both rain rates MA=126 MWM=160

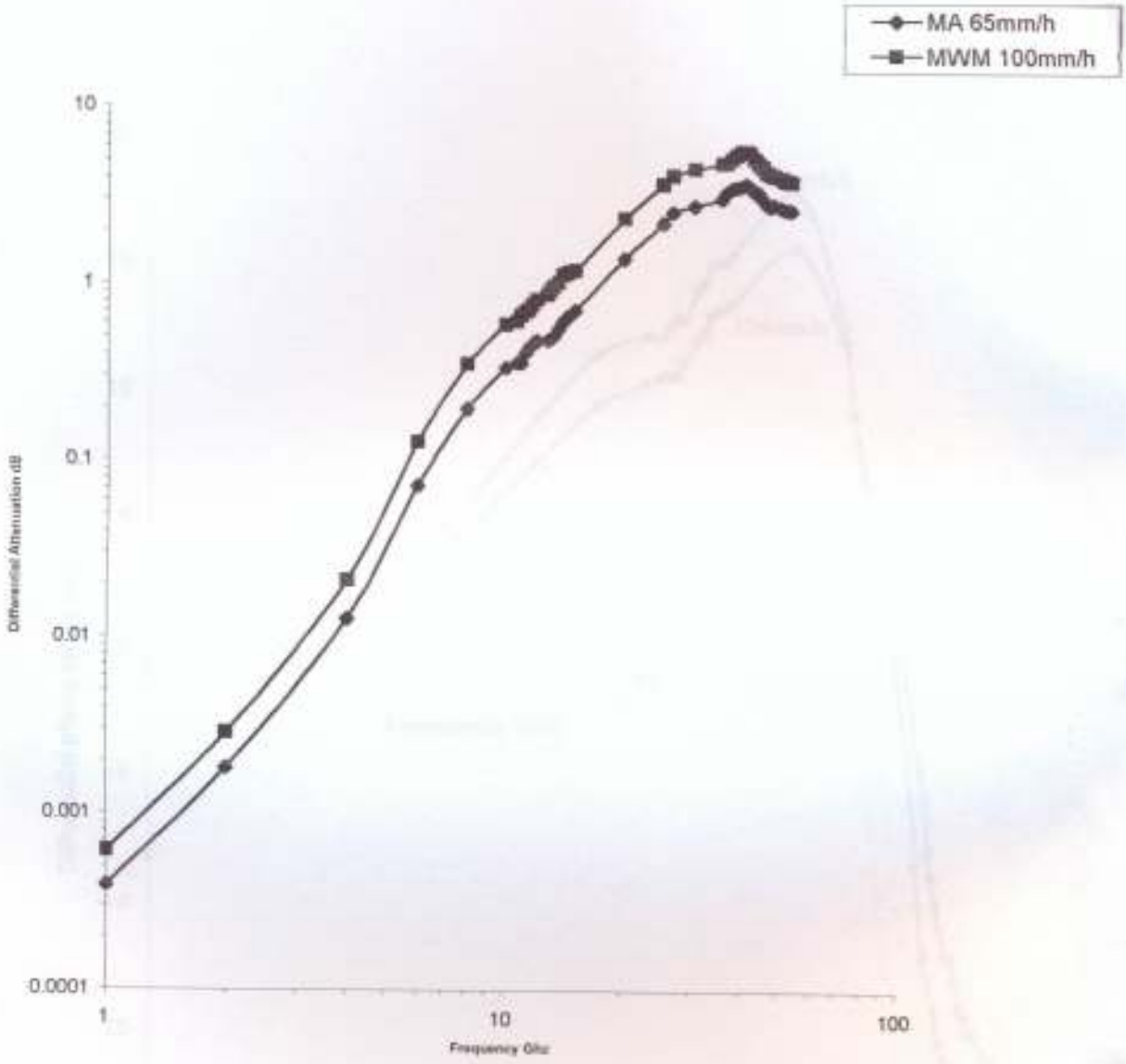


**Fig 3.8 Frequency charateristics of differential attenuation for Nairobi at both rain rates MA=100 MWM=65**

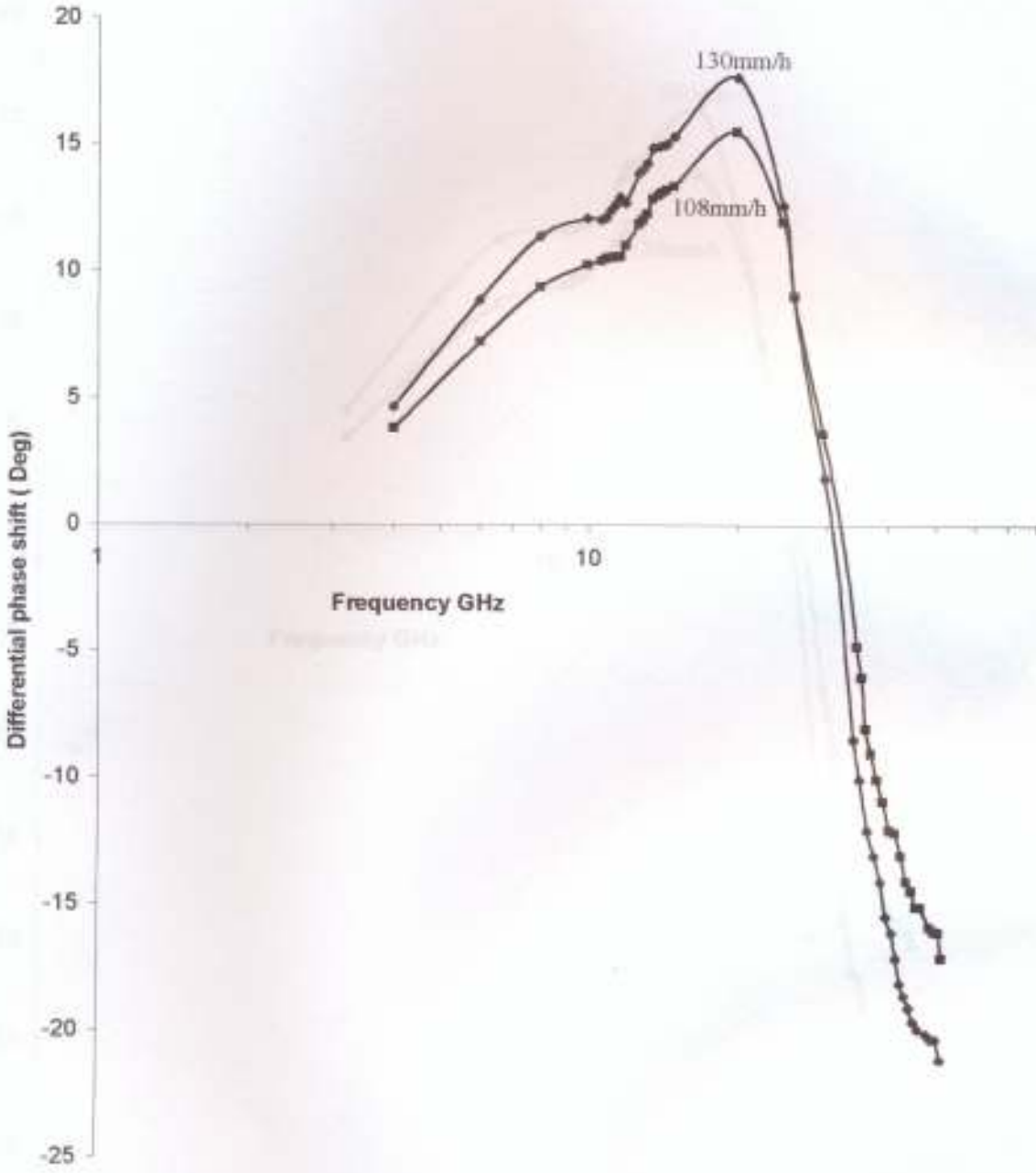


**Fig 3.9 Frequency charateristics of Differential phase shift Ile-Ife a both rain rates MA=108 MWM=130**

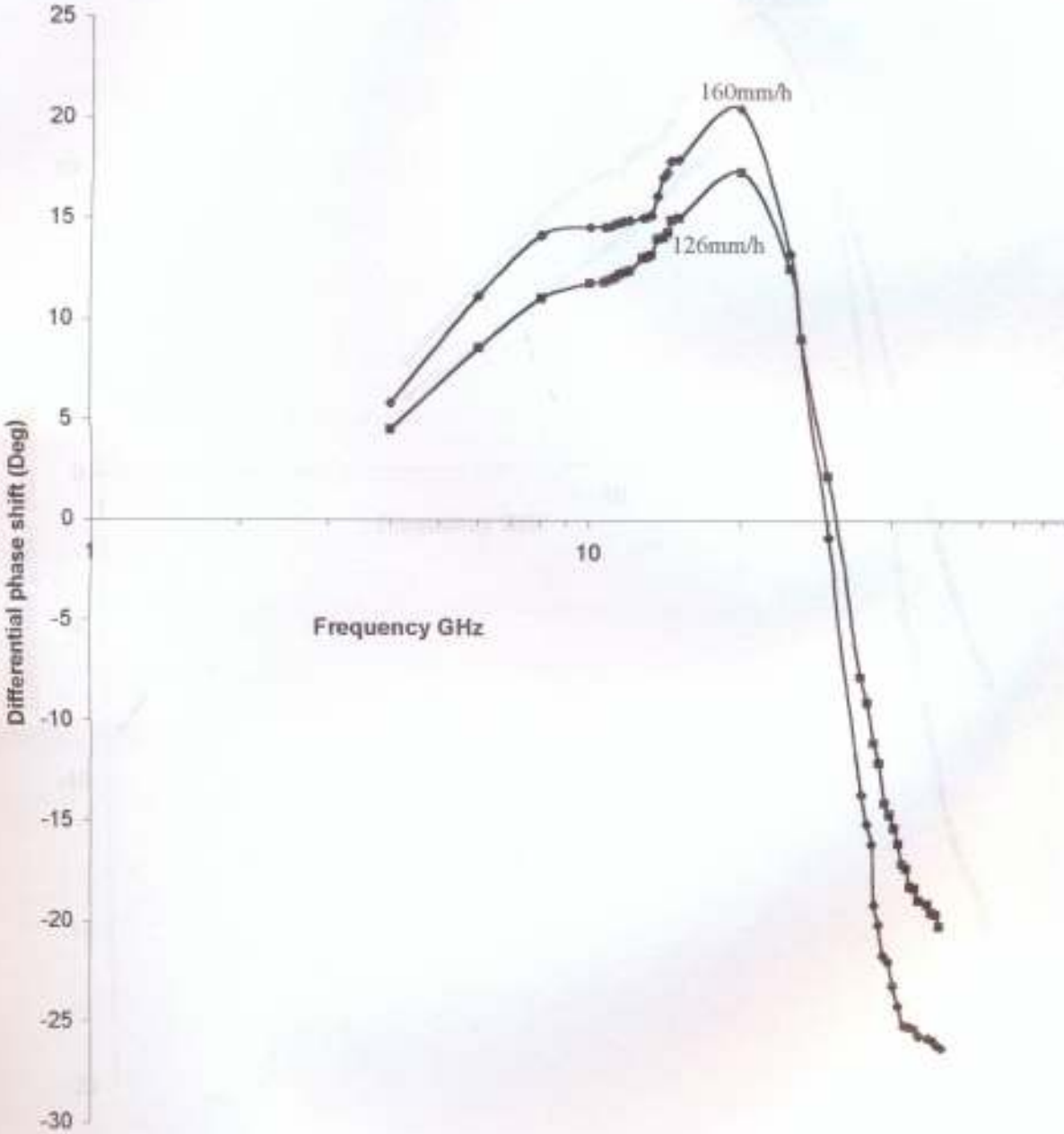


**Fig 3.10 Frequency charateristics of Differential phase shift Douala at both rain rates MA=126 MWM=160**

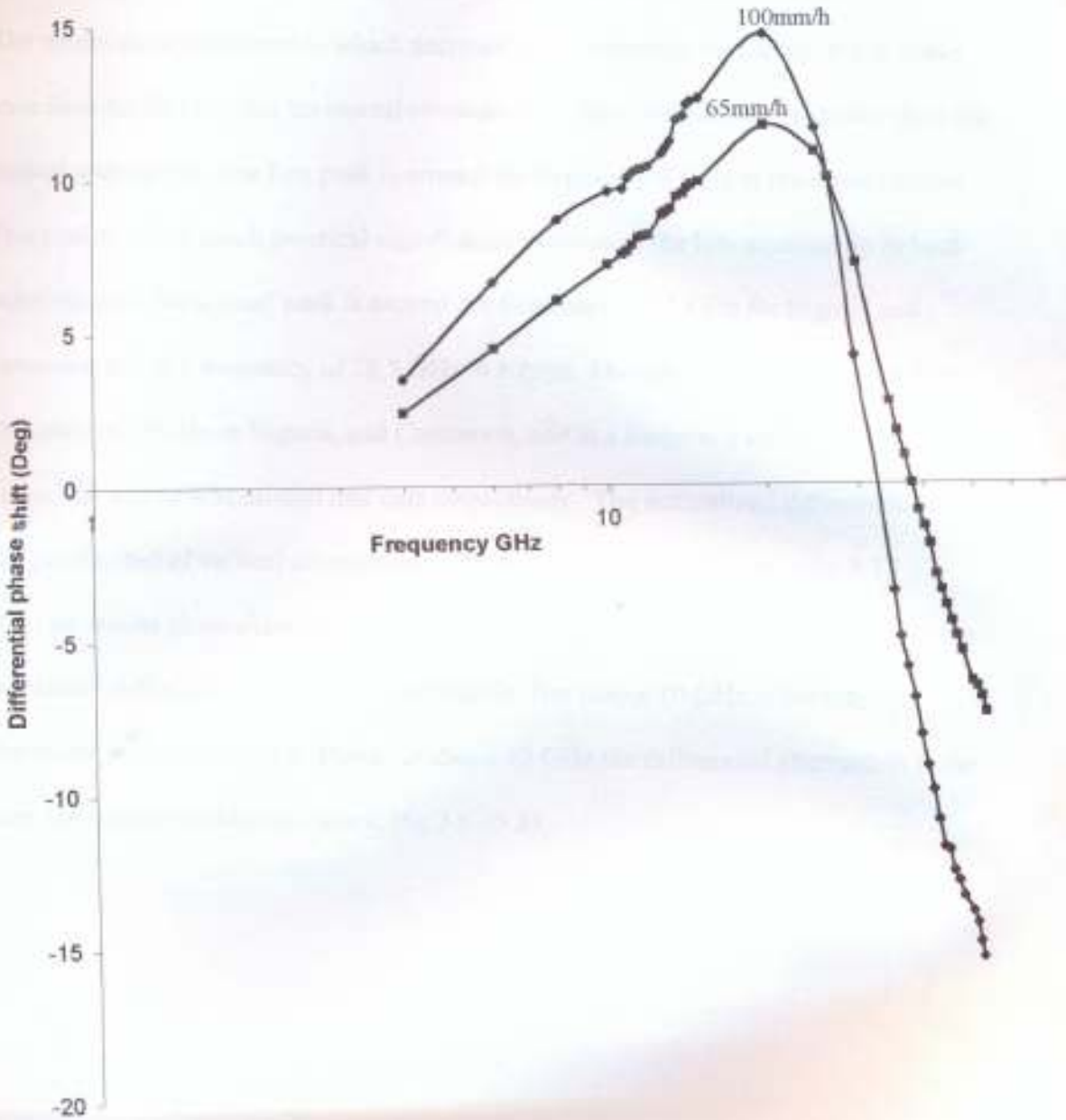


**Fig 3.11 Frequency charateristics of Differential phase shift Nairobi at both rain rates MA=65 MWM=100**

### 3.2.2 Normalized differential attenuation and normalized differential phase shift

The frequency characteristics of the normalized differential attenuation and normalized differential phase shift with respect to vertical attenuation are shown in figs 3.12 – 3.17. The results show some peaks, which decrease with increasing frequency; these peaks arise from the fact that the horizontal attenuation at those frequencies is greater than the vertical attenuation. The first peak is around the frequency 6 GHz at the three stations. This peak is not of much practical significance because of the low attenuation in both polarizations. The second peak is around the frequency of 25 GHz for Nigeria and Cameroon and at a frequency of 26.5 GHz in Kenya. The third peak occurs around the frequency of 39GHz in Nigeria, and Cameroon, and at a frequency of 38 and 39 GHz in Kenya MA and MWM rainfall rate data respectively. The normalized differential phase shift per decibel of vertical attenuation at the three locations is shown in fig 3.15 – 3.17.The results show sharp decrease with increasing frequency and above 10 GHz the normalized differential phase shift is negligible. But below 10 GHz is the major contributor to depolarization. However above 10 GHz the differential attenuation is the major contributor to depolarization, (fig 3.6 –3.8).

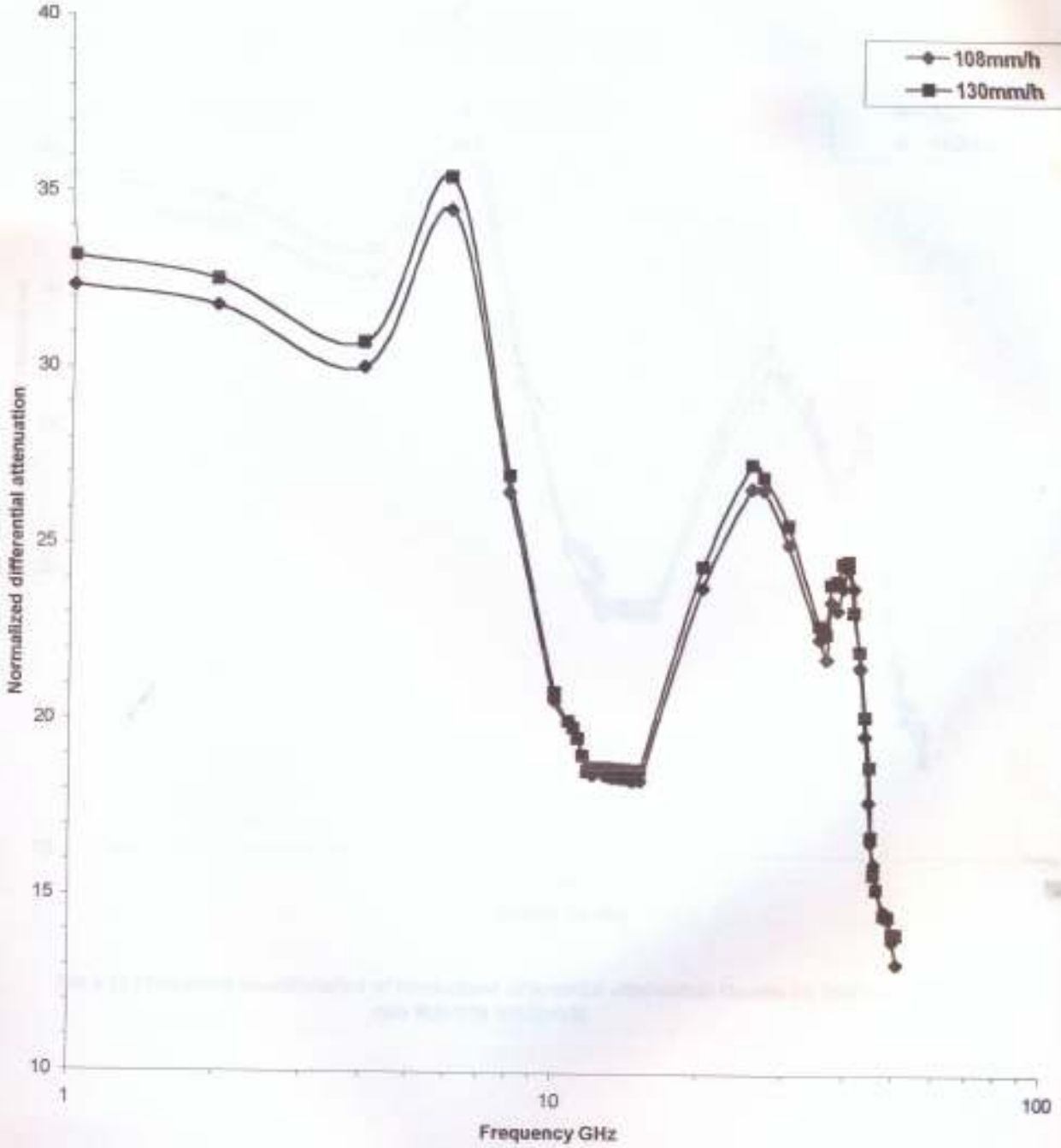


**Fig 3.13 Frequency charateristics of normalized differential attenuation Ile-Ife for both rain rate MA=108 MWM=130**

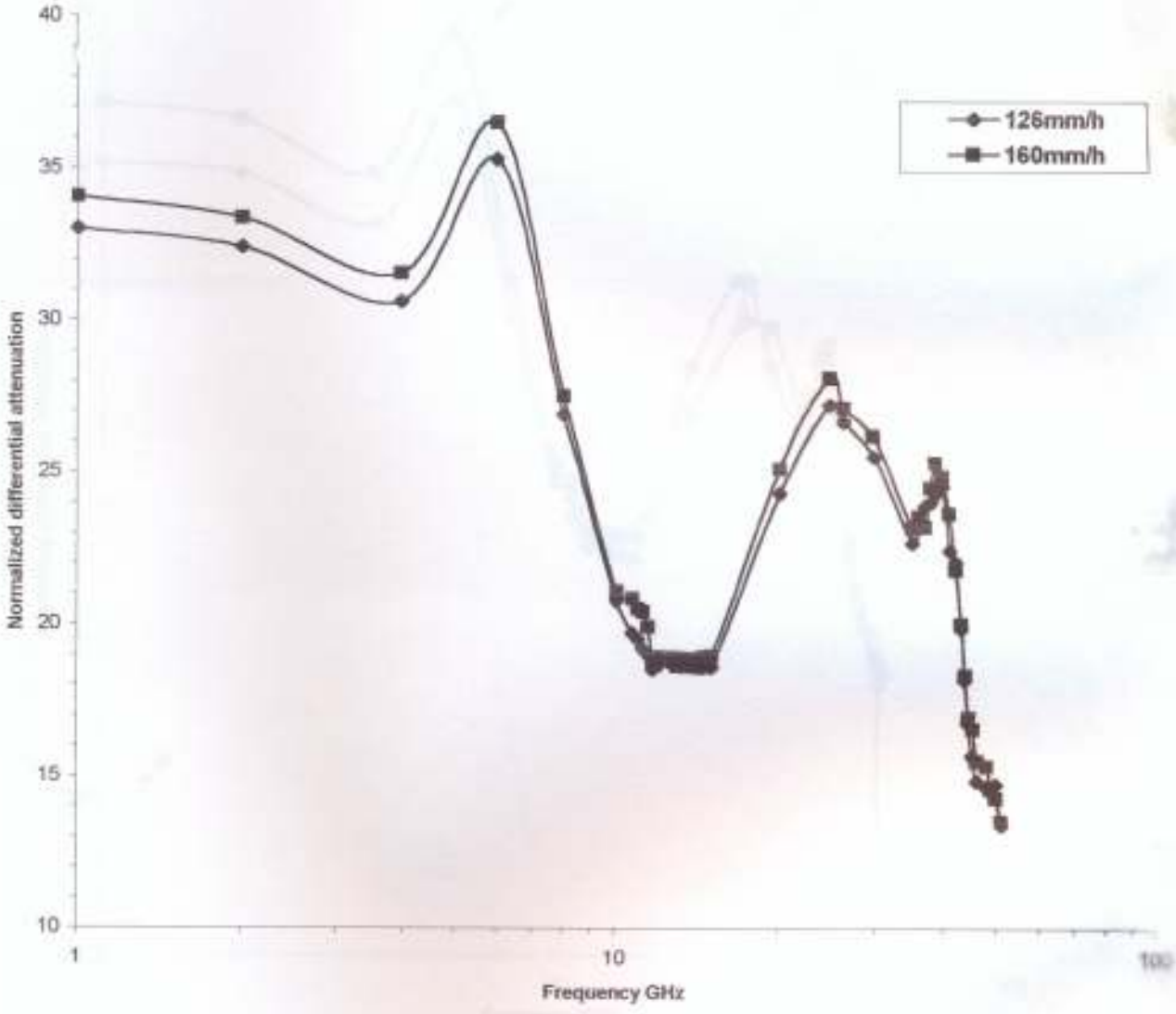


Fig 3.13 Frequency charateristics of normalized differential attenuation Douala for both rain rate MA=126 MWM=160

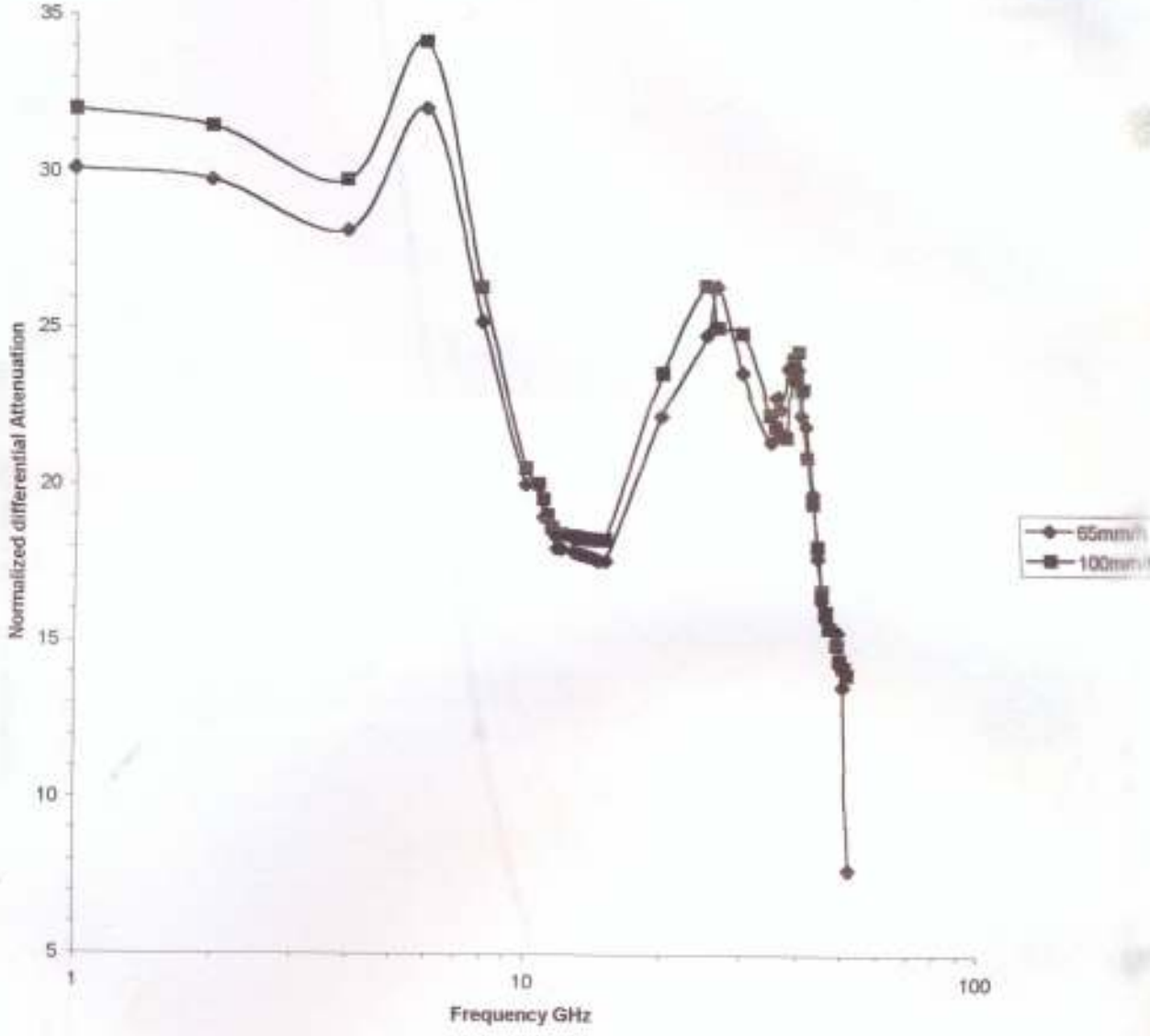


Fig 3.14 Frequency charateristics of normalized differential attenuation Nairobi for both rain rate MA=65 MWM=100

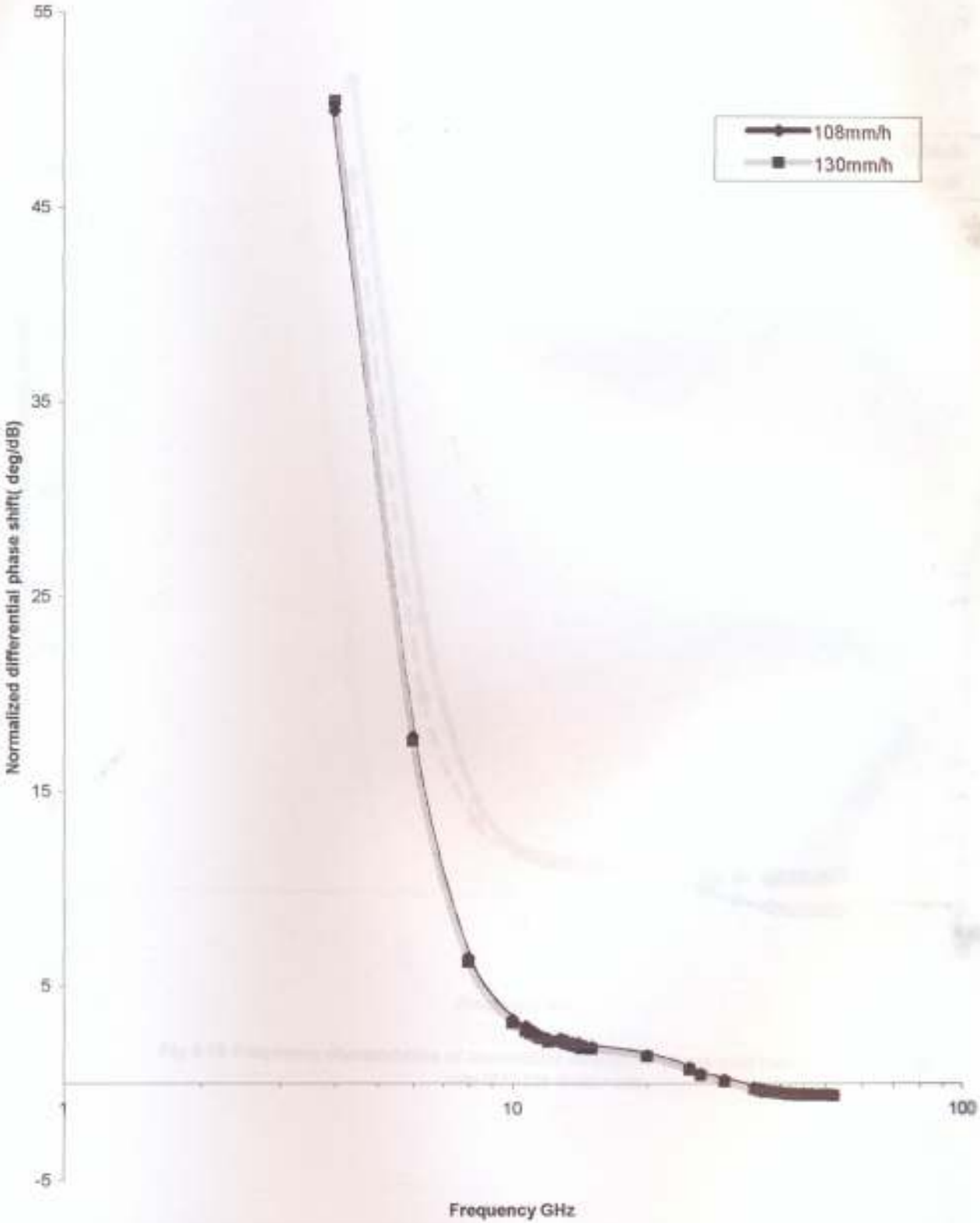


**Fig 3.15 Frequency charateristics of normalized differential phase shift Ile-Ife for both rain rate MA=108 MWM=130**

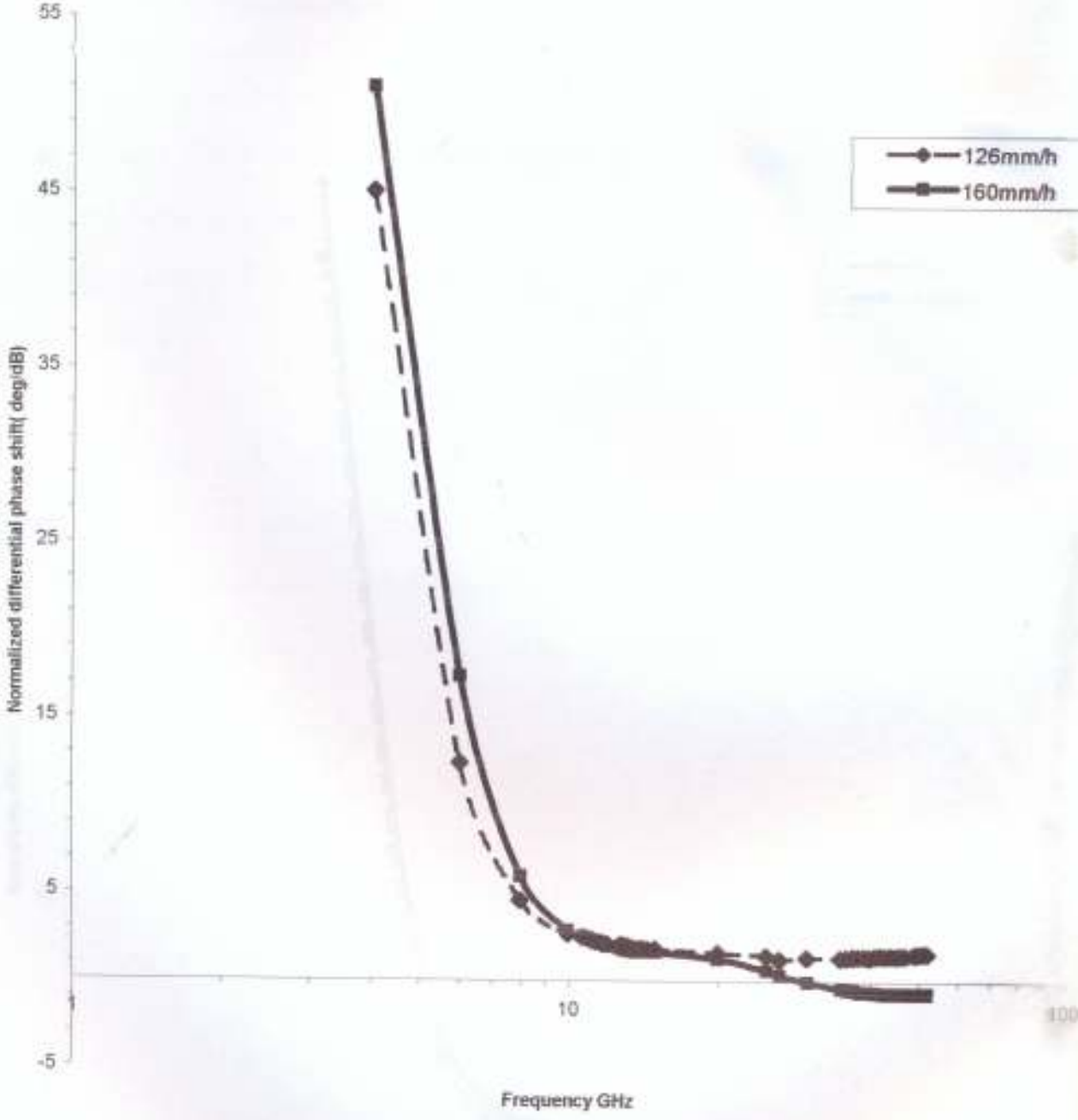


Fig 3.16 Frequency charateristics of normalized differential phase shift Douala for both rain rate MA=126 MWM=160

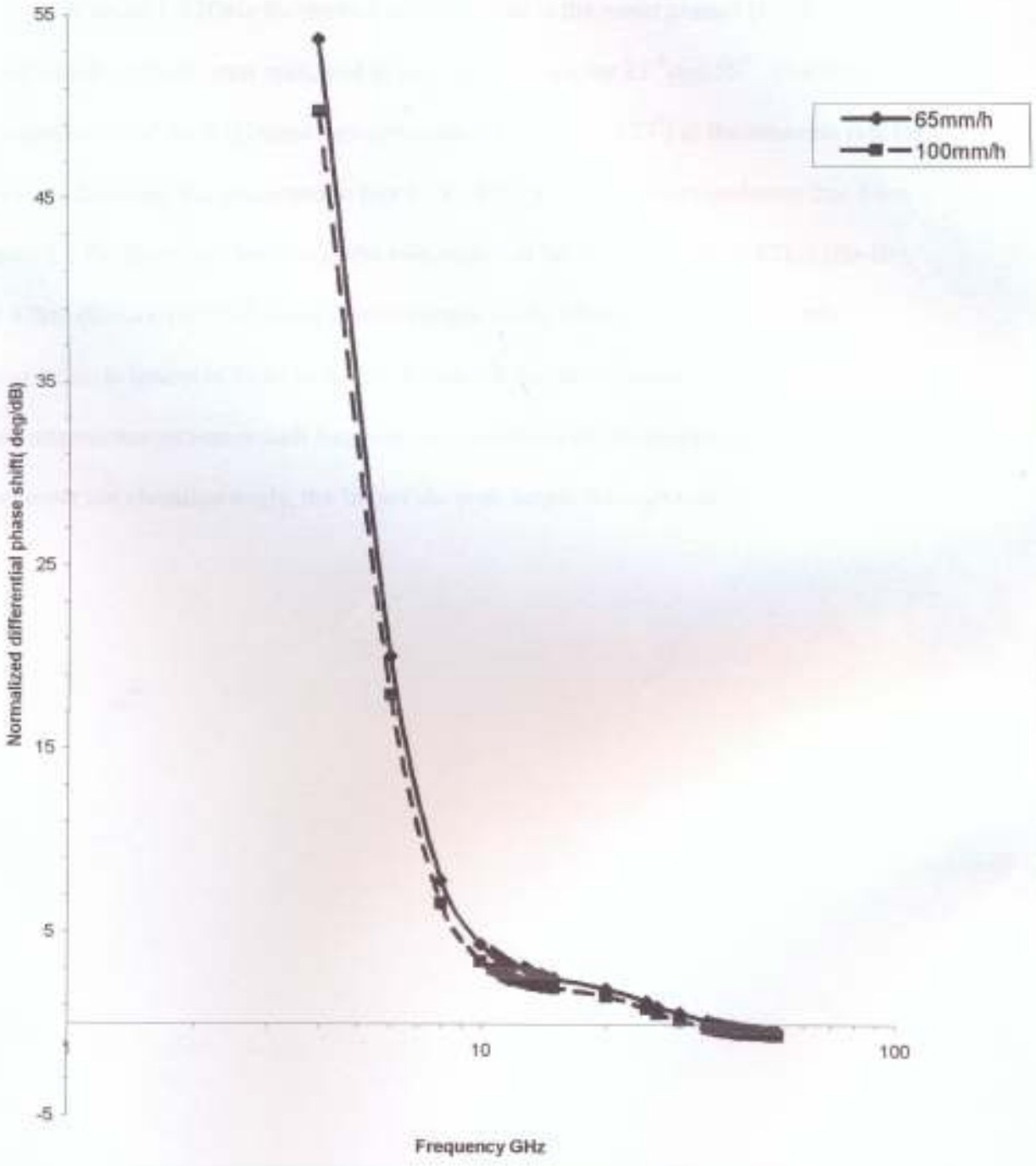


**Fig 3.17 Frequency charateristics of normalized differential phase shift Nairobi for both rain rate MA=65 MWM=100**

### 3.2.3 Total slant path Attenuation

The total slant path attenuation has been calculated for the three stations in the frequency range 1-52GHz for the two rain rates that is the mean annual (MA) and mean worst month (MWM) rain rates, and at two elevation angles 23 $^0$and 55$^0$ . The frequency characteristics of the total slant path attenuation (for 55$^0$ and 23$^0$) at the two-rain rate for the three locations are presented in figs 3.18 –3.23. It should be remembered that from Table 2.2 the slant path lengths to the rain region in the locations are 10.82km (Ile-Ife), 11.47km (Douala) and 6.91km (Nairobi) respectively. Hence the total slant path attenuation is lowest in Nairobi due to its short distance to the rain region. The total slant path attenuation increases with frequency and decrease in elevation angle, since generally the lower the elevation angle, the longer the path length through rain.

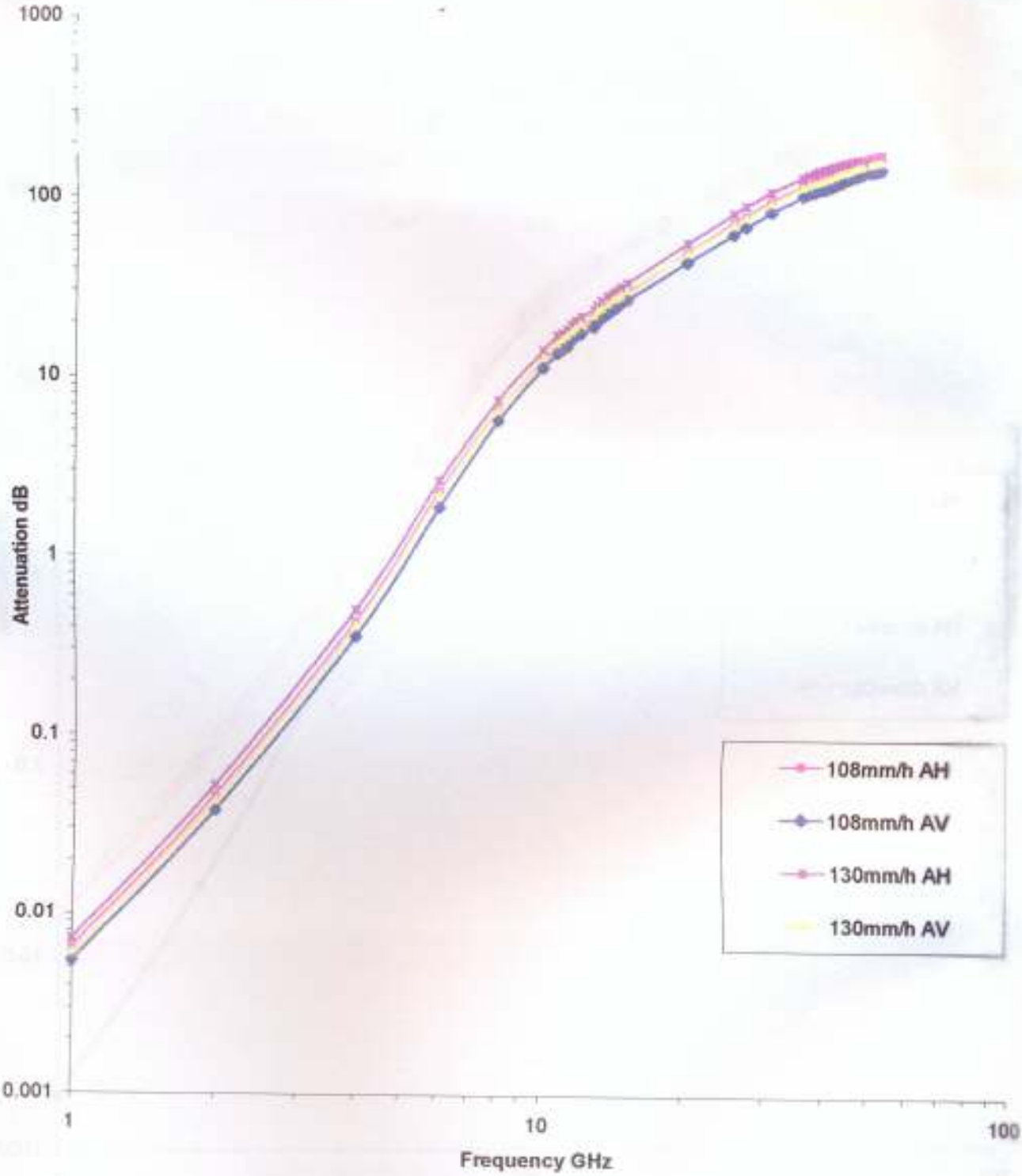


**Fig 3.18 Predicted slant-path attenuation for the rain region at Ile-Ife and at Elevation angle of 55**

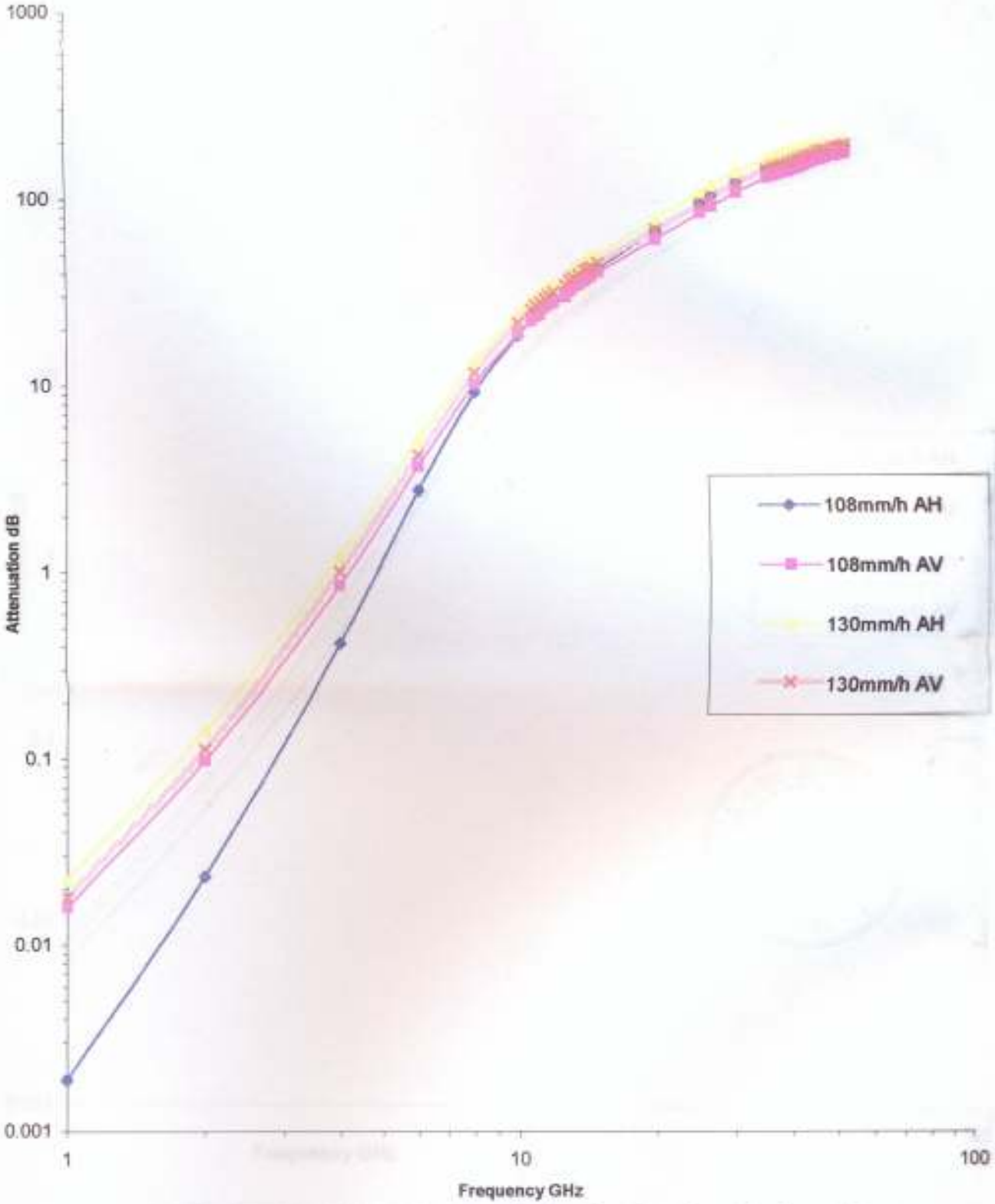


**Fig 3.19 Predicted slant-path attenuation for the rain region at Ile-Ife and at Elevation angle of 23**

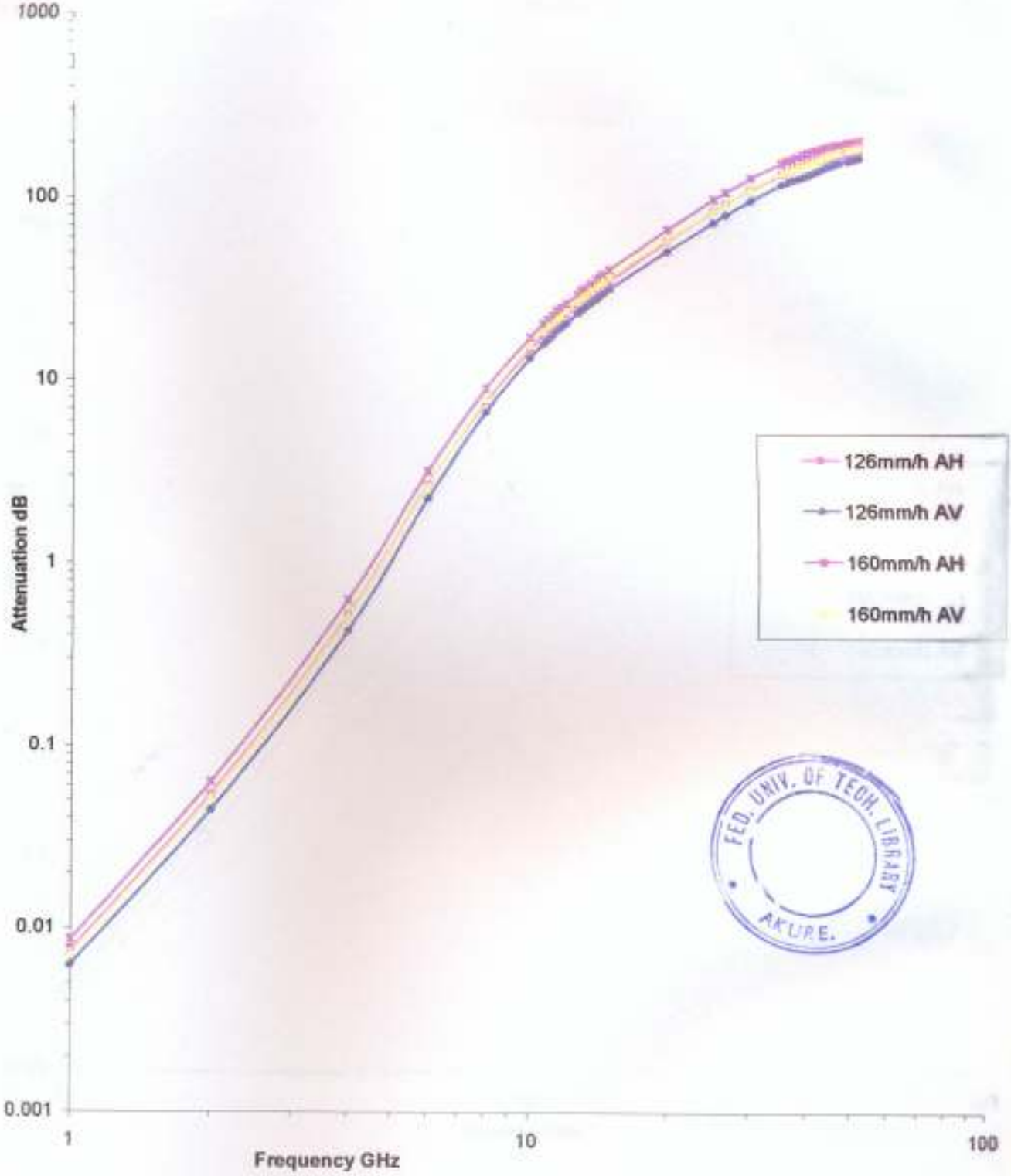




**Fig 3.20 Predicted slant-path attenuation for the rain region at Douala and at Elevation angle of 55**

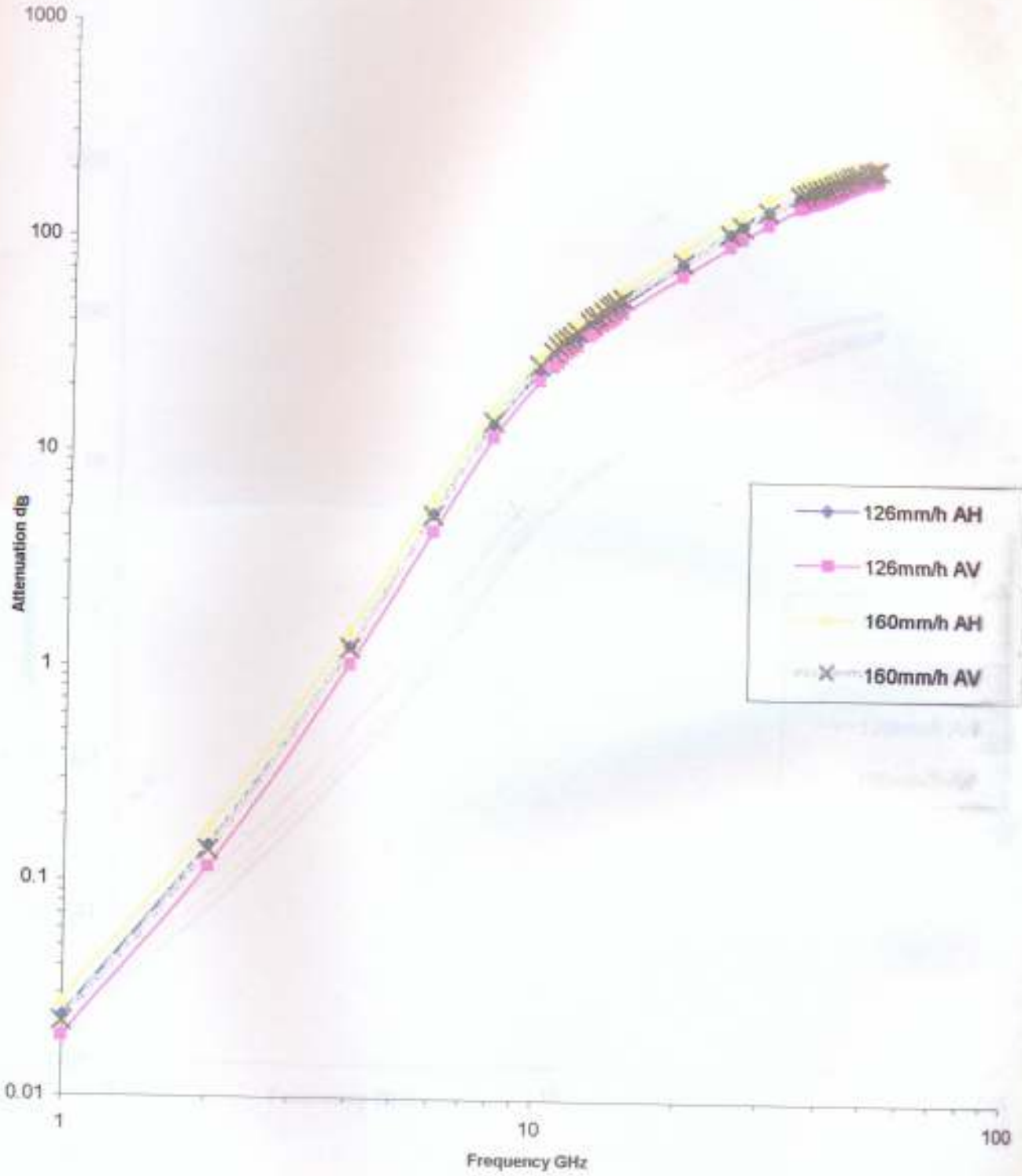


**Fig 3.21 Predicted slant-path attenuation for the rain region at Douala and at Elevation angle of 23**

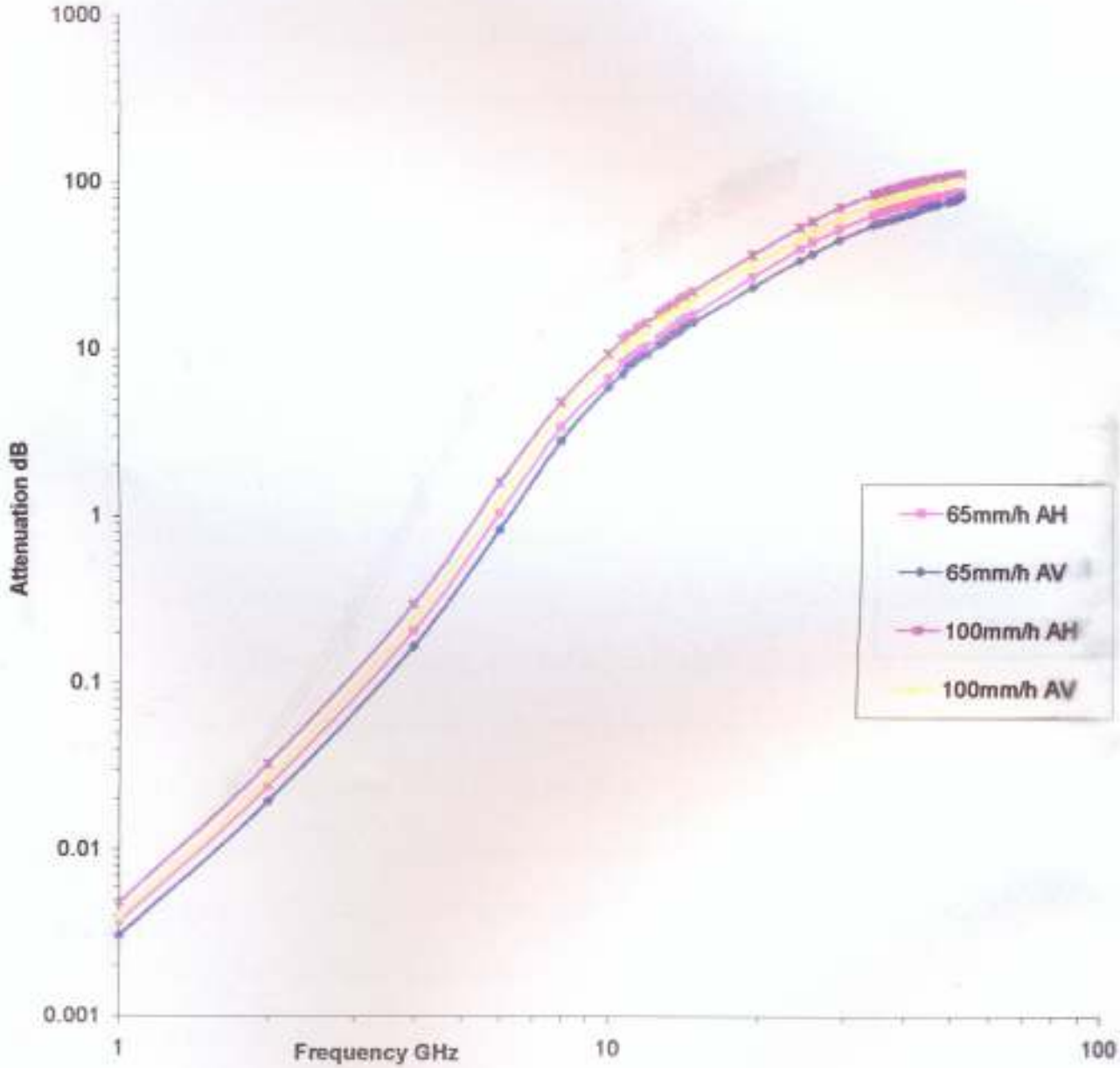


**Fig 3.22 Predicted slant-path attenuation for the rain region at Nairobi and at Elevation angle of 55**

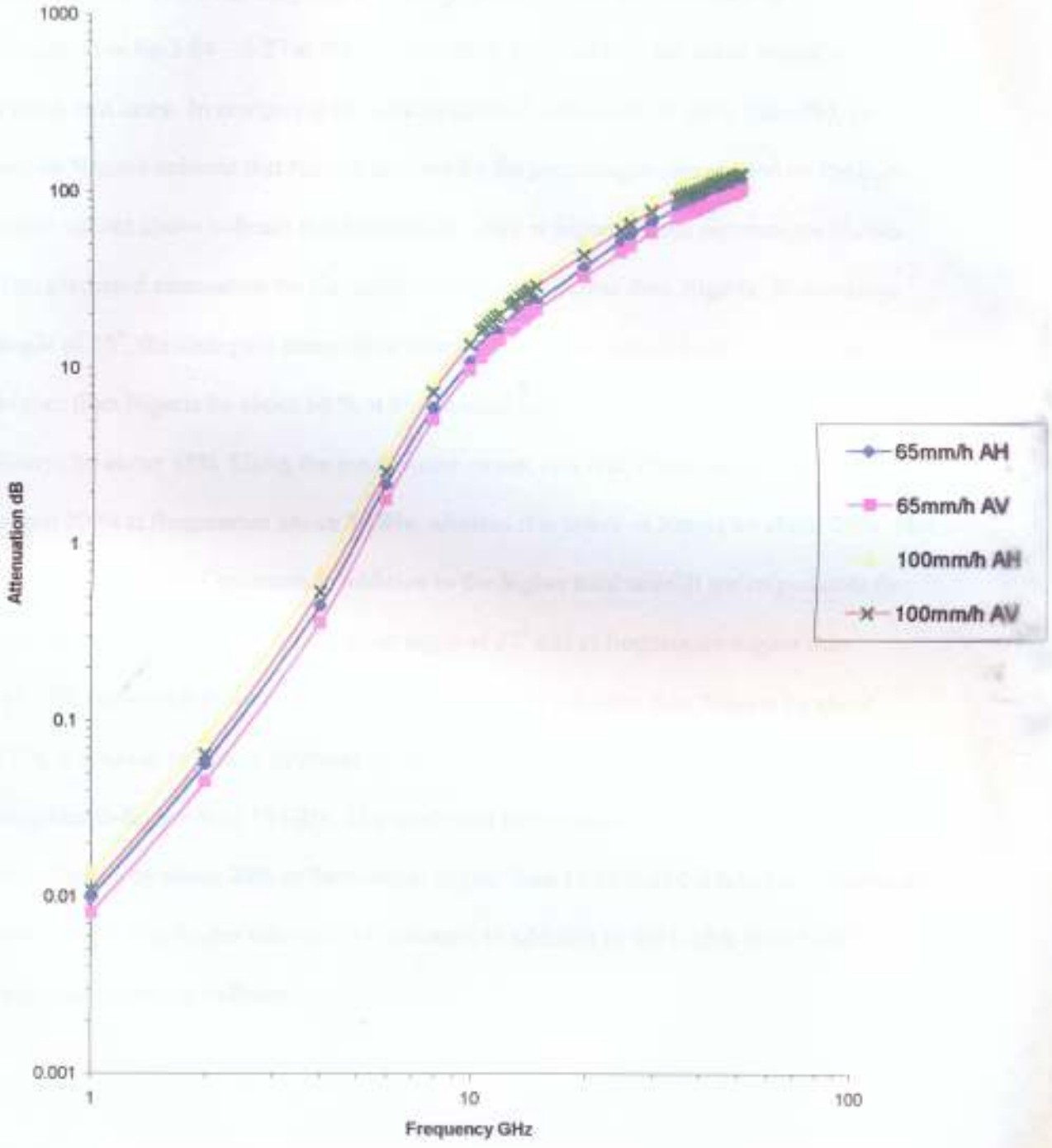


**Fig 3.23 Predicted slant-path attenuation for the rain region at Nairobi and at Elevation angle of 23**

### 3.2.4 Comparison of the Total slant path Attenuation

The result of the total slant path attenuation in Cameroon and Kenya are compared with Nigeria. The frequency characteristics of the percentage difference of the results are presented in fig 3.24 – 3.27 at the two-elevation angle and for the mean annual and worst month rain rates. In comparing the percentage difference with Nigeria (Ile –Ife), curves below Nigeria indicate that Nigeria is lower by the percentages represented on the curves, while curves above indicate that Nigeria (Ile –Ife), is higher by the percentages shown. The predicted attenuation for Cameroon is generally higher than Nigeria. At elevation angle of $55^0$, the slant path attenuation using the mean annual rain rate in Cameroon is higher than Nigeria by about 16 % at frequencies higher than 10 GHz. It is lower in Kenya by about 45%. Using the mean worst month rain rate, Cameroon is higher by about 20 % at frequencies above 5 GHz, whereas it is lower in Kenya by about 26%. The higher rain rates in Cameroon in addition to the higher total rainfall are responsible for this difference. At the lower elevation angle of $23^0$ and at frequencies higher than 10 GHz, using the mean annual rain rate, Cameroon is higher than Nigeria by about 13%, it is lower in Kenya by about 44 %. Using the mean worst month rain rate, at frequencies higher than 10 GHz. The total slant path attenuation in Cameroon is higher than Nigeria by about 24% at frequencies higher than 10 GHz and it is lower in Kenya by about 44 %. The higher rain rate in Cameroon in addition to the higher total rainfall is responsible for this difference.

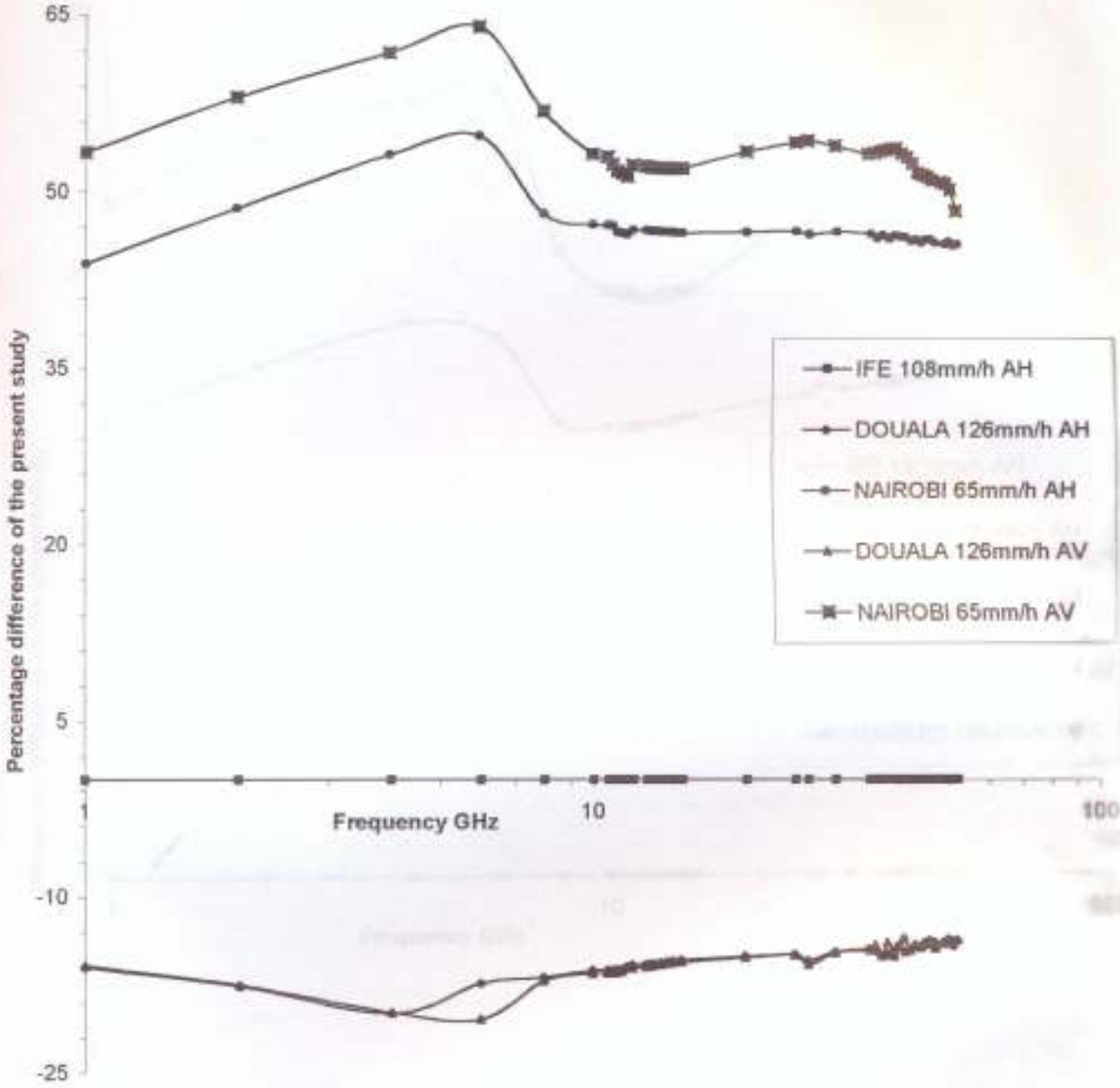


**Fig 3.24 Frequency charateristics of the percentage difference in total slant- path attenuation for 55 elevation angle at the three stations using the mean annuall rainfall rate**

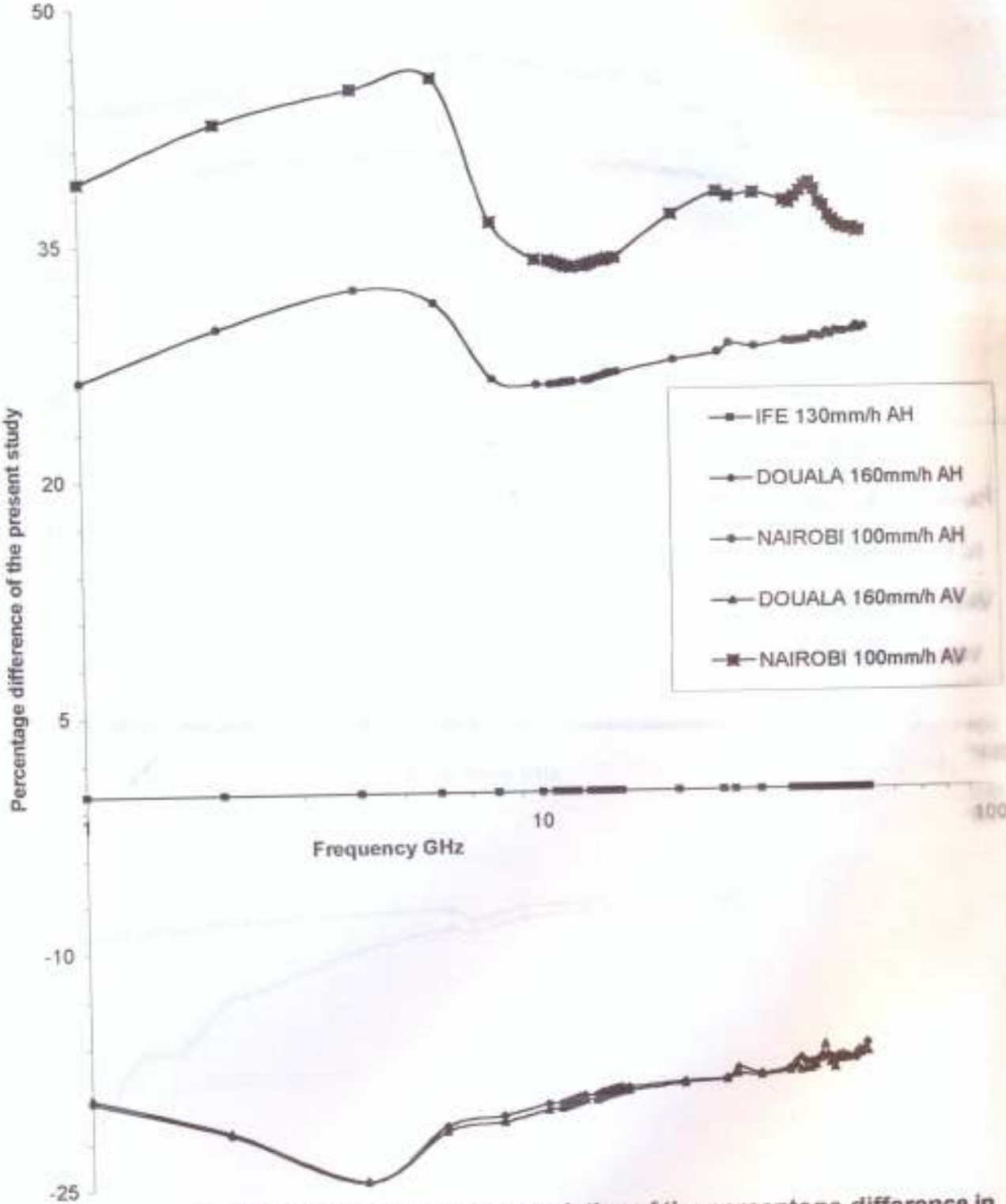


**Fig 3.25 Frequency charateristics of the percentage difference in total slant- path attenuation for 55 elevation angle at the three stations using the mean worst month rainfall rate**

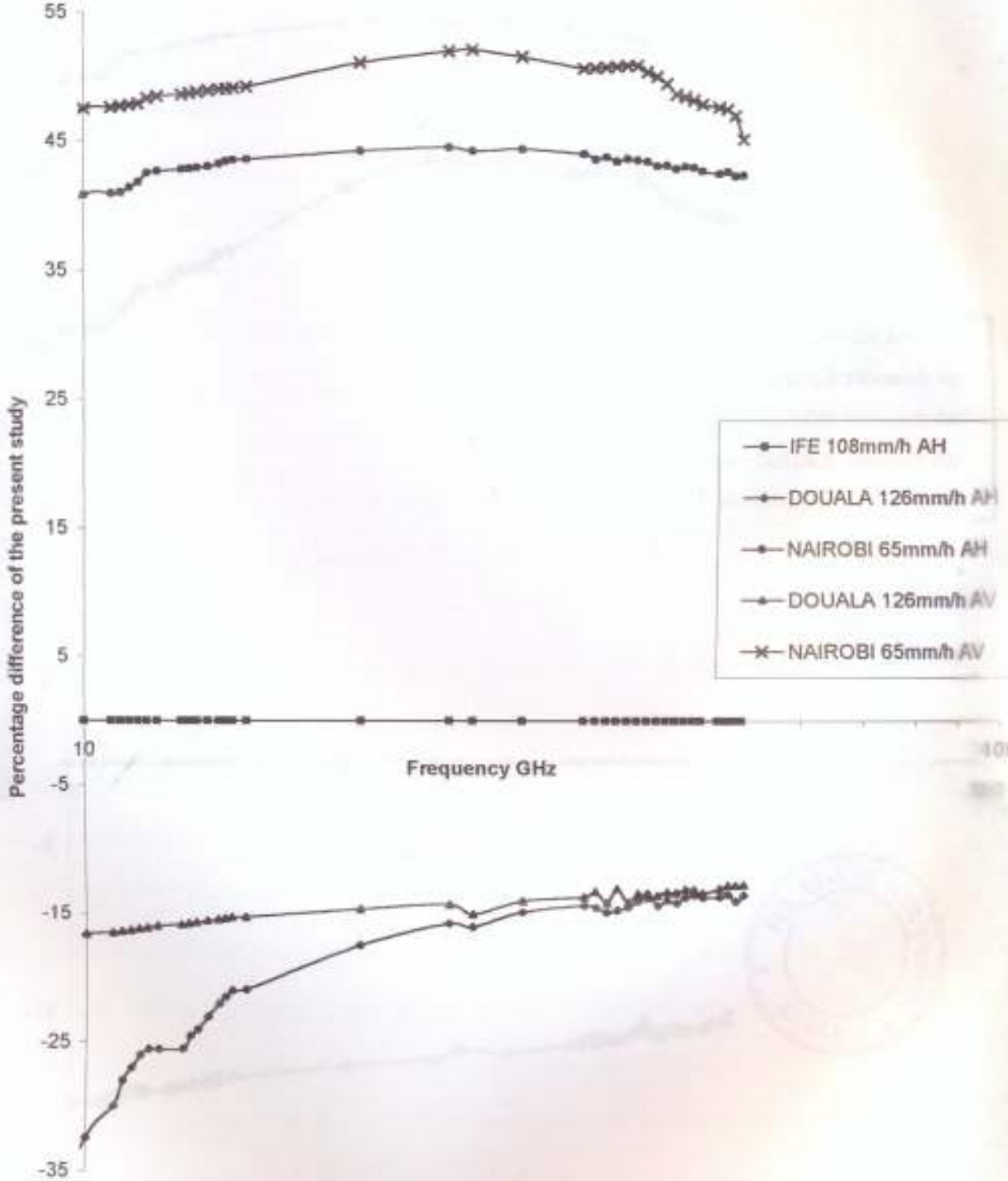


**Fig 3.26 Frequency charateristics of the percentage difference in total slant- path attenuation for 23 elevation angle at the three stations using the mean annuall rainfall rate**

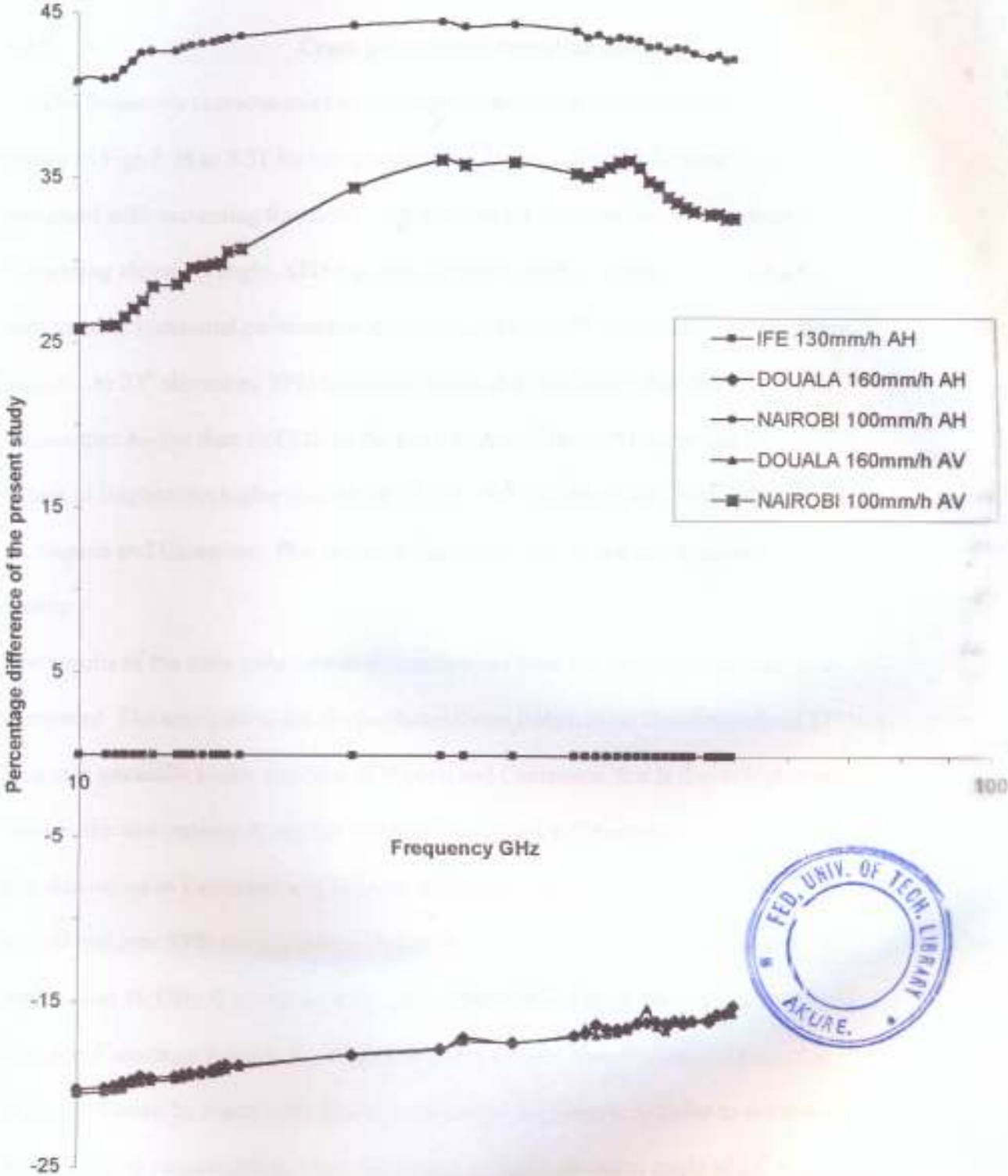




**Fig 3.27 Frequency charateristics of the percentage difference in total slant- path attenuation for 23 elevation angle at the three stations using the mean worst month rainfall rate**

### 3.2.5 Cross polarization Discrimination

The frequency characteristics of the Cross Polarization Discrimination (XPD) are shown in Figs 3.28 to 3.31 for two elevation angles investigated. Generally, the XPD decreases with increasing frequency, and rain rate for the locations. It also decreases with decreasing elevation angle. XPD for vertical polarization is worst by about 16 dB compared to horizontal polarization at all frequency for $55^0$ elevations in all the three station. At $23^0$ elevations XPD horizontal is about 16 dB better than the vertical for frequencies higher than 10 GHz, in the three stations. The XPD decreases to negative values at frequencies higher than about 25 GHz for vertical polarization at $23^0$ elevations in, Nigeria and Cameroon. This is due to higher rain rate of the two countries compare to Kenya.

The results of the cross polarization discrimination from the three locations are also compared. The result show that the predicted Cross Polarization Discrimination (XPD) in Kenya is generally higher than that of Nigeria and Cameroon, this is due to higher rainfall rates in the two stations. It implies that satellite signals will experience more depolarization in Cameroon and Nigeria. At elevation angle of $55^0$, using the mean annual rain rate XPD in Cameroon is lower than Nigeria by about 8 % at frequencies higher than 10 GHz. It is higher in Kenya by about 16%. Using the mean worst month rain rate, Cameroon is lower by about 9 % at frequencies about 5 GHz, whereas it is higher in Kenya by about 21%. The lower rain rate in Kenya in addition to the lowest total rainfall is responsible for this difference. At lower elevation angle of $23^0$ and at frequencies higher than 10 GHz, using the mean annual rain rate, Cameroon is lower than

Nigeria by about 81%, it is higher in Kenya by about 54 %. Using the mean worst month rain rate, at frequencies higher than 10 GHz, Cameroon is lower than Nigeria by about 31% at a frequency of 10 GHz and it is higher in Kenya by about 14 %. The lower rain rate in Kenya in addition to the lowest total rainfall is responsible for this difference. We can conclude that;

(1). The XPD values for Cameroon at $55^0$ elevation angle are comparable to Nigeria than that of Kenya.

(2). The minimum XPD for most communication systems is between 20 – 30 dB for discriminating the unwanted polarization during a severe rainfall. It can be seen that from the results for Kenya at $55^0$ elevations, and frequencies between 38 – 42 GHz, the XPD for horizontal polarization decreases to a minimum value of 27 dB this is closer to 30 dB.

(3). For Nigeria it decreases to a minimum of 21 dB between the frequencies 39 – 41 GHz and at Cameroon it decreases to a minimum of 20 dB between the frequencies 38 – 42 GHz.

(4). But at $23^0$ elevation, the XPD for horizontal polarization is much more poorer, above 20 GHz and it reduces to a minimum values of 17 dB for Kenya, while for Nigeria above 15 GHz it reduces to a minimum of 11 dB, for Cameroon above 13.625 GHz it reduces to a minimum of 10 dB.

(5). Generally at all frequencies (1 – 52GHz) XPD horizontal polarization for $55^0$ elevation is 10 dB better than XPD $23^0$ horizontal polarization.

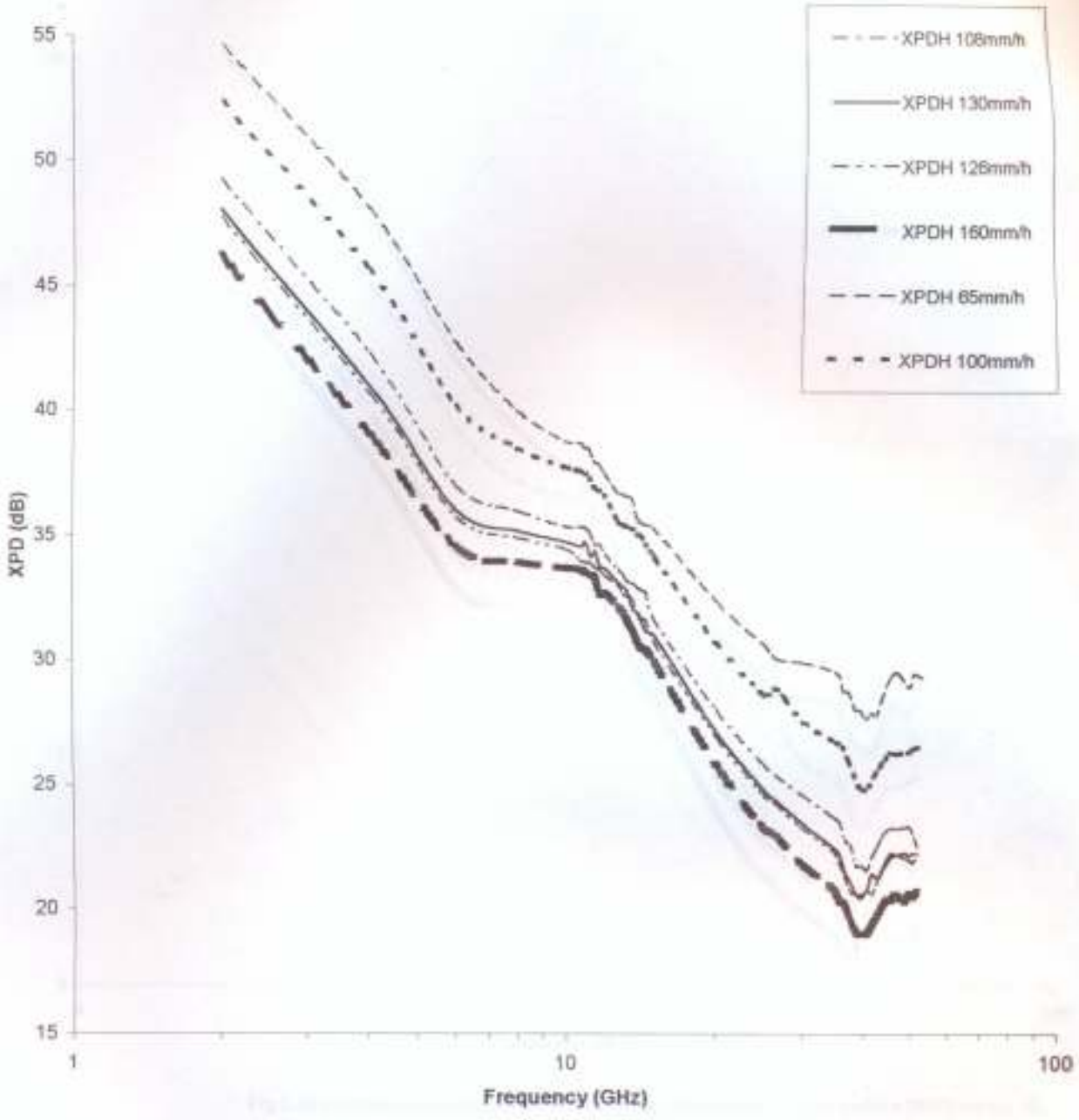


**Fig 3.28 Frequency charateristics of the cross polarization Discrimination (XPD) for Ile -Ife, Douala, Nairobi at both rain rate mean annual=108,126,65 and mean worst month= 130,160,100 respectively at elevation angle of 55**

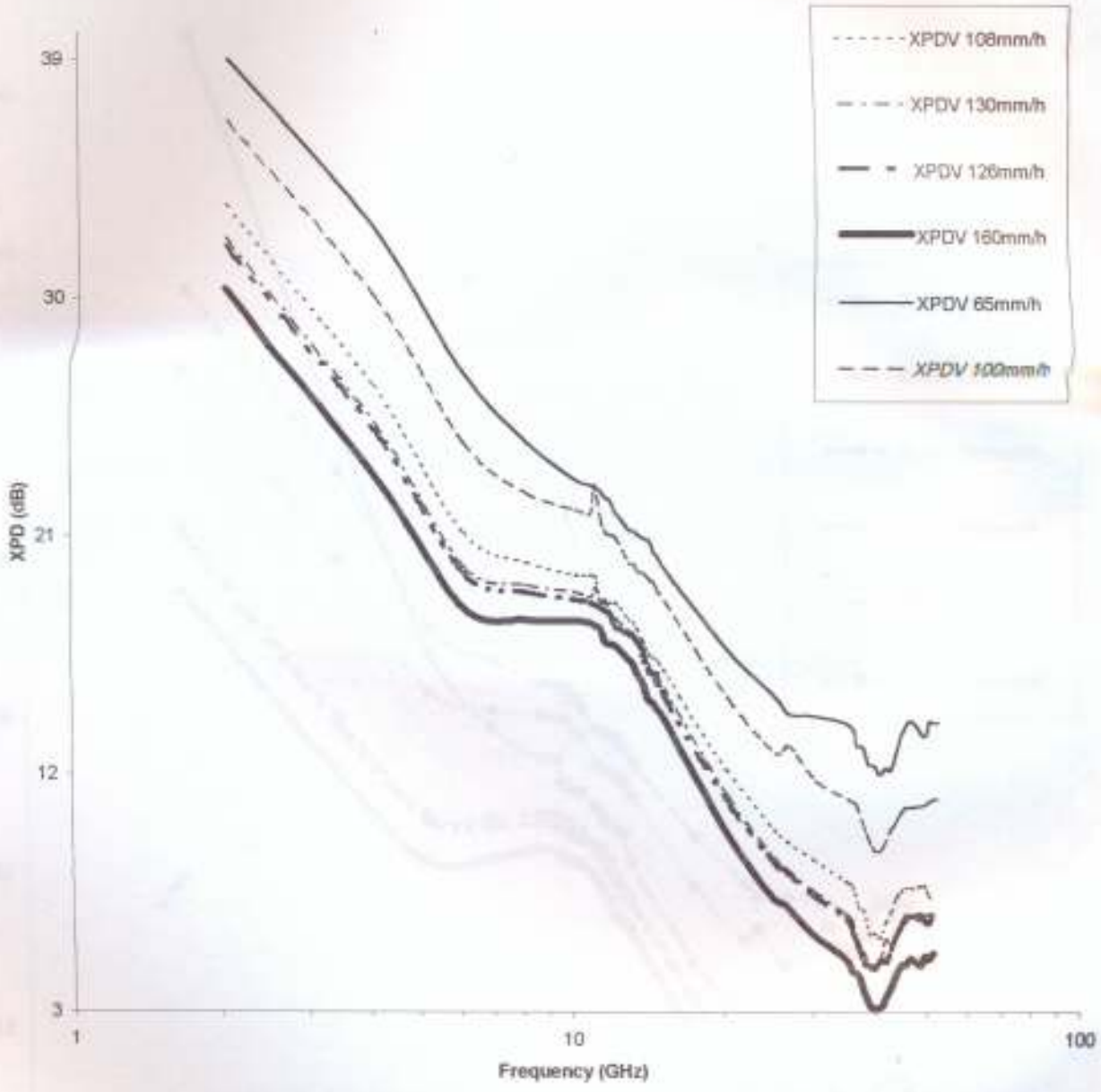


**Fig 3.29 Frequency charateristics of the cross polarization Discrimination (XPD) for Ile -Ife, Douala, Nairobi at both rain rate mean annual=108,126,65 and mean worst month= 130,160,100 respectively at elevation angle of 55**

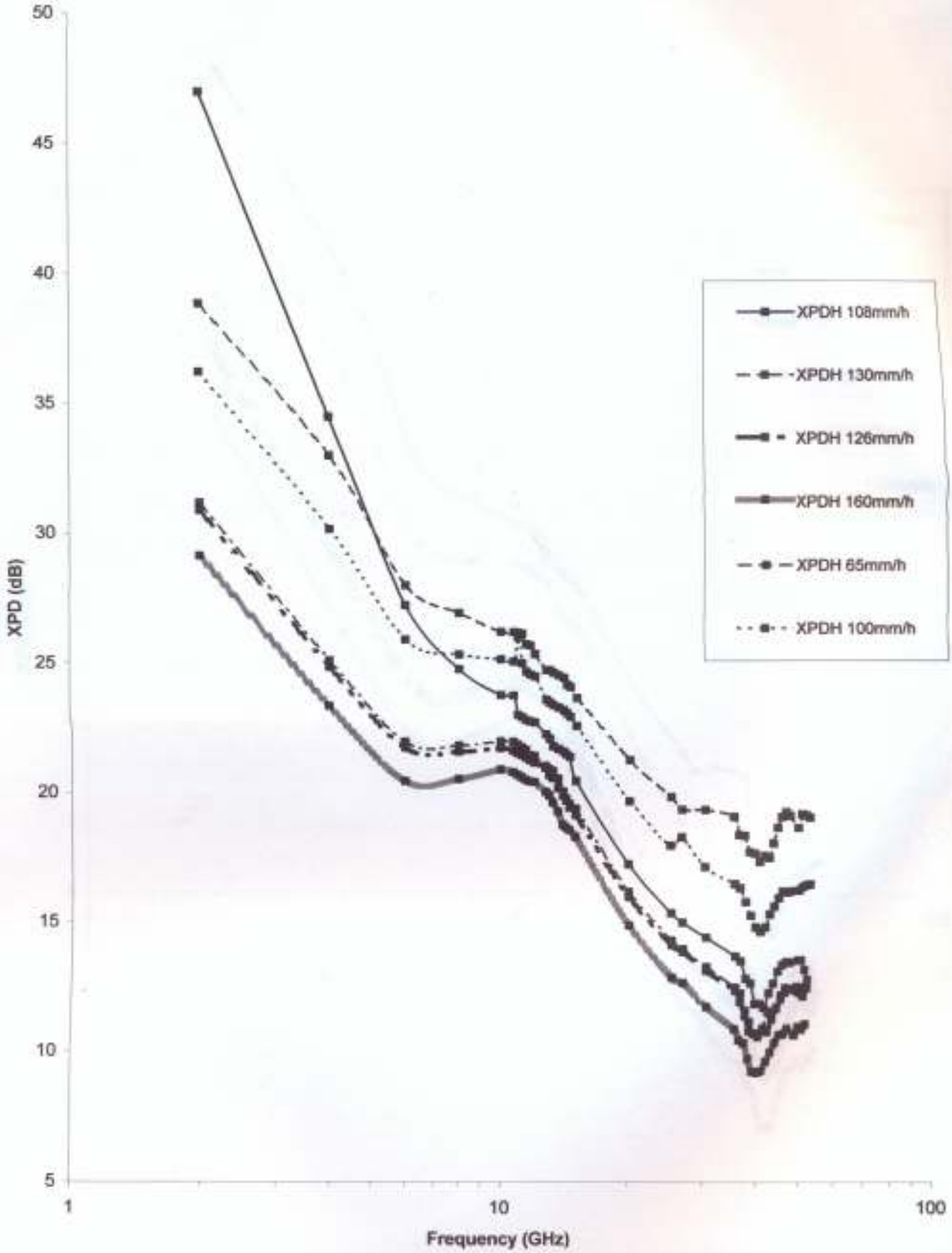


**Fig 3.30 Frequency charateristics of cross polarization Discrimination XPD for Ile-Ife, Doualal, and Nairobi at both rain rate mean annual=108,126,65and mean worst month= 130,160,100mm/h respectively at elevation angle of 23**

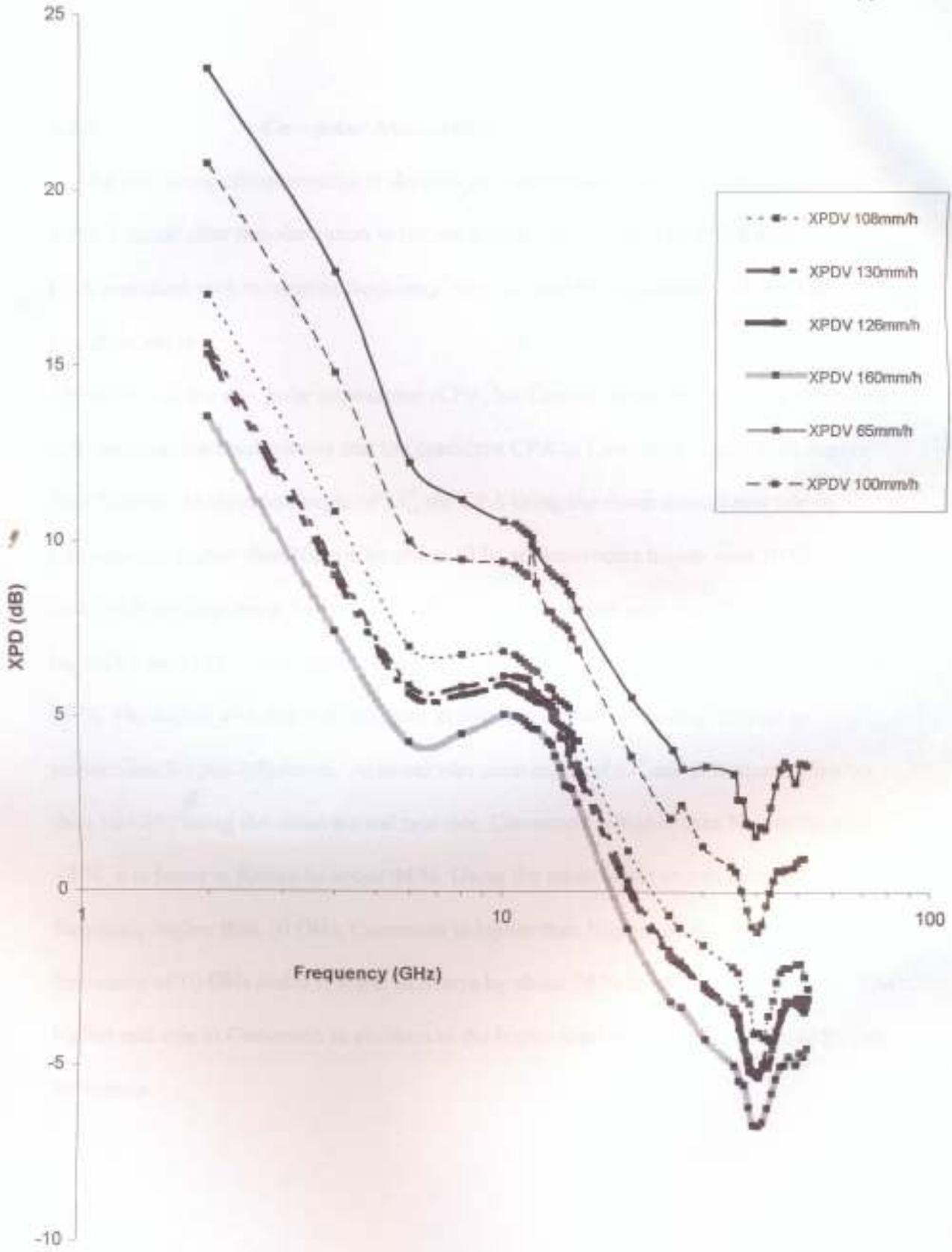


**Fig 3.31 Frequency charateristics of cross polarization Discrimination XPD for Ile-Ife, Doualal, and Nairobi at both rain rate mean annual=108,126,65and mean worst month= 130,160,100mm/h respectively at elevation angle of 23**

### 3.2.6 Co – polar Attenuation

The frequency characteristics of the copolar attenuation, that is the attenuation of the wanted signal after depolarization is shown in figs 3.32 – 3.35. The result shows that CPA increases with increasing frequency, rain rate and also increases with decrease in elevation angle.

The results of the co - polar attenuation (CPA) for Cameroon and Kenya were compared with Nigeria; the result shows that the predicted CPA of Cameroon is generally higher than Nigeria. At elevation angle of $55^0$, the CPA using the mean annual rain rate in Cameroon is higher than Nigeria by about 13 % at frequencies higher than 10 GHz. It is lower in Kenya by about 54 %. Using the mean worst month rain rate, Cameroon is higher by about 16 % at frequencies above 5 GHz, whereas it is lower in Kenya by about 26 %. The higher rain rate in Cameroon in addition to the higher total rainfall is responsible for this difference. At lower elevation angle of $23^0$ and at frequency higher than 10 GHz, using the mean annual rain rate, Cameroon is higher than Nigeria by about 13 %, it is lower in Kenya by about 44 %. Using the mean worst month rain rate, at frequency higher than 10 GHz, Cameroon is higher than Nigeria by about 15 % at frequency of 10 GHz and it is lower in Kenya by about 26 % for the same frequency. The higher rain rate in Cameroon in addition to the higher total rainfall is responsible for this difference.

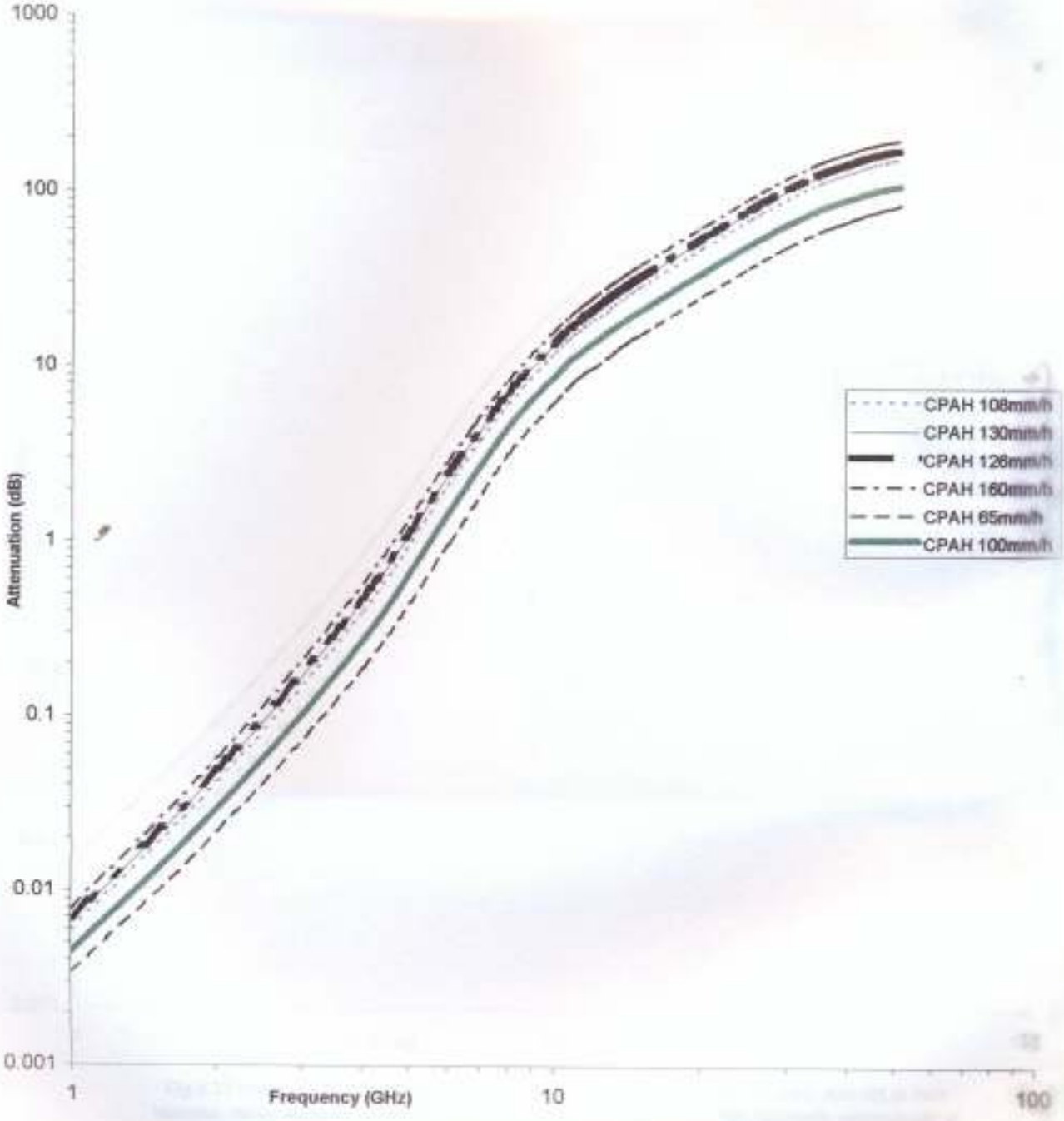


**Fig 3.32 Frequency charateristics of copolar attenuation for Ile-Ife, Douala, *Nairobi*,at both rainrate, mean annuall =108,126,65, and mean worst month=130,160,100mm/h respectively at elevation angle of *55***

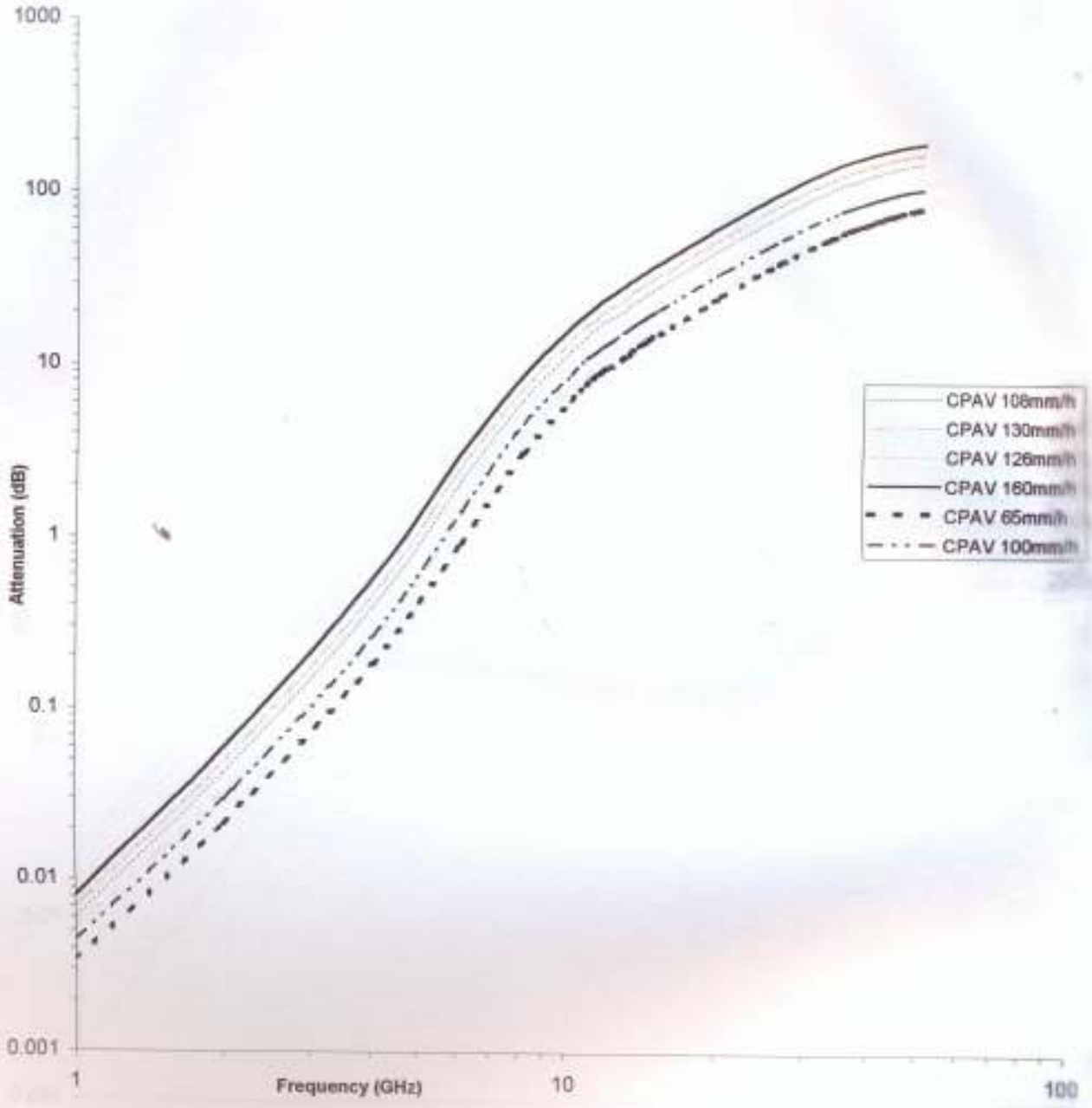


**Fig 3.33 Frequency charateristics of copolar attenuation for Ile-Ife, Douala, Nairobi,at both rainrate, mean annuall =108,126,65, and mean worst month=130,160,100mm/h respectively at elevation angle of 55**

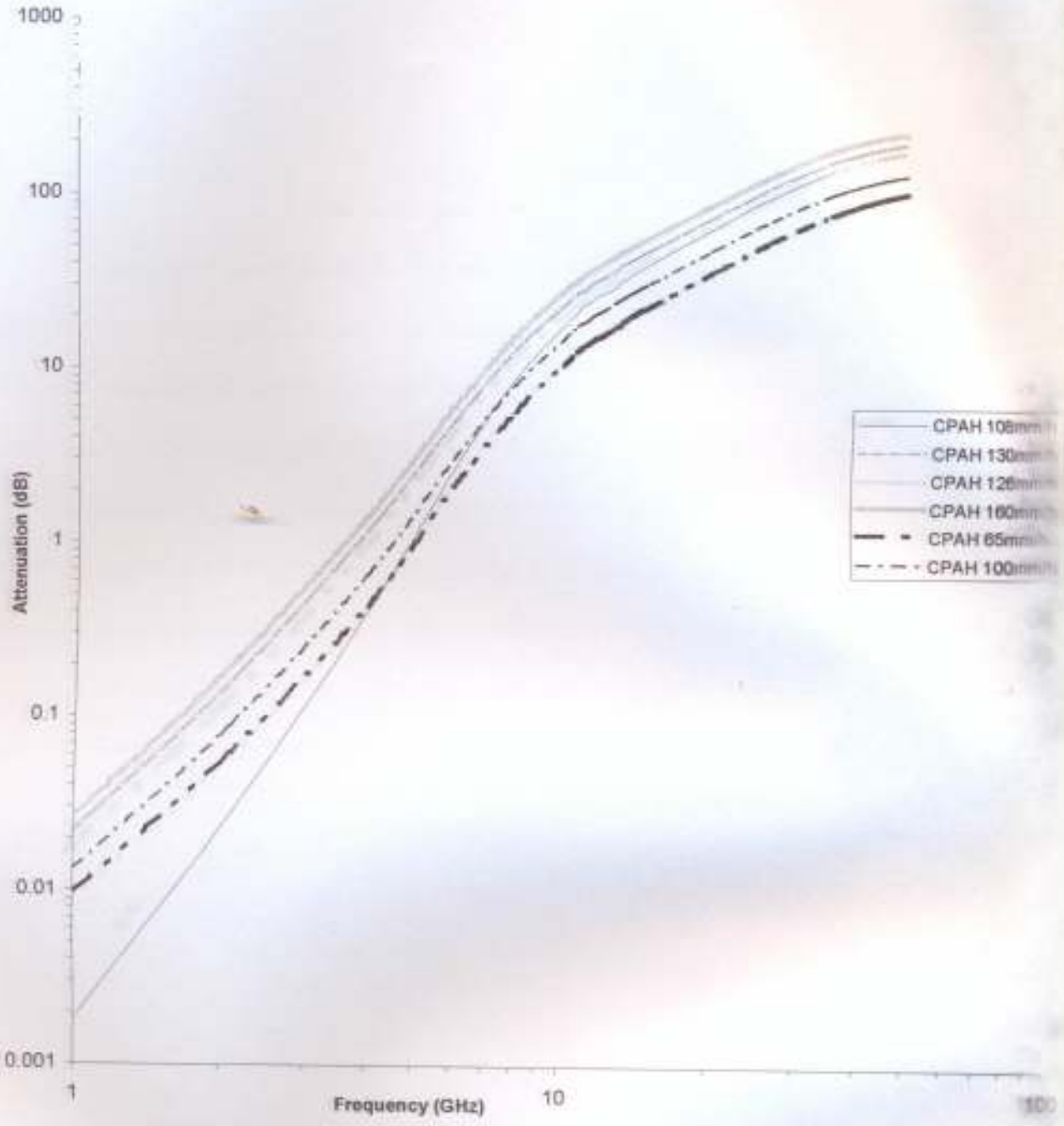


**Fig 3.34 Frequency charateristics of copolar attenuation for Ile-Ife, Douala, Nairobi,at both rainrate, mean annuall =108,126,65, and mean worst month=130,160,100mm/h respectively at elevation angle of 23**

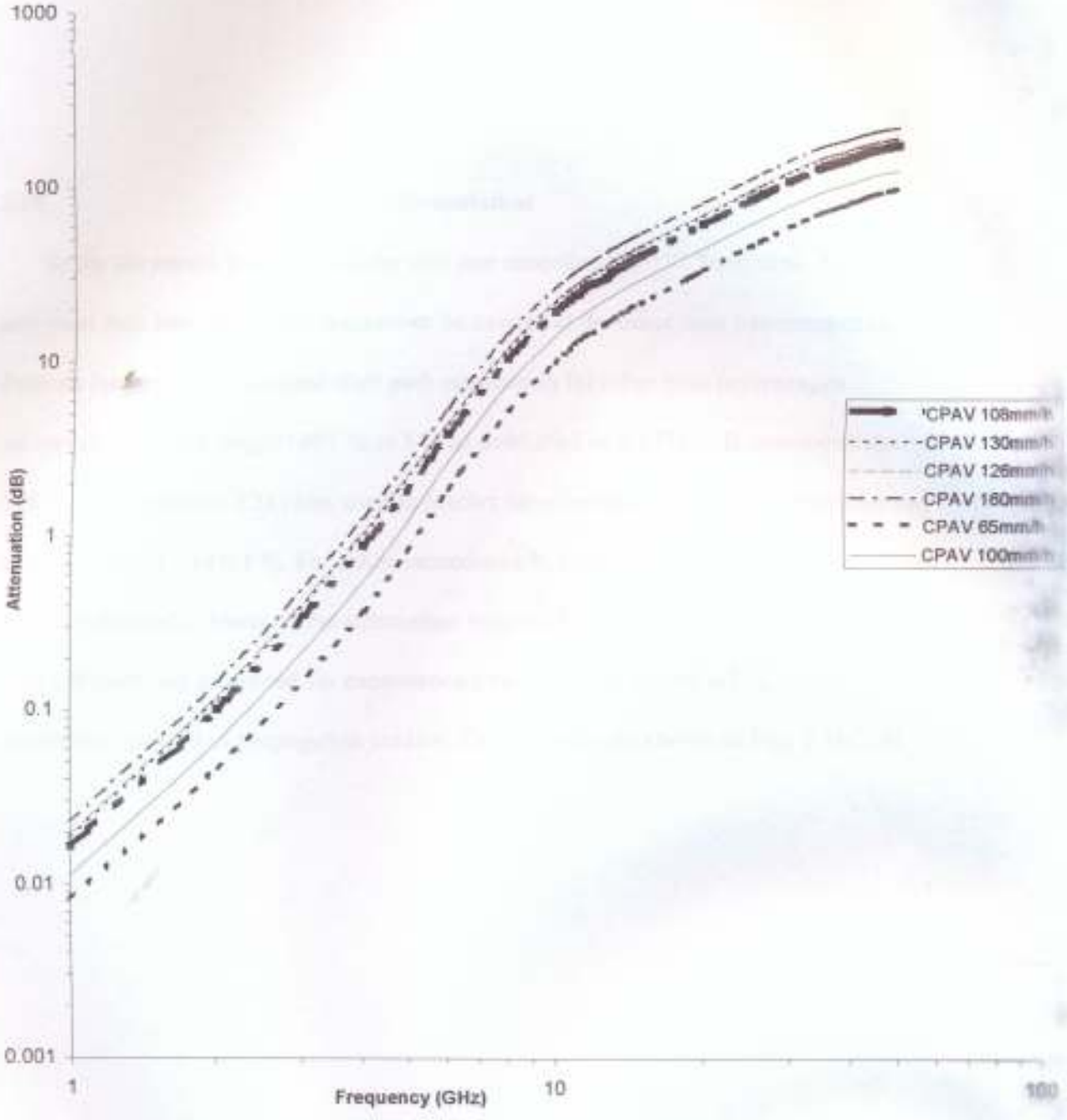


**Fig 3.35 Frequency charateristics of copolar attenuation for Ile-Ife, Douala, Nairobi,at both rainrate, mean annuall =108,126,65, and mean worst month=130,160,100mm/h respectively at elevation angle of 23**

### 3.28 Scaling formulation

So far the results presented are for rain rate exceeded for 0.01 % of time. XPD, CPA and slant path attenuation can sometimes be needed at the other time percentages scaling formula for estimating the total slant path attenuation for other time percentages unavailability in the range 0.001 % to 5 % as published in the ITU – Recommendation P. 618 – 8 (see equation 2.21) was used to predict for other time percentages unavailability such as 0.001 % and 0.1 %. For other exceedance % times, the attenuation for other % of time is estimated in terms of the attenuation exceeded for 0.01% of time using equation (2.21). Results are presented for exceedance times of 0.001 % and 0.1 %, which are also sometimes relevant to propagation studies. These results are shown in Figs 3.36-3.41

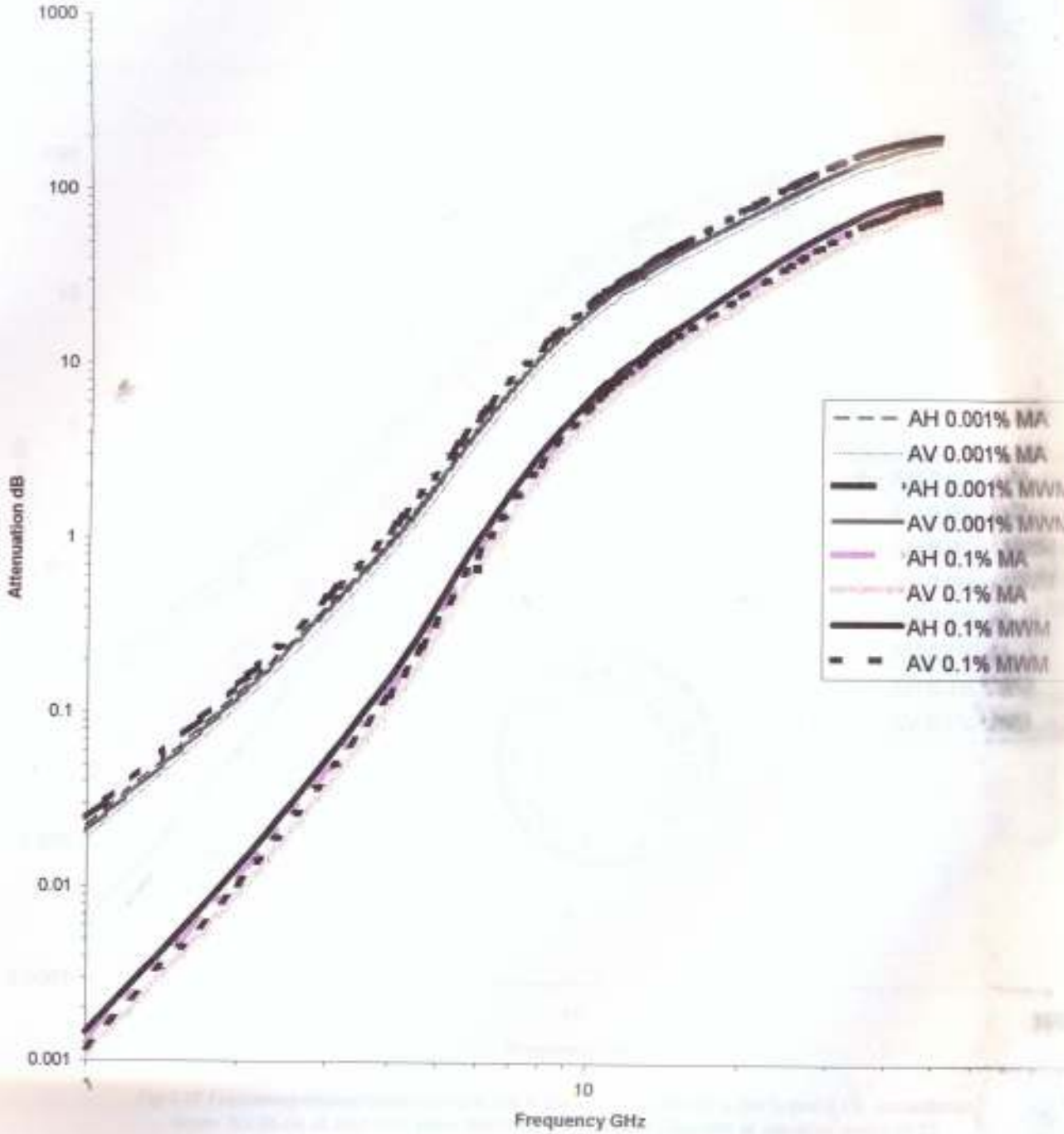


Fig 3.36 Frequency characteristis of total slant-path attenuation for 0.001% and 0.1% exceedance times for Ile-ife at both rain rates MA=108mm/h, MWM=130mm/h at elevation angle of 55

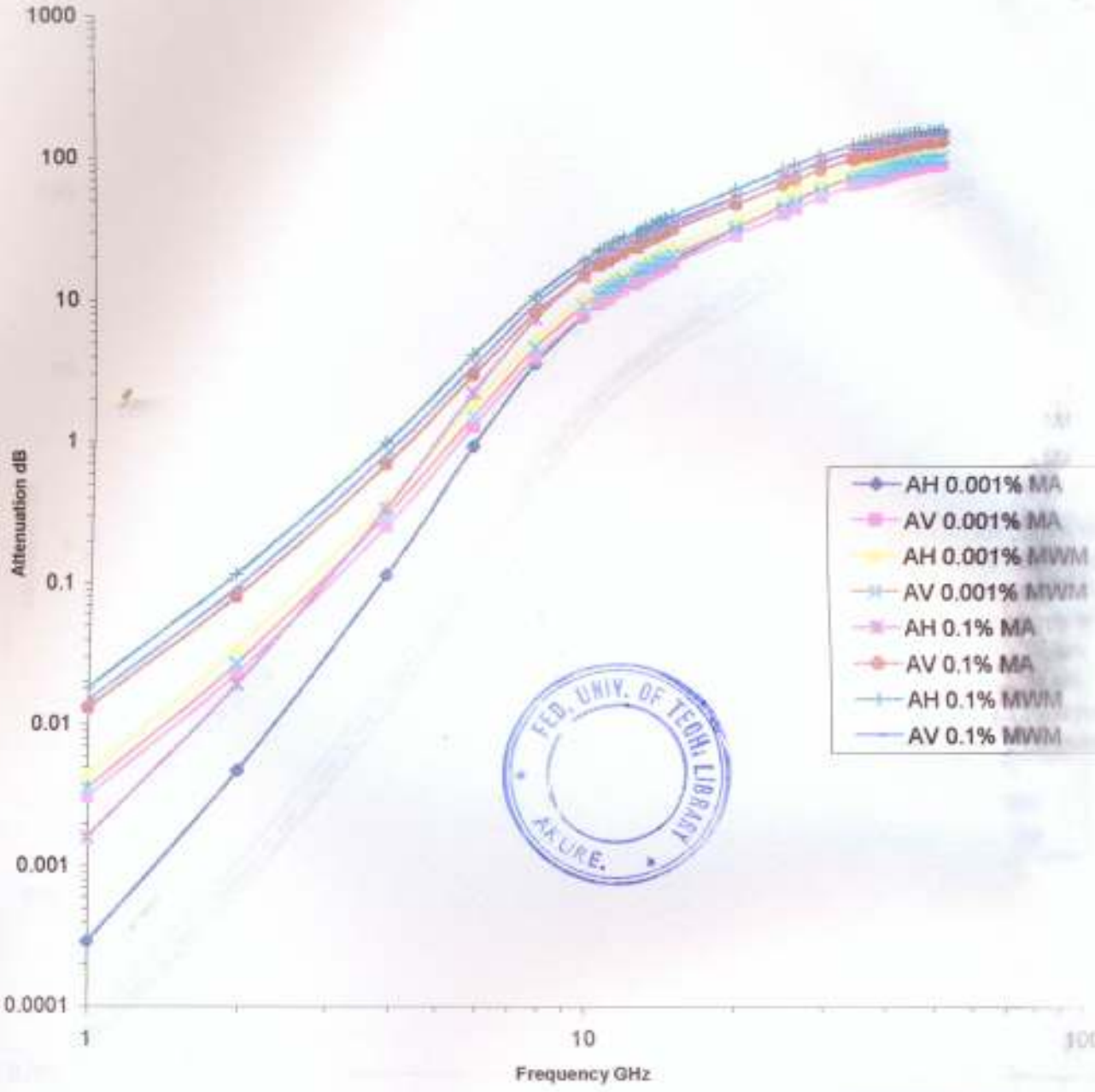




**Fig 3.37 Frequency characteristis of total slant-path attenuation for 0.001% and 0.1% exceedance times for Ile-ife at both rain rates MA=108mm/h, MWM=130mm/h at elevation angle of 23**

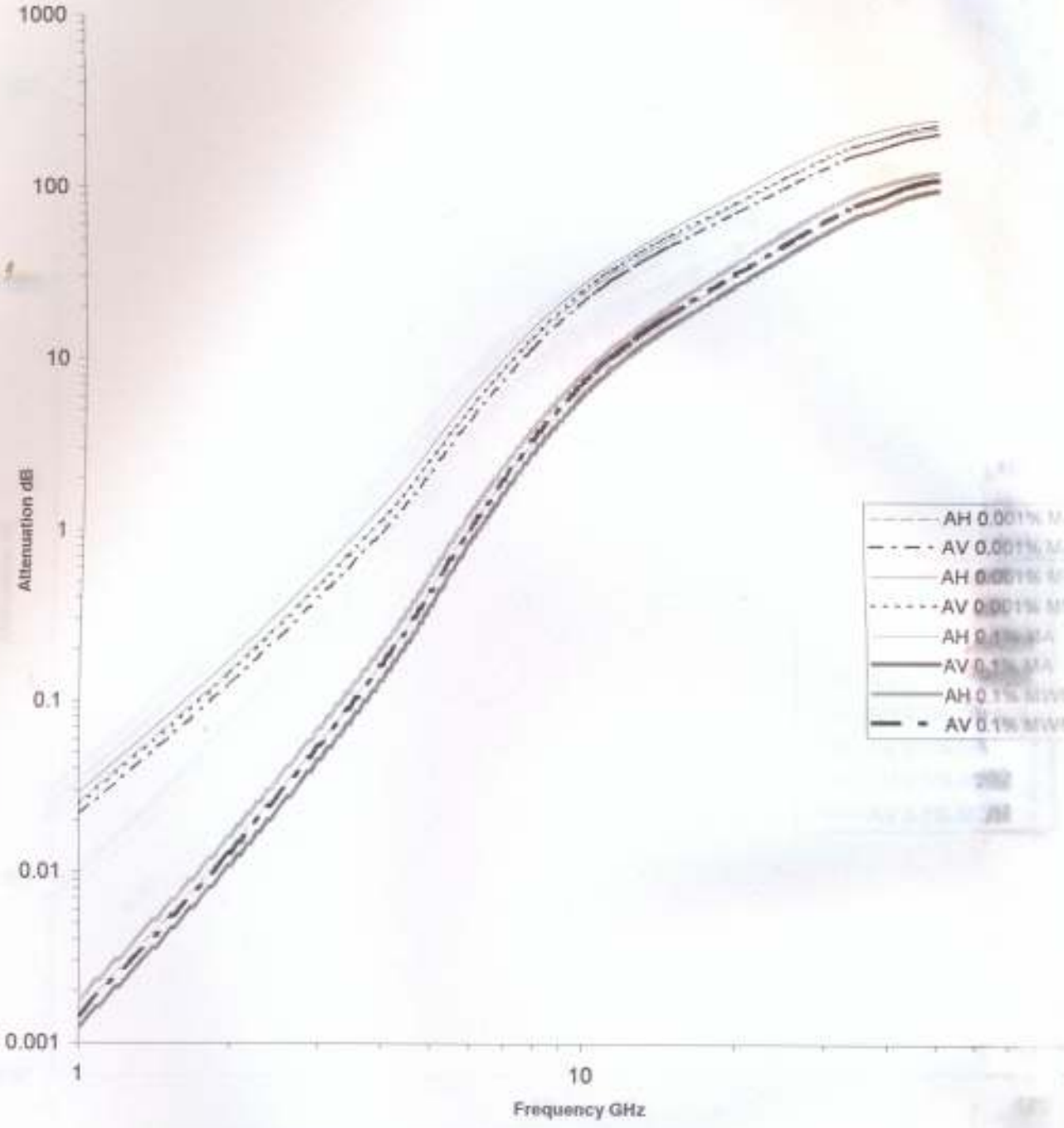


**Fig 3.38 Frequency characteristis of total slant-path attenuation for 0.001% and 0.1% exceedance times for Douala at both rain rates MA=126mm/h, MWM=160mm/h at elevation angle of 55**

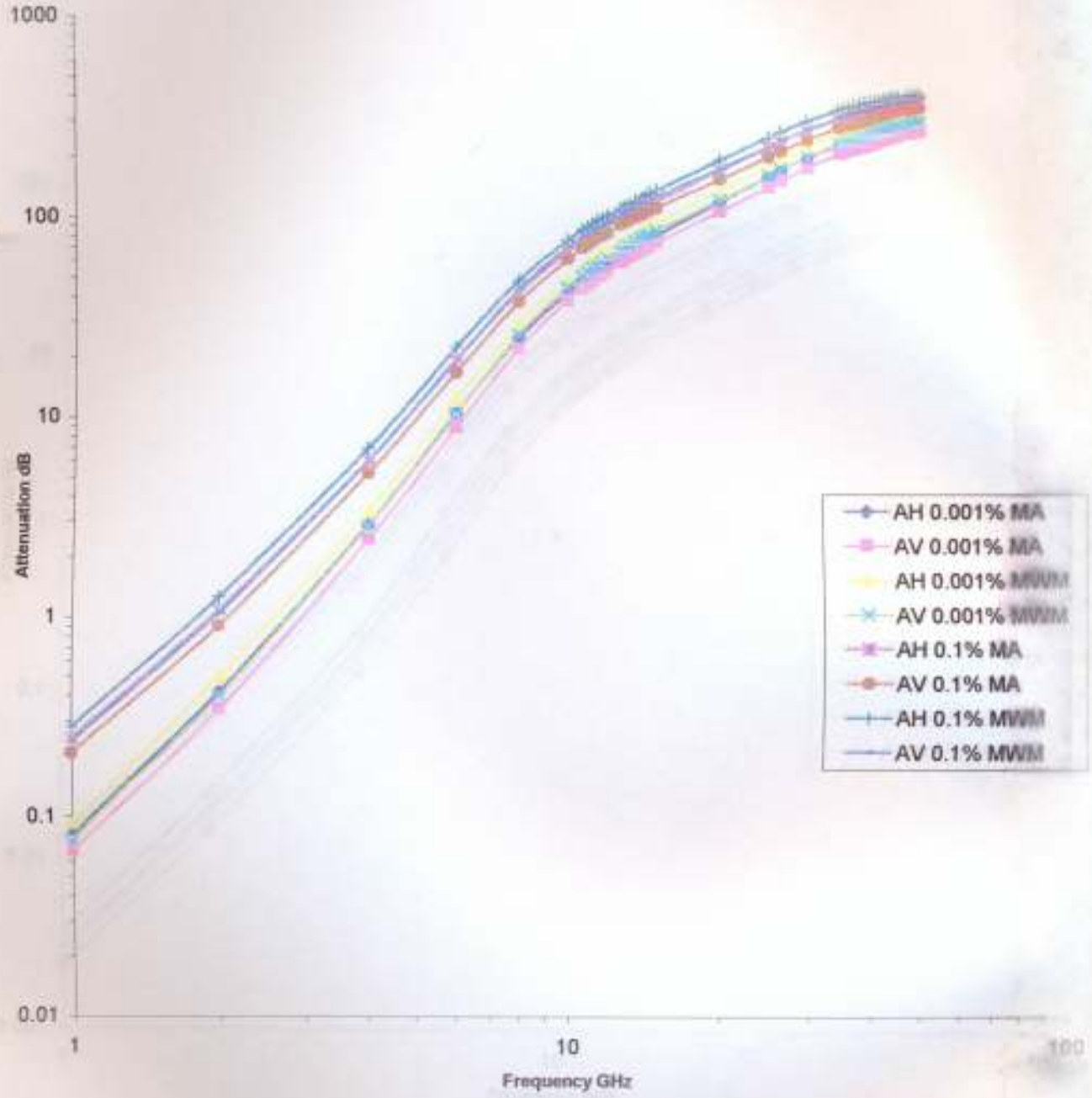


Fig 3.39 Frequency characteristis of total slant-path attenuation for 0.001% and 0.1% exceedance times for Douala at both rain rates MA=126mm/h, MWM=160mm/h at elevation angle of 23

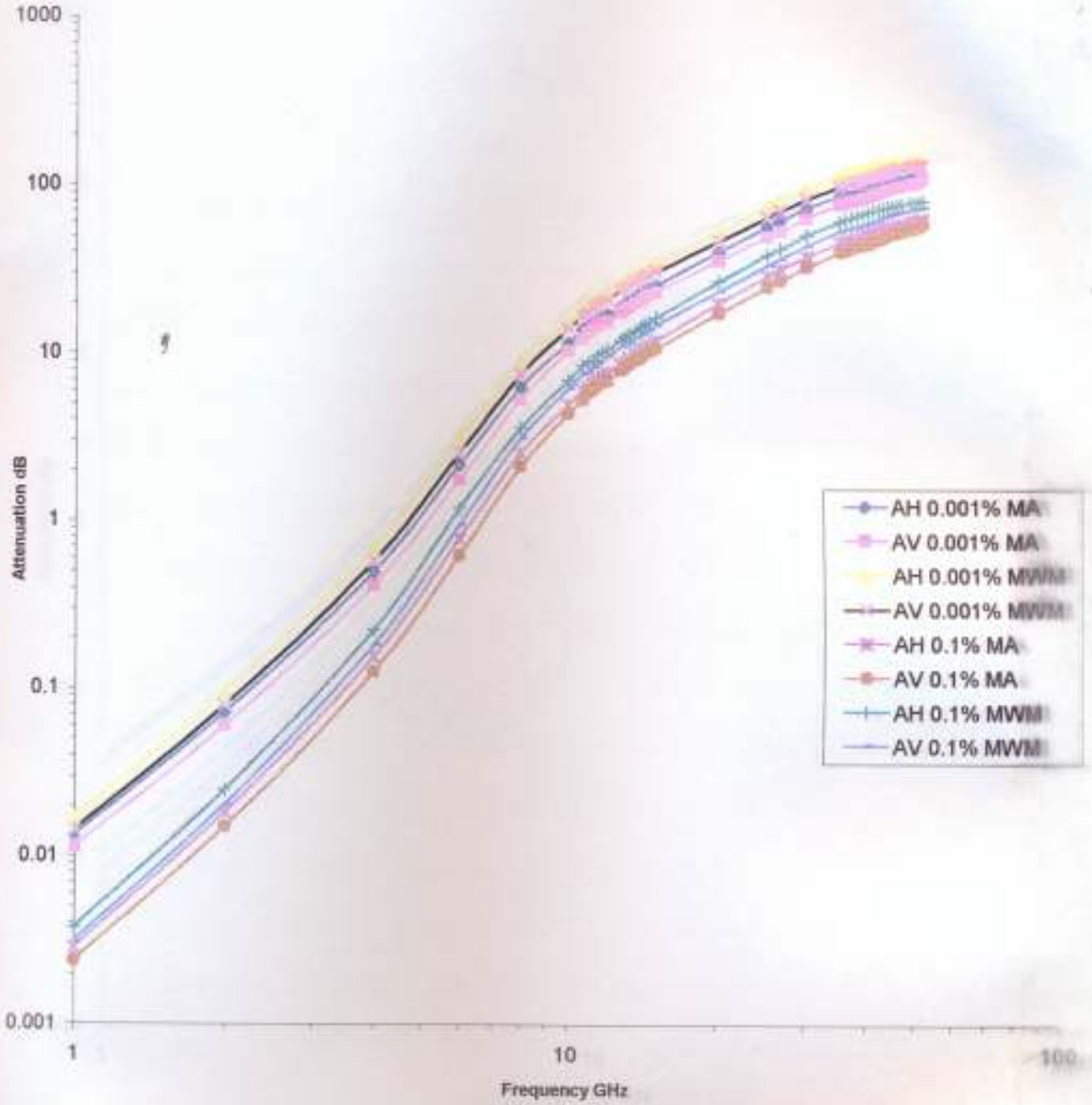


Fig 3.40 Frequency characteristis of total slant-path attenuation for 0.001% and 0.1% exceedance times for Nairobia at both rain rates MA=65mm/h, MWM=100mm/h at elevation angle of 55

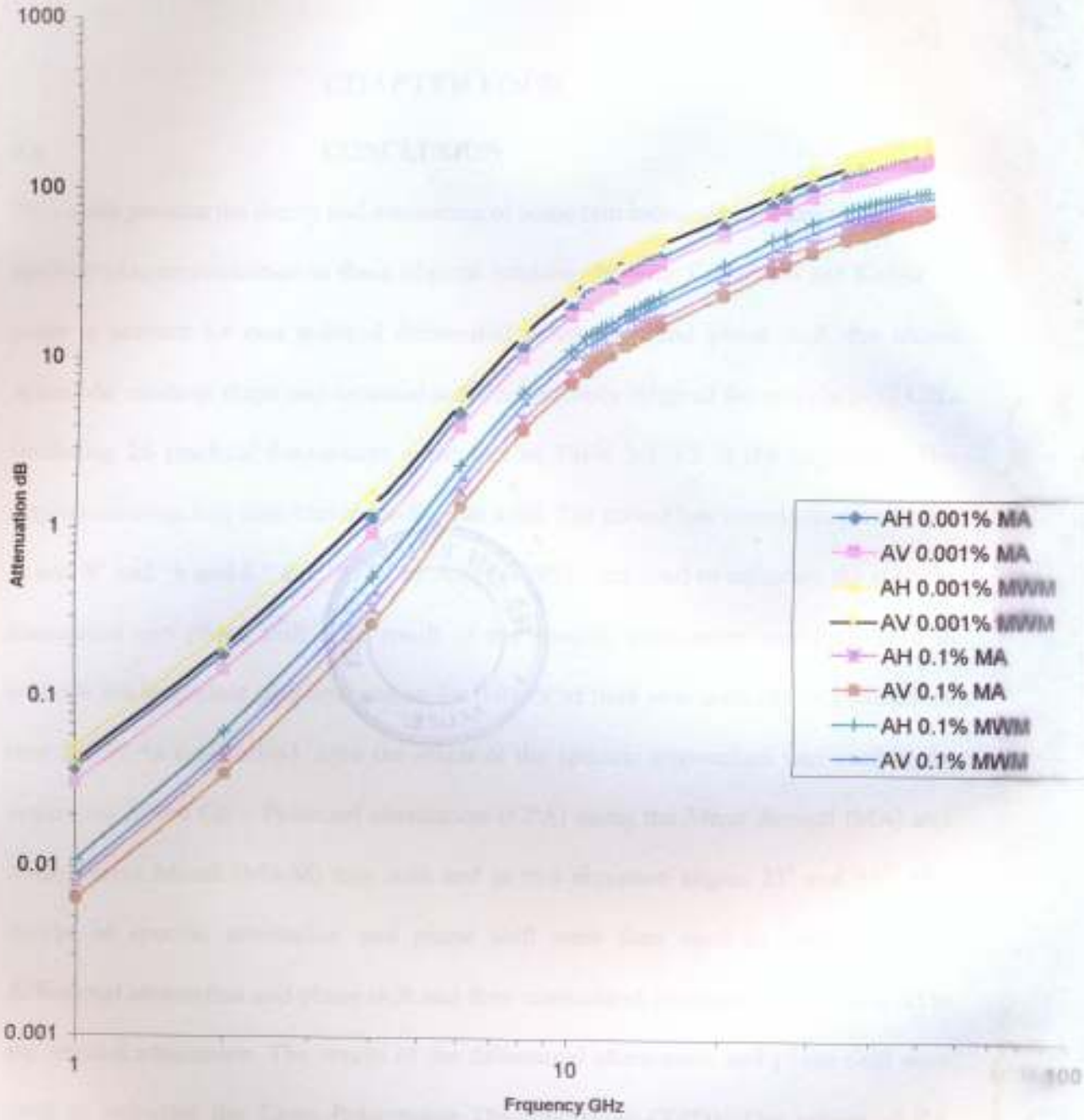


Fig 3.41 Frequency characteristis of total slant-path attenuation for 0.001% and 0.1% exceedance times for Nairobia at both rain rates MA=65mm/h, MWM=100mm/h at elevation angle of 23

# CHAPTER FOUR

## 4.1 CONCLUSION

This work presents the theory and evaluation of some rain induced propagation effects on satellite telecommunication in three tropical locations Nigeria, Cameroon and Kenya. In order to account for rain induced differential attenuation and phase shift, the oblate spheroidal raindrop shape was assumed and the frequency range of the study is 1–52 GHz (including 26 practical frequencies asterisked in Table 3.1-3.3 in the appendix). The tropical raindrop size distribution model was used. The power law regression parameters "a and b" and "h and k " calculated by Ajayi (1985) were used to calculate the specific attenuation and phase shift. The result of the specific attenuation was then used to evaluate the total slant path attenuation for 0.01 % of time unavailability or exceedance time (99.99 % availability). Also the result of the specific attenuation was used in the evaluation of the Co – Polarized attenuation (CPA) using the Mean Annual (MA) and Mean Worst Month (MWM) rain rates and at two elevation angles $23^0$ and $55^0$. The results of specific attenuation and phase shift were then used in calculating the differential attenuation and phase shift and their normalized components with respect to the vertical attenuation. The results of the differential attenuation and phase shift were used to calculate the Cross-Polarization Discrimination (XPD). The values of the predicted slant path attenuation, CPA, and XPD for Cameroon, and Kenya were compared with Nigeria. The results show that the predicted slant path attenuation, CPA, and XPD at elevation angle of $55^0$ for Cameroon are within about 24 % of that for Nigeria when the MA rain rate exceeded for 0.01 % of time is used. It is about

36 % when the MWM rain rate exceeded for 0.01 % of time is used. At the elevation angle of $23^0$, the values are unusually high and are about 1136 % and 466 % respectively.

## 4.2 RECOMMENDATIONS

In the framework of brotherliness and for the purpose of quick integration and expansion of telecommunications services in the region, further studies are recommended particularly in Cameroon where there is a dearth of information on propagation studies. There is very little interaction between or cooperation between scientists in radio communication in these regions, therefore an intergovernmental platform can be created to bring researchers in these countries together for the development of Africa. Furthermore, the available experts in Nigeria can be encouraged to assist their colleagues in Cameroon and Kenya to measure and analysis propagation parameters relevant to Earth-space communication in their region. This is with the view to improving the quality of telecommunication deliverables across the region.

## REFERENCES

Adimula I.A and Ajayi G.O (1996) Variation in raindrop size distribution and specific Attenuation due to rain in Nigeria. Ann.Telecom, Vol.51, No.1-2 p87-93

Ajayi G.O (1990), Some aspect of tropical rainfall and their effect on microwave propagation Int. satellite commun. Vol. 8, pp 163-172

Ajayi G.O and Balbaliscia F. (1990): Prediction of attenuation due to rain characteristics of the $0^0$ C Isothermal in temperate and tropical climates. Int. J Sat Comms. Vol 8, p 187-196.

Ajayi G. O., Feng, S., Radicella, S. M, Reddy B. M, (1996) Hand Book on Radio propagation Related to satellite communications in Tropical and Subtropical countries UNESCO and ICTP, U. R. S. I Standing committee on developing countries.

Ajayi G.O (1985), Characteristics of rain induced Attenuation and phase shift at CM and MM waves using a tropical raindrop size distribution model. Int. J. Infr. And mm waves Vol. 6, P771 – 806.

Ajayi G.O and Owolabi I. E (1987): Rainfall parameters from distrometer drop size measurements at a tropical station Ann. Telecom, vol 42, No. 1-2, p 3-12

Ajayi G.O, Owolabi I. E and Adimula I.A (1987), Rain induced depolarization from 1 GHz – 300 GHz in a tropical environment. Int. infrared milli meter waves, vol. 8, pp 177-197.

Ajayi G. O and R. L Olsen, (1985) modeling of a raindrop size distribution for microwave and millimeter wave applications Radio Sci., vol. 20, No. 2, pp. 193-202.

Ajewole M.O, L.B Kolawole and G.O Ajayi (1999), Cross polarization on Line – of – sight Links in a Tropical location: Effect of the Variation in canting Angle and Rain drop size distribution. IEEE transaction on antennas and propagation. Vol 47, NO 8. pp 1254-1259

Ajewole, M.O (1997) Scatering and attenuation of centimeter and millimeter radio signals by tropical rainfall. Ph. D thesis, Federal University of Technology Akure Nigeria

Allnut J. E and Haidara F (1998) Ku – band diurnal rain fade statistics from three two-year, earth-space experiments in equatorial Africa, U.R.S.I conference

Ajose S.O, Sadiku M.O, Goini U (1995), Computation of Attenuation, Phase rotation and Cross polarization of radio waves due to rainfall in tropical region IEEE transaction on antennas and propagation., vol 4b No 1. pp 1-5

Battan, L. J. (1973), Radar observation of the atmosphere Univ. of Chicago press Chicago, IL.

Brussaard, G. (1976) A meteorology model for rain – induced cross polarization, IEEE Trans, Antennas Propagat, Vol, Ap – 24, pp 5 – 11.

CCIR, (1986) Propagation in non-ionized media, report 732-2: Worst month statistic. Recommendations and reports of CCIR XVITH plenary Assembly, Dubro Vnik.

CHU T. S (1974), Rain – induced Cross polarization at centimeter and millimeter wavelength. American Telephone and Telegraph company. The Bell system technical Journal vol . 53 NO 8 october 1974.

Cox D. C. and Arnold H. W, (1984) Comparison of Measureed XPD and XPI for rain and ice space-earth path Radio – science 19, pp617 - 628

Hall, M. P. M and Barclay, L. W (1989) Radio wave propagation. Peter Peregrinus Ltd, London, p1-279.

ITU –Recommendation (1994) Cross polarization due to the atmosphere REP. 882 – 1, 722 – 2

ITU – Recommendation (2001) P. 839 – 3 Rain height model for prediction methods

ITU – Recommendation (2003) P. 618 – 8 Propagation data and prediction methods required for design of Earth – space telecommunication system.

ITU-Recommendation (1982) Draft handbook on radio meteorology. Int. Telecomms union study groups Doc. 3/11-E

ITU-Recommendation (1995) Draft handbook on radio meteorology. Int. Telecomms union study groups Doc. 3/11-D

Joss, J., Thams, J. C and Waldvogel, A. (1968) The variation of raindrop size distribution at Lorano, Switzerland. Proc. Int. Conf. On cloud Physics, Toronto, Canada. P369-373.

Laws, J. O. and Parsons, D. A. (1943) The relation of raindrop sizes to intensity. Trans. Amer. Geophys. Union, Vol. 24, p 432-460

Maggiori, D. (1981) Computed transmission through rain in the 1 – 400GHz frequency range for spherical and elliptical drops and any Polarization. FUB. Rept. IC 379 Alta Freq. Vol. 1. P 262-273

Maher, B. O. Murphy, P. J. and Sexon, M. C. (1977) A theoretical model of the effect of wind – gusting on rain – induced cross – polarization Ann Telecommunic, Vol 32, pp 404 - 408

Marshall, J. S and Palmer, W. M. K. (1948) The distribution of raindrops with size. J. of Meteorology, Vol. 5, p 165-166

McCarthy , D.k, Allnutt J.E, Salazar W.E, Wanmi F Tchinda M. Ndinayi T. D and Zaks C, 1994(a), Results of an 11.6 GHz radiometric experiment in Cameroon, second year Electronics Letters; 30(17) 1449-1450.

McCarthy , D.k, Allnutt J.E, Salazar W.E, Sitati R.w., Okoth M, Mutungi M.J, Odhiambo C.D. Zaks. C 1994(b), Results of an 11.6 GHz radiometric experiment in Kenya, second year Electronics Letters; 30(17) 1450-1452.

McCarthy , D.k, Allnutt J.E, Salazar W.E, Omeata E.C, Owolabi B.R., Oladiran T., Ojeba E.B, Ajayi G.O, Raji T. and , C.Zaks, 1994(c) Results of an 11.6 GHz radiometric experiment in Nigeria, second year Electronics Letters; 30(17) 1452-1453.

Olsen, R. L. Rogers, D. V. and Hodge, D. B. (1978) The $aR^b$ Relation in the calculation of rain attenuation. IEEE transaction on antennas and propagation. vol. AP – 26, No. 2, p 318-329.

Olsen, R. L. (1981). Cross polarization during precipitation on terrestrial links. A review Radio Sci., Vol. 16 No 5, PP. 761- 779.

Oguchi, T. (1973) Scattering properties of oblate raindrops and cross polarization of radiowaves due to rain calculation at 19.3 and 34.8 GHz J. Radio research Labs., Vol. 20, No 102, p 79 - 118

Oguchi, T. (1975) Rain depolarization studies at centimeter and millimeter wavelength; theory and mearsurements. J . Radio Res. Labs (Japan), Vol22, 107, 165-211

Oguchi, T. (1977). Scattering properties of pruppacher and pitter form raindrops and cross polarization due to rain, calculation at 11,13,19.3 and 34.8 GHz, Radio Sci, Vol. 12, No. 1 PP. 41-51

Saunders, M. J. (1971) Cross polarization at 18 and 30 GHz due to rain, IEEE Trans. Antennas Propagat., Vol. AP – 19, pp. 273 – 277.

Ugai, S. and Akimoto H. (1983) Proceeding of IEEE. Vol. 71. No 9. September p 1020-1078

Watson, P. A, (1974) Microphysics of hydrometers and polarization working group report III J. de Recherches Atm, Vol.8, ½, 477- 484

Watson, P. A. (1976) Survey of measurement of attenuation by rain and other hydrometeors Proceeding of IEEE. Vol. 123. No 9 p 863-871.

## Appendix

**Tables 3.1 – 3.3**

**Table 3.1**
**Results of the calculation of total slant path attenuation in Nigeria at elevation angles of $55^0$ and $23^0$ at both rain rates mean annual=108mm/h and mean worst month 130mm/h. Practical Frequencies are indicated by (*)**

| | ILE-IFE ELEVATION 55 PREDICTED SLANT PATH ATTENUATION | | | | | ILE-IFE ELEVATION 23 PREDICTED SLANT PATH ATTENUATION | | | | |
|---|---|---|---|---|---|---|---|---|---|---|
| | MA=108mm/h | | MWM=130mm/h | | | MA=108mm/h | | MWM=130mm/h | | |
| Freq/GHz | AH | AV | AH | AV | Freq/GHz | AH | AV | AH | AV | |
| 1 | 0.006464 | 0.005397 | 0.007207 | 0.006008 | 1 | 0.001866 | 0.015851 | 0.022182 | 0.017957 | |
| 2 | 0.045842 | 0.037656 | 0.051938 | 0.04262 | 2 | 0.023136 | 0.096956 | 0.14054 | 0.111824 | |
| 4 | 0.429161 | 0.351683 | 0.497578 | 0.407422 | 4 | 0.409376 | 0.839029 | 1.197503 | 0.991494 | |
| 6 | 2.276445 | 1.854218 | 2.599716 | 2.17177 | 6 | 2.713126 | 3.636337 | 5.05933 | 4.186402 | |
| 8 | 6.452881 | 5.640145 | 7.354235 | 6.443744 | 8 | 9.087492 | 10.02378 | 13.23039 | 11.5174 | |
| 10 | 12.41002 | 11.17096 | 14.08493 | 12.70921 | 10 | 18.21747 | 18.58377 | 23.64863 | 21.24307 | |
| *10.7 | 14.83148 | 13.38881 | 16.94954 | 15.28076 | *10.7 | 21.81865 | 21.81819 | 27.86478 | 25.01347 | |
| *10.95 | 16.12459 | 14.13089 | 17.48296 | 16.12459 | *10.95 | 23.86052 | 22.86191 | 28.49776 | 26.19997 | |
| *11.2 | 16.70886 | 14.57165 | 18.26384 | 16.9787 | *11.2 | 24.5844 | 23.39674 | 29.5436 | 27.38922 | |
| *11.45 | 17.38859 | 15.94525 | 19.5471 | 17.8428 | *11.45 | 25.47519 | 25.45463 | 31.41699 | 28.58119 | |
| *11.7 | 18.26031 | 16.81454 | 20.43347 | 18.71658 | *11.7 | 26.70046 | 26.66669 | 32.60846 | 29.77582 | |
| 12 | 19.04914 | 17.3047 | 21.54406 | 19.61028 | 12 | 27.69799 | 27.21367 | 34.09885 | 30.94089 | |
| *12.75 | 20.9559 | 18.87093 | 23.74032 | 21.9246 | *12.75 | 30.04427 | 29.11611 | 36.82023 | 33.92995 | |
| *13 | 22.35984 | 20.32264 | 25.10364 | 23.31167 | *13 | 32.12466 | 31.19251 | 38.71688 | 35.8806 | |
| *13.25 | 23.28158 | 21.23965 | 26.47441 | 24.23825 | *13.25 | 33.36659 | 32.4192 | 40.60597 | 37.08985 | |
| *13.625 | 24.43108 | 22.35887 | 28.1194 | 25.40465 | *13.625 | 34.81787 | 33.84693 | 42.76203 | 38.53934 | |
| *14 | 25.89182 | 23.48913 | 29.34896 | 26.96671 | *14 | 36.77112 | 35.27764 | 44.24886 | 40.58224 | |
| *14.25 | 26.5388 | 24.43186 | 30.32086 | 27.53342 | *14.25 | 37.52162 | 36.50958 | 45.46705 | 41.20808 | |
| *14.5 | 27.49319 | 25.38064 | 31.65417 | 28.49249 | *14.5 | 38.77203 | 37.74167 | 47.22823 | 42.42671 | |
| 15 | 29.51549 | 26.76572 | 33.26878 | 30.20893 | 15 | 41.42896 | 39.42164 | 49.12369 | 44.5391 | |
| 20 | 49.30735 | 43.36926 | 55.4661 | 48.79867 | 20 | 65.77592 | 59.40196 | 75.75469 | 66.7188 | |
| 25 | 72.13986 | 62.43307 | 81.08398 | 70.17059 | 25 | 92.72814 | 81.61537 | 105.2616 | 91.40589 | |
| *26.5 | 79.03577 | 68.36886 | 89.15609 | 77.24117 | *26.5 | 100.6427 | 88.4138 | 114.3746 | 99.47653 | |
| 30 | 94.92835 | 82.62519 | 106.5324 | 92.74683 | 30 | 118.6024 | 104.6019 | 133.58 | 116.8611 | |
| 35 | 114.9918 | 101.2541 | 128.7392 | 113.4204 | 35 | 140.6671 | 125.3951 | 157.6432 | 139.6728 | |
| *36 | 118.3018 | 104.4315 | 132.6984 | 116.9971 | *36 | 144.2222 | 128.8988 | 161.8874 | 143.569 | |
| *37 | 121.4842 | 106.2947 | 136.5612 | 119.4981 | *37 | 147.6334 | 130.8769 | 166.0248 | 146.2193 | |
| *38 | 124.6496 | 109.148 | 139.9237 | 121.9646 | *38 | 151.035 | 134.0175 | 169.5905 | 148.8443 | |
| *39 | 127.7992 | 110.7999 | 143.2618 | 124.3984 | *39 | 154.4278 | 135.7777 | 173.1391 | 151.4454 | |
| 40 | 130.8467 | 113.791 | 146.0603 | 127.1836 | 40 | 157.7094 | 139.0923 | 176.0806 | 154.4621 | |
| *41 | 133.9165 | 116.7359 | 149.2368 | 130.8634 | *41 | 161.0271 | 142.3569 | 179.4676 | 158.5091 | |
| *42 | 135.7675 | 119.6941 | 151.8598 | 135.3474 | *42 | 162.9292 | 145.6401 | 182.2364 | 163.4718 | |
| *43 | 136.5666 | 123.4145 | 154.4481 | 137.4325 | *43 | 165.9564 | 149.7932 | 184.9798 | 165.7092 | |
| *44 | 140.4907 | 126.3658 | 156.7387 | 140.4907 | *44 | 167.9778 | 153.0719 | 187.4007 | 169.0591 | |
| 45 | 142.8311 | 129.2446 | 158.9576 | 143.9744 | 45 | 170.4975 | 156.2716 | 189.7552 | 172.8933 | |
| *46 | 144.8218 | 131.4683 | 160.9349 | 146.5767 | *46 | 172.6275 | 158.736 | 191.8524 | 175.7393 | |
| *47 | 146.6515 | 133.6078 | 163.1131 | 148.8708 | *47 | 174.5869 | 161.1123 | 194.1881 | 178.2471 | |
| *49 | 149.9149 | 137.0295 | 166.6653 | 152.6437 | *49 | 178.0961 | 164.9248 | 197.9994 | 182.3781 | |
| 50 | 151.7522 | 138.8519 | 168.4215 | 154.2584 | 50 | 180.1042 | 166.9675 | 199.9013 | 184.1551 | |
| *51 | 152.8959 | 140.3616 | 170.0651 | 156.1546 | *51 | 181.3382 | 168.6678 | 201.6896 | 186.2547 | |
| *52 | 154.5771 | 142.4137 | 171.7854 | 157.7146 | *52 | 183.1926 | 170.9797 | 203.5737 | 187.989 | |

**Table 3.2**
**Results of the calculation of total slant path attenuation in Cameroon at elevation angles of $55^0$ and $23^0$ at both rain rates mean annual=126mm/h and mean worst month 160mm/h. Practical Frequencies are indicated by (*)**

| | DOUALA ELEVATION 55 PREDICTED SLANT PATH ATTENUATION | | | | | DOUALA ELEVATION 23 PREDICTED SLANT PATH ATTENUATION | | | | |
|---|---|---|---|---|---|---|---|---|---|---|
| | MA=126mm/h | | MWM=160mm/h | | | MA=126mm/h | | MWM=160mm/h | | |
| Freq/GHz | AH | AV | AH | AV | Freq/GHz | AH | AV | AH | AV | |
| 1 | 0.007495 | 0.00625 | 0.008608 | 0.007164 | 1 | 0.023085 | 0.018691 | 0.027105 | 0.021904 | |
| 2 | 0.053888 | 0.044232 | 0.063139 | 0.051761 | 2 | 0.145755 | 0.115995 | 0.175166 | 0.139113 | |
| 4 | 0.5144 | 0.421289 | 0.620429 | 0.507685 | 4 | 1.232322 | 1.024048 | 1.460794 | 1.217631 | |
| 6 | 2.670445 | 2.231873 | 3.149782 | 2.638243 | 6 | 5.179626 | 4.288465 | 6.167736 | 5.113764 | |
| 8 | 7.536778 | 6.604695 | 8.864013 | 7.79234 | 8 | 13.50854 | 11.76228 | 16.03377 | 13.99126 | |
| 10 | 14.42147 | 13.01332 | 16.87792 | 15.27594 | 10 | 24.12294 | 21.67126 | 28.46332 | 25.62354 | |
| *10.7 | 17.29811 | 15.50923 | 20.00376 | 18.11933 | *10.7 | 28.32797 | 25.28639 | 32.99496 | 29.73597 | |
| *10.95 | 17.9293 | 16.38816 | 20.92436 | 19.41475 | *10.95 | 29.11944 | 26.52428 | 34.23227 | 31.64371 | |
| *11.2 | 19.08584 | 17.27744 | 22.21915 | 20.32637 | *11.2 | 30.7854 | 27.76431 | 36.09395 | 32.87582 | |
| *11.45 | 20.25347 | 18.46202 | 23.52851 | 21.24875 | *11.45 | 32.44862 | 29.477 | 37.95543 | 34.11192 | |
| *11.7 | 20.91638 | 19.09603 | 24.49171 | 22.18148 | *11.7 | 33.25743 | 30.25095 | 39.21101 | 35.35175 | |
| 12 | 22.05088 | 20.07286 | 25.70301 | 23.45596 | 12 | 34.7746 | 31.55804 | 40.79306 | 37.07776 | |
| *12.75 | 24.79607 | 22.90728 | 28.94423 | 26.542 | *12.75 | 38.34519 | 35.34534 | 45.01369 | 41.13635 | |
| *13 | 26.12629 | 23.86249 | 30.341 | 27.94746 | *13 | 40.17214 | 36.60096 | 46.90335 | 43.06738 | |
| *13.25 | 26.92272 | 24.82574 | 31.36659 | 28.68887 | *13.25 | 41.14122 | 37.85843 | 48.18059 | 43.92534 | |
| *13.625 | 28.44921 | 26.03322 | 33.11457 | 30.40934 | *13.625 | 43.10009 | 39.35929 | 50.40955 | 46.15718 | |
| *14 | 29.89996 | 27.25111 | 34.88378 | 31.97702 | *14 | 44.91986 | 40.86251 | 52.64474 | 48.1248 | |
| *14.25 | 30.71723 | 28.24135 | 35.94107 | 33.00196 | *14.25 | 45.8942 | 42.12783 | 53.93116 | 49.39399 | |
| *14.5 | 32.20379 | 29.2383 | 37.32741 | 34.03335 | *14.5 | 47.87941 | 43.39448 | 55.71637 | 50.66485 | |
| 15 | 34.04036 | 30.91538 | 39.52925 | 35.96008 | 15 | 50.09551 | 45.43175 | 58.37694 | 52.97866 | |
| 20 | 56.71304 | 49.9211 | 65.72329 | 57.87383 | 20 | 77.23559 | 68.06201 | 89.50435 | 78.80959 | |
| 25 | 82.85428 | 71.74849 | 95.94725 | 83.08586 | 25 | 107.2917 | 93.23233 | 123.959 | 107.5855 | |
| *26.5 | 91.19661 | 79.12378 | 104.929 | 91.19661 | *26.5 | 116.7087 | 101.6542 | 133.913 | 116.7087 | |
| 30 | 108.8338 | 94.80518 | 125.8165 | 109.6335 | 30 | 136.1658 | 119.1943 | 156.7744 | 137.1345 | |
| 35 | 131.5428 | 115.9467 | 151.6412 | 133.7541 | 35 | 160.7576 | 142.5013 | 184.3061 | 163.3467 | |
| *36 | 135.5537 | 119.1401 | 156.1636 | 137.4183 | *36 | 165.0517 | 145.9425 | 189.0597 | 167.2227 | |
| *37 | 139.669 | 122.2637 | 159.9682 | 140.928 | *37 | 169.4724 | 149.3111 | 192.9895 | 170.9305 | |
| *38 | 143.1353 | 124.2878 | 164.3088 | 143.7746 | *38 | 173.1492 | 151.4201 | 197.554 | 173.8859 | |
| *39 | 146.448 | 127.4496 | 168.281 | 146.5778 | *39 | 176.6606 | 154.8547 | 201.7048 | 176.8094 | |
| 40 | 149.3108 | 130.0702 | 171.5178 | 149.6544 | 40 | 179.6697 | 157.6767 | 205.0284 | 180.0621 | |
| *41 | 152.0637 | 133.8496 | 174.8284 | 153.3967 | *41 | 182.5685 | 161.8305 | 208.455 | 184.0849 | |
| *42 | 155.428 | 137.0322 | 177.8555 | 157.446 | *42 | 186.1748 | 165.307 | 211.5771 | 188.4617 | |
| *43 | 158.0898 | 140.9508 | 180.8376 | 161.4884 | *43 | 188.9964 | 169.6219 | 214.6664 | 192.8339 | |
| *44 | 160.5798 | 144.4188 | 183.7771 | 165.5241 | *44 | 191.6377 | 173.428 | 217.7247 | 197.2018 | |
| 45 | 162.5953 | 147.3148 | 186.0942 | 168.8071 | 45 | 193.7598 | 176.5937 | 220.1017 | 200.7284 | |
| *46 | 164.6007 | 149.9659 | 188.763 | 171.5041 | *46 | 195.8861 | 179.491 | 222.8905 | 203.6082 | |
| *47 | 166.9814 | 152.7937 | 191.0539 | 174.5301 | *47 | 198.4454 | 182.5935 | 225.2737 | 206.866 | |
| *49 | 170.6171 | 156.2075 | 195.3587 | 178.5166 | *49 | 202.3461 | 186.3195 | 229.7615 | 211.1153 | |
| 50 | 172.3887 | 157.9325 | 196.6401 | 180.3764 | 50 | 204.2638 | 188.2184 | 231.096 | 213.1117 | |
| *51 | 174.5551 | 159.6524 | 198.5109 | 182.3467 | *51 | 206.6296 | 190.1213 | 233.078 | 215.2424 | |
| *52 | 175.7075 | 161.9042 | 199.7222 | 184.2075 | *52 | 207.8849 | 192.6218 | 234.3484 | 217.2633 | |

**Table 3.3**

**Results of the calculation of total slant path attenuation in Kenya at elevation angles of $55^0$ and $23^0$ at both rain rates mean annual=65mm/h and mean worst month 100mm/h. Practical Frequencies are indicated by (*)**

| | NAIROBI ELEVATION 55 PREDICTED SLANT PATH ATTENUATION | | | | | NAIROBI ELEVATION 23 PREDICTED SLANT PATH ATTENUATION | | | | |
|---|---|---|---|---|---|---|---|---|---|---|
| | MA=65mm/h | | MWM=100mm/h | | | MA=65mm/h | | MWM=100mm/h | | |
| Freq/GHz | AH | AV | AH | AV | Freq/GHz | AH | AV | AH | AV | |
| 1 | 0.003628 | 0.003017 | 0.004763 | 0.003947 | 1 | 0.009879 | 0.007979 | 0.013555 | 0.010892 | |
| 2 | 0.023587 | 0.019267 | 0.032274 | 0.026278 | 2 | 0.056222 | 0.044746 | 0.080338 | 0.063553 | |
| 4 | 0.201323 | 0.164151 | 0.29174 | 0.237082 | 4 | 0.444949 | 0.355169 | 0.672937 | 0.533589 | |
| 6 | 1.031645 | 0.820753 | 1.568024 | 1.24222 | 6 | 2.17491 | 1.773641 | 3.134525 | 2.560166 | |
| 8 | 3.352435 | 2.788018 | 4.760135 | 4.113728 | 8 | 5.858291 | 5.025301 | 8.381884 | 7.217207 | |
| 10 | 6.558633 | 5.817662 | 9.200687 | 8.207743 | 10 | 10.77933 | 9.558775 | 15.17482 | 13.51432 | |
| *10.7 | 8.088351 | 6.988958 | 11.25616 | 10.00151 | *10.7 | 13.04755 | 11.27611 | 18.20335 | 16.15128 | |
| *10.95 | 8.460068 | 7.697941 | 11.83176 | 10.39551 | *10.95 | 13.56043 | 12.34152 | 19.00172 | 16.67329 | |
| *11.2 | 8.940471 | 8.067696 | 12.16968 | 11.06144 | *11.2 | 14.24202 | 12.85686 | 19.40887 | 17.62747 | |
| *11.45 | 9.319035 | 8.553724 | 13.00023 | 11.55413 | *11.45 | 14.75664 | 13.55111 | 20.60277 | 18.29586 | |
| *11.7 | 9.806808 | 8.929785 | 13.51098 | 12.23032 | *11.7 | 15.43866 | 14.06721 | 21.2757 | 19.24851 | |
| 12 | 10.15963 | 9.113319 | 14.08819 | 12.69719 | 12 | 15.88867 | 14.25733 | 22.0208 | 19.84036 | |
| *12.75 | 11.39513 | 10.49038 | 15.89922 | 14.58359 | *12.75 | 17.54418 | 16.16996 | 24.42691 | 22.40804 | |
| *13 | 11.78919 | 10.87875 | 16.59981 | 15.0102 | *13 | 18.06278 | 16.68869 | 25.36546 | 22.94296 | |
| *13.25 | 12.51646 | 11.38648 | 17.30516 | 15.53107 | *13.25 | 19.07906 | 17.38364 | 26.30411 | 23.61834 | |
| *13.625 | 13.33748 | 12.09416 | 18.15787 | 16.55105 | *13.625 | 20.18639 | 18.33732 | 27.39099 | 24.98169 | |
| *14 | 14.16467 | 12.45205 | 19.19059 | 17.20527 | *14 | 21.29235 | 18.76728 | 28.73752 | 25.78866 | |
| *14.25 | 14.57317 | 13.20677 | 19.73919 | 17.92697 | *14.25 | 21.81443 | 19.81077 | 29.4214 | 26.74565 | |
| *14.5 | 15.0937 | 13.60805 | 20.46522 | 18.36796 | *14.5 | 22.49817 | 20.33136 | 30.36347 | 27.28506 | |
| 15 | 15.81354 | 14.19468 | 21.66433 | 19.50258 | 15 | 23.39173 | 21.05526 | 31.86357 | 28.72635 | |
| 20 | 26.38428 | 23.01888 | 35.82484 | 31.2528 | 20 | 36.71283 | 32.22491 | 49.27774 | 43.19322 | |
| 25 | 38.54161 | 33.09962 | 52.09427 | 44.70321 | 25 | 51.53487 | 44.639 | 68.6138 | 59.31063 | |
| *26.5 | 42.45573 | 36.13728 | 56.62088 | 49.22409 | *26.5 | 56.23746 | 48.32539 | 73.86338 | 64.67273 | |
| 30 | 50.7751 | 43.84389 | 68.22481 | 58.91809 | 30 | 66.10955 | 57.62825 | 87.29212 | 76.01725 | |
| 35 | 61.71138 | 53.90151 | 82.28157 | 71.94382 | 35 | 78.97361 | 69.64372 | 103.3084 | 91.11334 | |
| *36 | 63.91433 | 55.3464 | 84.70667 | 74.18918 | *36 | 81.56068 | 71.36285 | 106.0567 | 93.70156 | |
| *37 | 65.34218 | 56.68639 | 86.94091 | 75.74127 | *37 | 83.2307 | 72.95991 | 108.5857 | 95.47789 | |
| *38 | 67.40402 | 58.01951 | 89.16526 | 77.2768 | *38 | 85.65284 | 74.55221 | 111.108 | 97.24198 | |
| *39 | 68.81694 | 59.34623 | 91.38033 | 78.79685 | *39 | 87.31297 | 76.1401 | 113.6242 | 98.99466 | |
| 40 | 70.53177 | 60.68357 | 93.21935 | 80.44228 | 40 | 89.33133 | 77.74351 | 115.7103 | 100.8994 | |
| *41 | 72.27375 | 62.69625 | 95.45091 | 82.89286 | *41 | 91.38378 | 80.14591 | 118.2552 | 103.7429 | |
| *42 | 73.66445 | 64.0112 | 96.8507 | 85.11793 | *42 | 93.02879 | 81.72646 | 119.848 | 106.3252 | |
| *43 | 75.04676 | 66.0408 | 98.45622 | 87.21825 | *43 | 94.66778 | 84.14814 | 121.6849 | 108.7646 | |
| *44 | 76.4212 | 68.07081 | 100.0454 | 89.3155 | *44 | 96.30112 | 86.56893 | 123.5096 | 111.2021 | |
| 45 | 77.33944 | 69.44818 | 101.3293 | 91.19528 | 45 | 97.40884 | 88.22648 | 124.9916 | 113.3916 | |
| *46 | 78.46205 | 70.68508 | 102.8258 | 92.87702 | *46 | 98.75781 | 89.7222 | 126.7228 | 115.3567 | |
| *47 | 79.81094 | 71.98554 | 104.1305 | 94.33371 | *47 | 100.372 | 91.29426 | 128.2414 | 117.0678 | |
| *49 | 81.78823 | 73.83325 | 106.3245 | 96.57625 | *49 | 102.7774 | 93.56933 | 130.8243 | 119.7363 | |
| 50 | 82.48105 | 74.93066 | 107.2242 | 97.64236 | 50 | 103.6442 | 94.91243 | 131.9007 | 121.0145 | |
| *51 | 83.58163 | 76.2501 | 108.3182 | 98.76274 | *51 | 104.9841 | 96.515 | 133.2025 | 122.3586 | |
| *52 | 84.31827 | 79.92315 | 109.2868 | 99.77072 | *52 | 105.9078 | 100.8409 | 134.3675 | 123.5785 | |